32ND INTERNATIONAL COSMIC RAY CONFERENCE, BEIJING 2011

The IceCube Neutrino Observatory I:

Point Source Searches

THE ICECUBE COLLABORATION

Keywords: *IceCube, neutrino astronomy, point sources, likelihood method, AGN, blazar, multi-wavelength astronomy, astrophysical neutrinos, Fermi bubbles, galactic plane, neutrino flares, time-dependent searches, supernovae, gamma-ray bursts, Swift, X-ray, multimessenger, fireball model, NToO*

32ND INTERNATIONAL COSMIC RAY CONFERENCE, BEIJING 2011

THE ICECUBE COLLABORATION

R. ABBASI[28], Y. ABDOU[22], T. ABU-ZAYYAD[33], M. ACKERMANN[39], J. ADAMS[16], J. A. AGUILAR[28], M. AHLERS[32], M. M. ALLEN[36], D. ALTMANN[1], K. ANDEEN[28,a], J. AUFFENBERG[38], X. BAI[31,b], M. BAKER[28], S. W. BARWICK[24], R. BAY[7], J. L. BAZO ALBA[39], K. BEATTIE[8], J. J. BEATTY[18,19], S. BECHET[13], J. K. BECKER[10], K.-H. BECKER[38], M. L. BENABDERRAHMANE[39], S. BENZVI[28], J. BERDERMANN[39], P. BERGHAUS[31], D. BERLEY[17], E. BERNARDINI[39], D. BERTRAND[13], D. Z. BESSON[26], D. BINDIG[38], M. BISSOK[1], E. BLAUFUSS[17], J. BLUMENTHAL[1], D. J. BOERSMA[1], C. BOHM[34], D. BOSE[14], S. BÖSER[11], O. BOTNER[37], A. M. BROWN[16], S. BUITINK[14], K. S. CABALLERO-MORA[36], M. CARSON[22], D. CHIRKIN[28], B. CHRISTY[17], F. CLEVERMANN[20], S. COHEN[25], C. COLNARD[23], D. F. COWEN[36,35], A. H. CRUZ SILVA[39], M. V. D'AGOSTINO[7], M. DANNINGER[34], J. DAUGHHETEE[5], J. C. DAVIS[18], C. DE CLERCQ[14], T. DEGNER[11], L. DEMIRÖRS[25], F. DESCAMPS[22], P. DESIATI[28], G. DE VRIES-UITERWEERD[22], T. DEYOUNG[36], J. C. DÍAZ-VÉLEZ[28], M. DIERCKXSENS[13], J. DREYER[10], J. P. DUMM[28], M. DUNKMAN[36], J. EISCH[28], R. W. ELLSWORTH[17], O. ENGDEGÅRD[37], S. EULER[1], P. A. EVENSON[31], O. FADIRAN[28], A. R. FAZELY[6], A. FEDYNITCH[10], J. FEINTZEIG[28], T. FEUSELS[22], K. FILIMONOV[7], C. FINLEY[34], T. FISCHER-WASELS[38], B. D. FOX[36], A. FRANCKOWIAK[11], R. FRANKE[39], T. K. GAISSER[31], J. GALLAGHER[27], L. GERHARDT[8,7], L. GLADSTONE[28], T. GLÜSENKAMP[39], A. GOLDSCHMIDT[8], J. A. GOODMAN[17], D. GÓRA[39], D. GRANT[21], T. GRIESEL[29], A. GROSS[16,23], S. GRULLON[28], M. GURTNER[38], C. HA[36], A. HAJ ISMAIL[22], A. HALLGREN[37], F. HALZEN[28], K. HAN[39], K. HANSON[13,28], D. HEINEN[1], K. HELBING[38], R. HELLAUER[17], S. HICKFORD[16], G. C. HILL[28], K. D. HOFFMAN[17], A. HOMEIER[11], K. HOSHINA[28], W. HUELSNITZ[17,c], J.-P. HÜLSS[1], P. O. HULTH[34], K. HULTQVIST[34], S. HUSSAIN[31], A. ISHIHARA[15], E. JACOBI[39], J. JACOBSEN[28], G. S. JAPARIDZE[4], H. JOHANSSON[34], K.-H. KAMPERT[38], A. KAPPES[9], T. KARG[38], A. KARLE[28], P. KENNY[26], J. KIRYLUK[8,7], F. KISLAT[39], S. R. KLEIN[8,7], J.-H. KÖHNE[20], G. KOHNEN[30], H. KOLANOSKI[9], L. KÖPKE[29], S. KOPPER[38], D. J. KOSKINEN[36], M. KOWALSKI[11], T. KOWARIK[29], M. KRASBERG[28], T. KRINGS[1], G. KROLL[29], N. KURAHASHI[28], T. KUWABARA[31], M. LABARE[14], K. LAIHEM[1], H. LANDSMAN[28], M. J. LARSON[36], R. LAUER[39], J. LÜNEMANN[29], J. MADSEN[33], A. MAROTTA[13], R. MARUYAMA[28], K. MASE[15], H. S. MATIS[8], K. MEAGHER[17], M. MERCK[28], P. MÉSZÁROS[35,36], T. MEURES[13], S. MIARECKI[8,7], E. MIDDELL[39], N. MILKE[20], J. MILLER[37], T. MONTARULI[28,d], R. MORSE[28], S. M. MOVIT[35], R. NAHNHAUER[39], J. W. NAM[24], U. NAUMANN[38], D. R. NYGREN[8], S. ODROWSKI[23], A. OLIVAS[17], M. OLIVO[10], A. O'MURCHADHA[28], S. PANKNIN[11], L. PAUL[1], C. PÉREZ DE LOS HEROS[37], J. PETROVIC[13], A. PIEGSA[29], D. PIELOTH[20], R. PORRATA[7], J. POSSELT[38], P. B. PRICE[7], G. T. PRZYBYLSKI[8], K. RAWLINS[3], P. REDL[17], E. RESCONI[23,e], W. RHODE[20], M. RIBORDY[25], M. RICHMAN[17], J. P. RODRIGUES[28], F. ROTHMAIER[29], C. ROTT[18], T. RUHE[20], D. RUTLEDGE[36], B. RUZYBAYEV[31], D. RYCKBOSCH[22], H.-G. SANDER[29], M. SANTANDER[28], S. SARKAR[32], K. SCHATTO[29], T. SCHMIDT[17], A. SCHÖNWALD[39], A. SCHUKRAFT[1], A. SCHULTES[38], O. SCHULZ[23,f], M. SCHUNCK[1], D. SECKEL[31], B. SEMBURG[38], S. H. SEO[34], Y. SESTAYO[23], S. SEUNARINE[12], A. SILVESTRI[24], G. M. SPICZAK[33], C. SPIERING[39], M. STAMATIKOS[18,g], T. STANEV[31], T. STEZELBERGER[8], R. G. STOKSTAD[8], A. STÖSSL[39], E. A. STRAHLER[14], R. STRÖM[37], M. STÜER[11], G. W. SULLIVAN[17], Q. SWILLENS[13], H. TAAVOLA[37], I. TABOADA[5], A. TAMBURRO[33], A. TEPE[5], S. TER-ANTONYAN[6], S. TILAV[31], P. A. TOALE[2], S. TOSCANO[28], D. TOSI[39], N. VAN EIJNDHOVEN[14], J. VANDENBROUCKE[7], A. VAN OVERLOOP[22], J. VAN SANTEN[28], M. VEHRING[1], M. VOGE[11], C. WALCK[34], T. WALDENMAIER[9], M. WALLRAFF[1], M. WALTER[39], CH. WEAVER[28], C. WENDT[28], S. WESTERHOFF[28], N. WHITEHORN[28], K. WIEBE[29], C. H. WIEBUSCH[1], D. R. WILLIAMS[2], R. WISCHNEWSKI[39], H. WISSING[17], M. WOLF[23], T. R. WOOD[21], K. WOSCHNAGG[7], C. XU[31], D. L. XU[2], X. W. XU[6], J. P. YANEZ[39], G. YODH[24], S. YOSHIDA[15], P. ZARZHITSKY[2], M. ZOLL[34]

[1] *III. Physikalisches Institut, RWTH Aachen University, D-52056 Aachen, Germany*
[2] *Dept. of Physics and Astronomy, University of Alabama, Tuscaloosa, AL 35487, USA*
[3] *Dept. of Physics and Astronomy, University of Alaska Anchorage, 3211 Providence Dr., Anchorage, AK 99508, USA*
[4] *CTSPS, Clark-Atlanta University, Atlanta, GA 30314, USA*
[5] *School of Physics and Center for Relativistic Astrophysics, Georgia Institute of Technology, Atlanta, GA 30332, USA*
[6] *Dept. of Physics, Southern University, Baton Rouge, LA 70813, USA*
[7] *Dept. of Physics, University of California, Berkeley, CA 94720, USA*
[8] *Lawrence Berkeley National Laboratory, Berkeley, CA 94720, USA*
[9] *Institut für Physik, Humboldt-Universität zu Berlin, D-12489 Berlin, Germany*
[10] *Fakultät für Physik & Astronomie, Ruhr-Universität Bochum, D-44780 Bochum, Germany*
[11] *Physikalisches Institut, Universität Bonn, Nussallee 12, D-53115 Bonn, Germany*
[12] *Dept. of Physics, University of the West Indies, Cave Hill Campus, Bridgetown BB11000, Barbados*
[13] *Université Libre de Bruxelles, Science Faculty CP230, B-1050 Brussels, Belgium*
[14] *Vrije Universiteit Brussel, Dienst ELEM, B-1050 Brussels, Belgium*
[15] *Dept. of Physics, Chiba University, Chiba 263-8522, Japan*
[16] *Dept. of Physics and Astronomy, University of Canterbury, Private Bag 4800, Christchurch, New Zealand*
[17] *Dept. of Physics, University of Maryland, College Park, MD 20742, USA*
[18] *Dept. of Physics and Center for Cosmology and Astro-Particle Physics, Ohio State University, Columbus, OH 43210, USA*
[19] *Dept. of Astronomy, Ohio State University, Columbus, OH 43210, USA*
[20] *Dept. of Physics, TU Dortmund University, D-44221 Dortmund, Germany*
[21] *Dept. of Physics, University of Alberta, Edmonton, Alberta, Canada T6G 2G7*
[22] *Dept. of Physics and Astronomy, University of Gent, B-9000 Gent, Belgium*
[23] *Max-Planck-Institut für Kernphysik, D-69177 Heidelberg, Germany*
[24] *Dept. of Physics and Astronomy, University of California, Irvine, CA 92697, USA*
[25] *Laboratory for High Energy Physics, École Polytechnique Fédérale, CH-1015 Lausanne, Switzerland*
[26] *Dept. of Physics and Astronomy, University of Kansas, Lawrence, KS 66045, USA*
[27] *Dept. of Astronomy, University of Wisconsin, Madison, WI 53706, USA*
[28] *Dept. of Physics, University of Wisconsin, Madison, WI 53706, USA*
[29] *Institute of Physics, University of Mainz, Staudinger Weg 7, D-55099 Mainz, Germany*
[30] *Université de Mons, 7000 Mons, Belgium*
[31] *Bartol Research Institute and Department of Physics and Astronomy, University of Delaware, Newark, DE 19716, USA*
[32] *Dept. of Physics, University of Oxford, 1 Keble Road, Oxford OX1 3NP, UK*
[33] *Dept. of Physics, University of Wisconsin, River Falls, WI 54022, USA*
[34] *Oskar Klein Centre and Dept. of Physics, Stockholm University, SE-10691 Stockholm, Sweden*
[35] *Dept. of Astronomy and Astrophysics, Pennsylvania State University, University Park, PA 16802, USA*
[36] *Dept. of Physics, Pennsylvania State University, University Park, PA 16802, USA*
[37] *Dept. of Physics and Astronomy, Uppsala University, Box 516, S-75120 Uppsala, Sweden*
[38] *Dept. of Physics, University of Wuppertal, D-42119 Wuppertal, Germany*
[39] *DESY, D-15735 Zeuthen, Germany*
[a] *now at Dept. of Physics and Astronomy, Rutgers University, Piscataway, NJ 08854, USA*
[b] *now at Physics Department, South Dakota School of Mines and Technology, Rapid City, SD 57701, USA*
[c] *Los Alamos National Laboratory, Los Alamos, NM 87545, USA*
[d] *also Sezione INFN, Dipartimento di Fisica, I-70126, Bari, Italy*
[e] *now at T.U. Munich, 85748 Garching & Friedrich-Alexander Universität Erlangen-Nürnberg, 91058 Erlangen, Germany*
[f] *now at T.U. Munich, 85748 Garching, Germany*
[g] *NASA Goddard Space Flight Center, Greenbelt, MD 20771, USA*

Acknowledgments

We acknowledge the support from the following agencies: U.S. National Science Foundation-Office of Polar Programs, U.S. National Science Foundation-Physics Division, University of Wisconsin Alumni Research Foundation, the Grid Laboratory Of Wisconsin (GLOW) grid infrastructure at the University of Wisconsin - Madison, the Open Science Grid (OSG) grid infrastructure; U.S. Department of Energy, and National Energy Research Scientific Computing Center, the Louisiana Optical Network Initiative (LONI) grid computing resources; National Science and Engineering Research Council of Canada; Swedish Research Council, Swedish Polar Research Secretariat, Swedish National Infrastructure for Computing

(SNIC), and Knut and Alice Wallenberg Foundation, Sweden; German Ministry for Education and Research (BMBF), Deutsche Forschungsgemeinschaft (DFG), Research Department of Plasmas with Complex Interactions (Bochum), Germany; Fund for Scientific Research (FNRS-FWO), FWO Odysseus programme, Flanders Institute to encourage scientific and technological research in industry (IWT), Belgian Federal Science Policy Office (Belspo); University of Oxford, United Kingdom; Marsden Fund, New Zealand; Japan Society for Promotion of Science (JSPS); the Swiss National Science Foundation (SNSF), Switzerland; D. Boersma acknowledges support by the EU Marie Curie IRG Program; A. Groß acknowledges support by the EU Marie Curie OIF Program; J. P. Rodrigues acknowledges support by the Capes Foundation, Ministry of Education of Brazil; A. Schukraft acknowledges the support by the German Telekom Foundation; N. Whitehorn acknowledges support by the NSF Graduate Research Fellowships Program.

32ND INTERNATIONAL COSMIC RAY CONFERENCE, BEIJING 2011

Time-independent searches for astrophysical neutrino sources with the combined data of 40 and 59 strings of IceCube.

THE ICECUBE COLLABORATION[1]
[1]*See special section in this proceedings*

Abstract: We present the results of time-independent searches for astrophysical neutrino sources performed over the whole sky using data collected between April 2008 and May 2010 with the 40-string and 59-string configurations of the IceCube Neutrino Observatory. Muon tracks arriving in the detector from neutrino interactions are reconstructed using the time and charge information detected by an array of photomultiplier tubes (PMTs). In the northern sky, the data sample consists of 14,121 events collected with 40 strings and 43,339 with 59 strings, mostly muons induced by atmospheric neutrinos. In this sky region the search is sensitive to point sources of neutrinos with E^{-2} spectra mainly in the TeV-PeV energy range. In the opposite hemisphere, a much larger background of high-energy atmospheric muons dominate the data set. A zenith dependent energy cut is used to reduce the number of background events. This weakens the sensitivity for point sources with E^{-2} spectra with respect to the upgoing region. The downgoing region is more sensitive to harder-spectrum sources for which the bulk of events can be detected between PeV-EeV energies. An unbinned maximum likelihood ratio test is used to search for astrophysical signals. For the first time it was adapted to combine data from different detector configurations. The combined sensitivity is about a factor ~ 2.5 better than the previous 1-year limit of the 40-string configuration alone. A dedicated search based on a catalog of sources is also presented.

Corresponding authors: J. A. Aguilar[2] *(aguilar@icecube.wisc.edu)*, M. Baker[2], J. Dumm[2], T. Montaruli[2], N. Kurahashi[2]
[2]*Dept. of Physics, University of Wisconsin, Madison, WI 53706, USA*

Keywords: neutrino astronomy; point sources; likelihood method

1 Introduction

The IceCube Neutrino Observatory is a neutrino telescope installed in the deep ice at the geographic South Pole. The final configuration comprises 5,160 photomultiplier tubes (PMTs) [1] along 86 strings instrumented between 1.5–2.5 km in the ice sheet. Its design is optimized for the detection of high energy astrophysical neutrinos with energies above $\sim$ 100 GeV. The observation of cosmic neutrinos will be a direct proof of hadronic particle acceleration and will reveal the origins of cosmic rays (CR) and the possible connection to shock acceleration in Supernova Remnants (SNR), Active Galactic Nuclei (AGN) or Gamma Ray Bursts (GRBs). The IceCube detector uses the Antarctic ice as the detection volume where muon neutrino interactions produce muons that induce Cherenkov light. The light propagates through the transparent medium and can be collected by PMTs housed inside Digital Optical Modules (DOMs). The DOMs are spherical, pressure resistant glass vessels each containing a 25 cm diameter Hamamatsu photomultiplier and its associated electronics. Detector construction finished during the austral summer of 2010-11.

During its construction, the IceCube telescope ran in various configurations. From April 2008 to May 2009, 40 strings of IceCube were operational and collecting scientific data. The data analyzed for that period has provided until now the best sensitivity to high energy neutrino point sources. In this article we describe the analysis of the combined data of the previous 40 strings of IceCube with the 59-string configuration data from May 2009 to May 2010 (see Fig. 1). With the combined information from both data samples we are able for the first time to probe beyond the initial estimates of the 1-year sensitivity of the completed IceCube detector [2].

2 Method

The method used for this analysis is an unbinned maximum likelihood ratio test [4]. This test allows to calculate the significance of an excess of neutrinos above the background for a given direction. The method uses both the reconstructed direction of the events as well as the reconstructed visible muon energy, to discriminate between signal and background [3]. This method improves the sensitivity to astrophysical sources over directional clustering

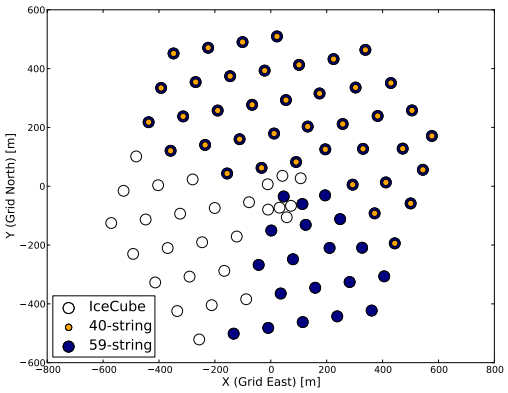

Figure 1: Detector layout. The empty circles represents the string positions that corresponds to the geometry of the whole IceCube detector. The 40-string configuration is represented with the small dots and the 59-string configuration with filled circles.

alone by leveraging the event energies in order to separate hard-spectrum signals from the softer spectra of the atmospheric neutrino or muon backgrounds. For each tested direction in the sky, the number of signal events over background, n_s, and the index of a power law, γ, for the spectrum of the signal events are determined that maximize the likelihood function. The likelihood ratio between the best-fit hypothesis and the null hypothesis ($n_s = 0$) forms the test statistic. The significance of the result is evaluated by performing the analysis on scrambled data sets, randomizing the events in right ascension but keeping all other event properties fixed. Uniform exposure in right ascension is ensured by the daily rotation of the detector with respect to the sky. Events that are close to the polar regions of the sky (declination $< -85^\circ$ or $> 85^\circ$) are excluded from the analysis, since the scrambling in right ascension does not work in these regions.

Two point-source searches are performed. The first is an all-sky search where the maximum likelihood ratio is evaluated for each direction in the sky on a grid of $0.1^\circ \times 0.1^\circ$, much finer than the angular resolution. The significance of any point on the grid is determined by the fraction of scrambled data sets containing at least one grid point with a likelihood ratio higher than the one observed in the data. This fraction is the post-trial p-value for the all-sky search. Because the all-sky search includes a large number of effective trials, the second search is restricted to the directions of *a priori* selected sources of interest. The post-trial p-value for this search is again calculated by performing the same analysis on scrambled data sets.

3 Data selection and Detector Performance

From April 2008 to May 2009, 40 strings of the IceCube detector were operational. The duty cycle at analysis level for that period was $\sim 90\%$ after selecting good runs based on the detector stability and the total livetime was 375.5 days. The event selection for the 40-string configuration data sample is described in detail in Ref. [3]. In the analysis of the data from the 40 strings of IceCube no significant excess over fluctuations of the background was found, and upper limits have been published (see Ref. [3]). Here we report on a combined analysis using the data corresponding to the 40 strings period plus the 59-string configuration data taken from May 2009 to May 2010. The livetime corresponding to the 59-string configuration is 348 days with a similar $\sim 90\%$ duty cycle at final analysis level as in the previous year.

The trigger rate of the 59-string configuration is of the order of 1.5 kHz for events based on a simple multiplicity trigger requiring 8 triggered DOMs. This trigger rate is strongly dominated by the muon background produced in cosmic rays interactions in the atmosphere. A first level of background rejection of poorly reconstructed up-going events and a selection of high energy muons for the southern sky is done on-site at the South Pole (Level 1 filter). The data sent through the satellite to the North undergo further processing that includes a broader range of more CPU consuming likelihood-based reconstructions at the so-called Level 2 and Level 3 filters. This offline processing also provides useful parameters for background rejection and measurements of the energy and of the angular uncertainty. The data rate at Level 3 is of the order of 3 Hz and still dominated by atmospheric muons. Because the northern sky and the southern sky present very different challenges, two separate techniques for background rejection are used for each hemisphere.

In the northern sky the 59-string configuration event selection was performed using a multi-variate classification algorithm. Boosted Decision Trees (BDTs) were used in the final analysis step to classify events as signal-like or background-like. Twelve event observables, split in two sets of 8 and 4 respectively, were selected by choosing variables with low correlation for a background dominated dataset (correlation coefficient $|c| < 0.5$), but high discriminating power between signal and background. Training was done using a subsample of the data as the background and simulated neutrino events as signal. We trained two sets of BDTs, one with a neutrino spectrum of E^{-2}, and one with a neutrino spectrum of $E^{-2.7}$ in order to account for softer neutrino spectra and possible TeV cut-offs in the expected neutrino emission. The usage of data as the background sample for training is an important aspect since it makes the analysis independent of the systematic uncertainties of the simulation of the muon background. The combination of the two BDT scores for both the softer neutrino spectrum and the standard E^{-2} is used as a selection criterion and the cut that optimizes the discovery potential

for neutrino point sources over a wide energy range is chosen.

The southern sky is filtered by using energy estimators to separate the large amount of down-going atmospheric muons from a hypothetical neutrino signal with a harder spectrum. For vertically down-going events with zenith angles between 0 and 50 degrees, we take advantage of the IceTop detector in order to reject atmospheric muons originating from a shower that produces a signal in at least two of the PMTs of the IceTop detector. This IceTop veto allows us to reject background with $\sim$ 99% efficiency in the very vertical zenith angles without losing signal neutrino efficiency ($<$ 1 %).

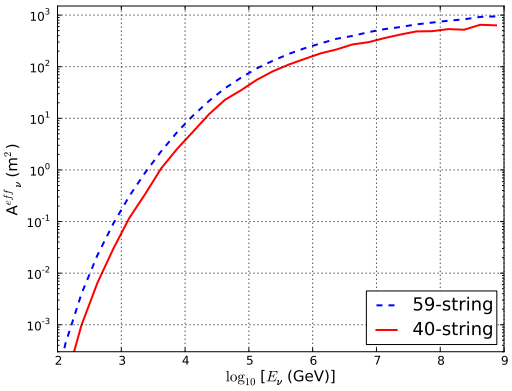

Figure 2: Solid angle averaged neutrino effective area in the northern sky for the 59-string IceCube configuration (dotted line) and the 40-string configuration (solid line) for an equal ratio of ν_μ and $\bar{\nu}_\mu$ as a function of the true neutrino energy.

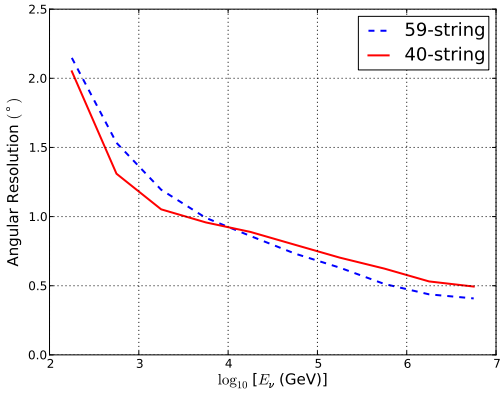

Figure 3: Nuetrino angular resolution as a function the true neutrino energy for the 59-string IceCube configuration and the 40-string configuration.

The final data sample for the 59-string configuration has a total number of 107,569 events, among them almost 2/3 come from the southern sky and the rest from the up-going region. The estimated atmospheric muon contamination in the northern sky is $\sim$5 %. The solid angle averaged neutrino effective area for both detector configurations in the northern sky is shown in Fig. 2 as a function of the true neutrino energy. The overall increase in neutrino effective area in the up-going region of the 59-string configuration with respect to the previous IceCube configuration of 40 strings is a factor of $\sim$ 1.3 for energies $>$ 1 TeV and up to a factor of 2 at lower energies due to the event selection based on BDTs trained with softer neutrino spectra. Fig. 3 shows the angular resolution defined as the median of the point spread function (PSF) as a function of the true neutrino energy. The PSF is defined as the angle between the reconstructed muon track and the true neutrino direction. The BDT used in the 59-string configuration allows more low energy signal events to pass the event selection with worse angular resolution, that explains why the median distribution is worse compared to the 40-string configuration at energies below 10 TeV.

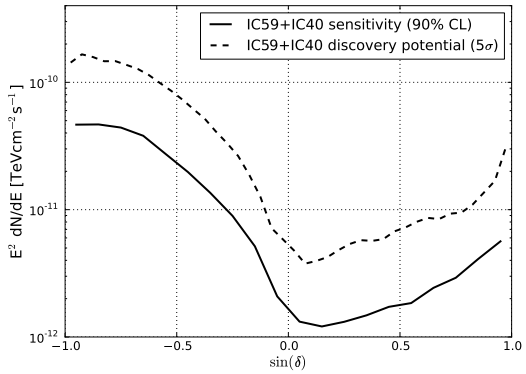

Figure 4: Expected sensitivity (solid line) for 90 % C.L. using the classical (frequentist) construction of upper limits, and discovery potential defined as the minimum flux required to have a 50% probability to claim a discovery of a point-source with a E^{-2} neutrino spectrum with confidence level equivalent to 5σ, (dotted line), for the combined analysis using the 40-string and 59-string configuration data. Both lines are shown as a function of the declination.

The expected sensitivity for the 2 years (375 + 348 days) of combined data and the discovery potential is shown in Fig. 4 as a function of declination for a E^{-2} neutrino spectrum. The overall improvement with respect to the 40-string configuration sensitivity is about a factor of $\sim$ 2.5 making it comparable to the projected 1-year sensitivity of the completed IceCube detector.

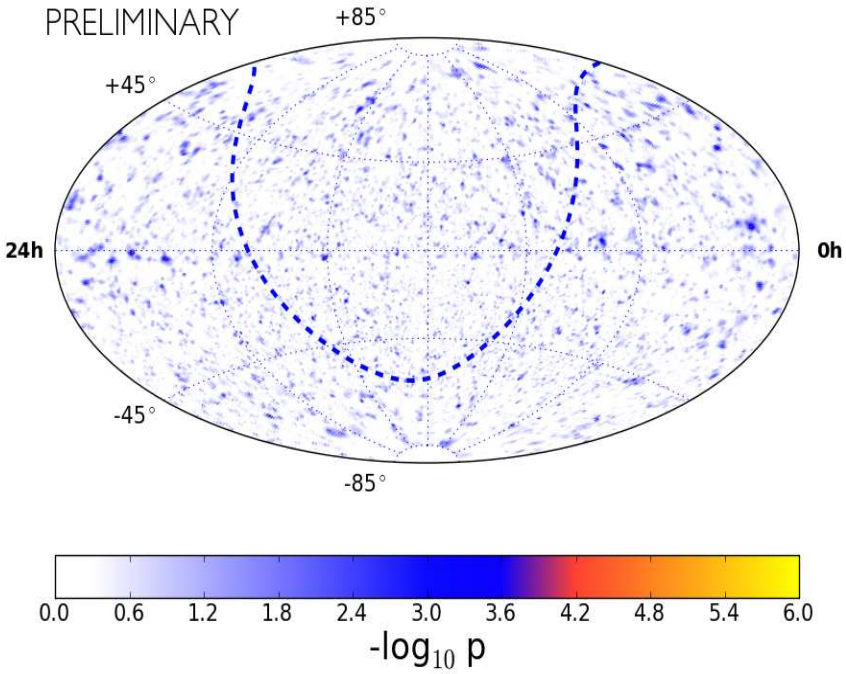

Figure 5: Significance skymap in equatorial coordinates (J2000) of the all-sky point source scan. The dotted line indicates the galactic plane.

4 Results

The results of the all-sky scan are shown in the preliminary pre-trial significance map in Fig. 5. The most significant deviation from background is located at 75.45° r.a. and $-18.15°$ dec. The best-fit parameters for this location are $\hat{n}_S$ = 18 and $\hat{\gamma}$ = 3.9. The pre-trial p-value is 2.23×10^{-5} which corresponds to a post-trial p-value of 67% calculated as the fraction of scrambled sky maps with at least one source with an equal or higher significance. The most significant source from the *a priori* source list is PKS 1454-354 with a pre-trial estimated p-value of 14%. The equivalent post-trial p-value was calculated as well using scrambled sky maps and correspond to a value of $\sim$ 95%. The 90% CL upper limits for both searches will be provided as the systematic uncertainties are evaluated and incorporated in the Feldman & Cousins confidence belt construction.

5 Conclusions

Between April 2008 and May 2009 the IceCube detector recorded 375 days of data with 40 instrumented strings. The analysis included 36,900 events in the whole sky where no evidence for a signal was found. The 40-string configuration analysis provided the best flux upper limits on point sources of astrophysical neutrinos up to now. Here we presented an analysis of a combined data sample in 40-string and 59-string configurations of IceCube. The sensitivity of this analysis is already beyond the initial estimates of the expected sensitivity of 1 year of the IceCube detector. Two searches were performed; an all-sky scan and a search on specific locations based on *a priori* list of candidate sources. In both cases no significant excess was found.

References

[1] R. Abbasi *et al.* [IceCube Coll.], Nucl. Inst. Meth. A, 2010, **618**: 139.
[2] J. Ahrens *et al.* [IceCube Coll.], Astropart. Phys., 2004, **20**: 507-532.
[3] R. Abbasi *et al.* [IceCube Coll.], Astrop. J., 2011, **732**: 18.
[4] J. Braun *et al.* , Astropart. Phys., 2010, **33**: 175.

32ND INTERNATIONAL COSMIC RAY CONFERENCE, BEIJING 2011

Searches for Time-Variable Neutrino Point Sources with the IceCube Observatory

THE ICECUBE COLLABORATION[1]
[1]*See special section of these proceedings.*

Abstract: We present searches for time-dependent emissions of neutrinos in the entire sky using the data collected between April 2008 and May 2010 with 40 and 59 strings of IceCube. An all-sky search is performed searching for any clustering of events in space and time. In the northern sky the sample is mainly atmospheric neutrinos, while in the southern sky the sample is dominated by atmospheric muons. In order to reduce the penalty of trials we also perform a search based on flares of AGNs observed by other experiments, using lightcurve information from bands where comprehensive coverage is available. Results from the 40-string detector are presented in this paper, while those from the 59 string detector will be presented at the conference.

Corresponding authors: M. Baker[2] (*mfbaker@icecube.wisc.edu*), J.A. Aguilar[2], J. Dumm[2], N. Kurahashi[2], T. Montaruli[2]
[2]*Dept. of Physics, University of Wisconsin, Madison, WI 53706, USA*

Keywords: neutrino astronomy, AGN, multi-wavelength astronomy

1 Introduction

The IceCube Neutrino Observatory is a kilometer-scale detector located at the geographic South Pole. Beneath the glacial surface, IceCube is composed of 5160 optical modules (DOMs) deployed on 86 vertical strings between 1450 and 2450 m to detect and reconstruct high energy neutrino-induced charged leptons. The main science goal of the IceCube experiment is the detection of astrophysical neutrino sources, which will help identify the origins of the highest energy cosmic rays.

Muons passing through the detector emit Čerenkov light allowing reconstruction with median angular resolution of less than 1° for > 10 TeV energy muons in the 40 and 59-string configurations.

Time-dependent analyses aim to reduce the background of atmospheric neutrinos and muons by searching over smaller time scales around a period of interest. The searches discussed in this paper are about a factor of four more powerful than time-integrated searches for flares with duration $\leq$ 100 s. In this paper we describe the addition of a time dependent term to the standard searches for steady emission of neutrinos presented in [1] [2]. We apply this term in searches for neutrino emission from an all-sky generic time-dependent search and from a catalogue of sources with photon flares occurring when IceCube was taking data in its 40 and 59-string configurations.

2 Time Dependent Point Source Searches

An unbinned maximum likelihood ratio method which models the data as a mixture of signal and background has been used for the search for point sources of neutrinos in IceCube [3]. We use the angular and energy distribution of events as information to characterize the signal with respect to the background. Astrophysical sources of neutrinos will cluster near the object and are expected to have a power-law energy spectrum harder than that measured of the atmospheric backgrounds [4]. An energy estimator is used based on the photon density along each reconstructed muon track. The atmospheric background has a roughly constant rate in time, but sources such as Active Galactic Nuclei exhibit significant variability in photon flux states, allowing for tests aimed at additional background rejection. The analysis returns a best-fit number of signal events and spectral index, as well as other free parameters from the time-dependent terms.

The IceCube 40-string data at analysis level consists of 36,900 selected events, 14,121 are upward-going neutrino candidate events and 22,779 are downward-going, mainly PeV energy muons from atmospheric air showers [1]. The 59-string data at analysis level consists of 107,569 selected events, 43,339 of which are upward-going neutrino candidates, and 64,230 are in the downward-going region [2]. The data used in this analysis were collected over 724 days of livetime between April 5, 2008 and May 31, 2010, cor-

responding to 92% of all data taken during that period. Selection cuts for the final sample are based on the quality of the reconstruction, such as the angular uncertainty of the track reconstruction, and on other variables such as the number of DOMs hit by the direct Čerenkov light produced by muons. These variables help reject misreconstructed events.

The signal probability distribution function (pdf) is:

$$S_i = S_i^{space}(\mid \vec{x}_i - \vec{x}_s \mid, \sigma_i) S_i^{energy}(E_i, \theta_i, \gamma_s) S_i^{time} \quad , \tag{1}$$

where σ_i is the reconstructed angular uncertainty of the event [5], $\mid \vec{x}_i - \vec{x}_s \mid$ the angular separation between the reconstructed event and the source, $S_i^{energy}(E_i, \theta_i, \gamma_s)$ is the energy pdf with the event energy E_i, zenith angle θ_i, and spectral index γ_s, which is built in 22 zenith bands to account for declination dependence of the background. S_i^{time} is the time pdf of the event. The background pdf is given by:

$$B_i = B_i^{space}(\theta_i, \phi_i) B_i^{energy}(E_i, \theta_i) B_i^{time}(t_i), \tag{2}$$

where $B_i^{space}(\theta_i, \phi_i)$ is the background event density (a function of the azimuth ϕ_i and zenith θ_i of the event), $B_i^{energy}(E_i, \theta_i)$ is the zenith-dependent energy distribution of the background, and $B_i^{time}(t_i)$ the inverse of the live-time, reflecting the fact that the probability density functions are normalized to one and the background rate is essentially flat in time. The background pdf is determined using the data, and the final p-value for each analysis is obtained by comparing equivalent experiments scrambled in time and right ascension to actually observed data.

3 All-Sky Time Scan

We perform a scan for any significant excess with respect to background over all time scales (from sub-seconds to a full year) over the entire sky. Since this analysis finds events clustered in time, independent scans are performed using the 40-string (April 5, 2008 to May 20, 2009) and 59-string (May 20, 2009 to May 31, 2010) samples. For flares shorter than $\sim$100 days, this provides a better discovery potential for the time-dependent hypothesis than a time-integrated analysis. In principle short bursts can be discovered at a 5σ threshold with only two events if they occur near enough in time. An advantage of an untriggered search such as this is the ability to probe all emission scenarios, including neutrino emission without any observed counterpart in the electromagnetic spectrum.

This analysis method was developed and tested using a simulation of a generic km^3 neutrino detector in [6], and has been adapted for use with a detector with non-uniform acceptance in zenith and azimuth and dead time [7]. The time-dependent probability density function for this search is a Gaussian function, with its mean and width as free parameters, returning the most significant flare from a particular direction. The method is applied as an all-sky scan over a 0.5°x 0.5° grid (smaller than the typical event angular uncertainty) in right ascension and declination, scanning for flares of all durations from 20 μs (the minimum time separation between events) to 150 days. The final result is the set of best fit parameters from the location with the strongest deviation from background.

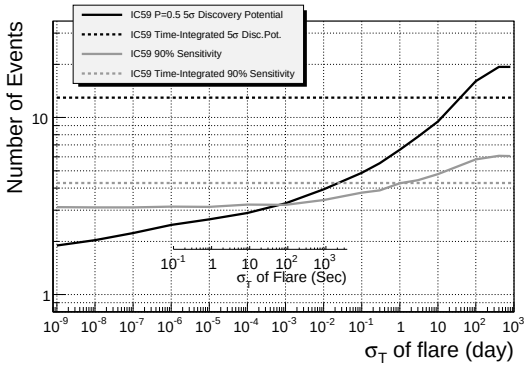

Figure 1: The 50% 5σ discovery potential and 90% sensitivity in terms of the mean number of events for a fixed source at $+16^o$ declination with the 59-string detector. The number of events for the sensitivity and discovery potential for the time-independent search are also shown. Flares with a σ_T of less than 40 days, or a FWHM of less than roughly 100 days during the 59-string data taking period, have a better discovery potential than the steady search.

3.1 40-String Results

Using the 40-string data, the location which deviates most from background is found at (RA,Dec)=(254.75°, +36.25°), and is presented in [7]. Two events are found (2.0° apart in space and 22 seconds in time), with a best-fit spectrum γ of 2.15 (with uncertainty of $\pm$0.4), mean of the flare T_o of MJD 54874.703125 and width σ_T of 15 seconds. A clustering of greater significance is seen in 56% of scrambled skymaps, which is consistent with a fluctuation of the background. The result of the scan with 59-strings data will be presented at the conference.

4 Triggered Search for Flares

When there is specific timing information about the photon activity of an astronomical object, that information can be used to reduce the background. For triggered sources, the focus is on objects such as blazars, which exhibit variability on timescales of hours to weeks. When flares are seen with comprehensive coverage, flux measurements are made on a regular basis and this continuous lightcurve can be used to define the activity at any point in time as low to high. This improves the ability to define periods of high flux state with a clear beginning and end. The assumption is that photon and neutrino emissions experience heightened states simultaneously. This analysis utilizes 1-day binned

lightcurves from the Fermi LAT. Results for 40-string data are presented in [7], while at the conference results including the 59 string period will be shown.

4.1 Method and Expected Performance

Sources for this search were selected considering alerts during the 40 and 59-string data taking periods for sources in outburst $> 1.5 \times 10^{-6}$ photons/s/cm^2. Sources with flares in the 40-string period (April 5, 2008 to May 20, 2009) are listed in table 1. A Maximum Likelihood Block (MLB) algorithm [8][9] is used to de-noise the lightcurves by iterating over the data points to select periods from the lightcurves which are consistent with a constant flux, taking statistical errors into account. The hypothesis is that the neutrino emission follows the lightcurve, but only when the photon flux goes above a certain threshold F_{th}. By looking only at these high states the atmospheric background is largely reduced. The value of F_{th} is used as a free parameter, finding the value of the threshold which maximizes the significance of the data. This method is designed to avoid any penalty from making an incorrect *a priori* choice on a flaring threshold, which is larger than the effect of one additional degree of freedom.

$F(t_i)$ is defined as the value of the denoised light curve at t_i and F_{th} is the flux threshold below which no neutrino emission is assumed (i.e. S_i^{time}=0 if $F(t_i) \leq F_{th}$). In the case of $F(t_i) \geq F_{th}$, the probability of neutrino emission is assumed to be proportional to the flux level above that threshold:

$$S_i^{time} = \frac{(F(t_i) - F_{th})}{N_f}; \quad (3)$$

where the normalization factor N_f is the integral of the denoised light curve above the threshold. Allowing a lead or lag of up to 50 days was also tested. This resulted in a markedly higher number of events for discovery, so we constrained the neutrinos to come within $\pm$ 1 day of the photons.

4.2 Results

The results from all sources tested during the 40-string data-taking are listed in table 1. The most significant source from the 40-string data-taking period is PKS 1502+106, which has a pre-trial p-value of 5%. With the method, we find one high-energy event during the August 2008 flare. The post-trial p-value is 29%, which is compatible with background fluctuations. Results extending the lightcurves and adding the 59-strings data will be presented at the conference.

Source	pre-trial p-value	Threshold (10^{-6} cm^{-2} s^{-1})	Duration above threshold (days)
PKS 1510-089	—	0	282
3C 66A/B	0.47	0.675	57
3C 454.3	0.20	9.47	2.5
PKS 1454-354	—	0	282
3C 279	0.47	2.34	6
PKS 0454-234	—	0	282
PKS 1502+106	0.049	3.13	8
J123939+044409	—	0	282

Table 1: Sources tested with the 40 string data and pre-trial p-values for the flare search with continuous lightcurves. In the event of an underfluctuation no p-value is calculated. The overlap between the Fermi public release data and the 40-string data taking period is 282 days, that being the maximum duration of the lightcurve above F_{th}.

5 Conclusion

We have analyzed data from the IceCube observatory from the season 2008-9 when the detector consisted of 40 strings. The all-sky scan over all directions finds that the most significant cluster of events is separated in time by 22 s and in space by 2° and has a trial-corrected p-value of 56%. The most significant observation of a flare from catalogues compiled using Fermi-LAT and IACT alerts during the 40-string configuration data taking is PKS 1502+106, with a p-value of 29% after trials. The results of time-dependent searches including the IceCube 59-string data will be presented at the conference.

References

[1] Abbasi, et al. ApJ **732** 2011 18.
[2] IceCube Collaboration, paper 909, These proceedings.
[3] Braun, J. et al. Astropart. Phys. **29**, 2008 299.
[4] Abbasi et al. Phys. Rev. D, **83** 2011 012001.
[5] T. Neunhöffer, Astropart. Phys. **25** 2006 220.
[6] Braun, J. et al. Astropart. Phys. **33** 2010 175.
[7] Abbasi, et al. arXiv:1104.0075
[8] Scargle, J. ApJ **504** 1998 405.
[9] Resconi, E. et al. A&A **502** 2009 499.

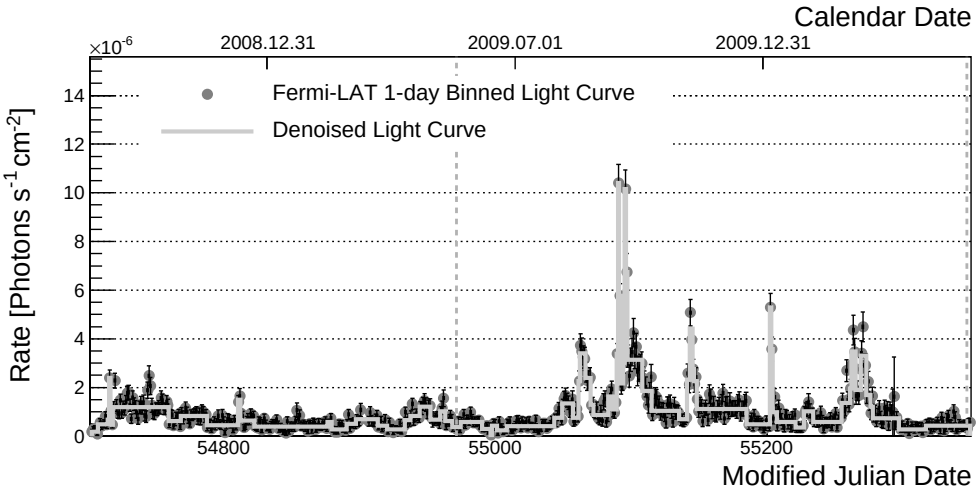

Figure 2: An example of the one-day binned Fermi lightcurve (gray points, with statistical errors) and denoised lightcurve (light gray solid line) for the blazar 3C273. The lightcurve begins here when Fermi science operations began, the time axis continues until the end of the 59-string data taking period.

Search for astrophysical neutrinos from extended and stacked sources with IceCube

THE ICECUBE COLLABORATION[1]
[1]*See special section in these proceedings*

Abstract: The combined data of IceCube's 40-string and 59-string configurations spanning over 700 days are used to search for astrophysical neutrinos originating from sources listed in several catalogs. A stacking method which stacks sources and searches for an integrated signal above the estimated background is employed. Very large scale sources such as neutrino emission from the galactic plane and the Fermi bubble region are also used as extended source hypotheses. To perform these searches, a likelihood method that tests the presence of signal using the shape of such sources, their energy spectra and the angular distribution of events is employed.

Corresponding authors N. Kurahashi[2] (*naoko@icecube.wisc.edu*), J.A. Aguilar[2], M. Baker[2], J. Dumm[2], T. Montaruli[2]
[2]*Dept. of Physics, University of Wisconsin, Madison, WI 53706, USA*

Keywords: Astrophysical neutrinos, Fermi bubbles, galactic plane

1 Introduction

A search for astrophysical neutrinos originating in galactic and extragalactic sources using a likelihood (LH) method extensively described in [1, 2] has been performed recently on IceCube data and is reported in [3]. This method uses energy and directional information that distinguish the softer backgrounds of atmospheric muons and neutrinos from the harder astrophysical neutrinos. Such neutrinos, yet to be observed, could originate in jets and shocks via Fermi acceleration. The background is estimated by scrambling real events in their arrival times (or right ascensions) in the LH method. In this way, the p-value (the fraction of randomized data sets with higher test-statistic values than the real data) comes only from data and has no dependency on the accuracy of the simulation [1]. While Ref. [3] is focused on the LH search for steady emissions from point sources from the whole sky and from selected sources of interest, the work reported in [4] and [5] is focused on extending the likelihood method by utilizing time dependence of emissions (GRBs and AGN flares). The work presented here extends the LH method to the stacking of sources belonging to the same source class and to very extended sources that cover a large fraction of the sky. In this work, as in [1, 3], the median sensitivity and upper limits at a 90% confidence level (CL) are calculated according to teh classical (frequentist) construction of upper limits (Neyman 1937). The discovery potential is the flux required for 50% of trials with simulated signal to yield a p-value less than 2.87×10^{-7} (i.e. 5σ significance if expressed as the one-sided tail of a Gaussian distribution) unless stated otherwise.

The data sample and its selection is described in [3]. For the first time the LH method has been adapted to combine data belonging to different configurations. We combine the data sample collected for 375.5 d in the 40-string configuration of IceCube during the period from 2008 April 5 to 2009 May 20 [1] and data collected during the 59-string configuration for 348.1 d from May 20, 2009 to May 30, 2010 [3]. The total data sample consists of 43,339 (64,230) events with 59 strings in the upgoing (downgoing) hemisphere and 14,121 (22,779) for 40 strings. Hence the total number of events on which this search is performed in the whole sky is 144,469. As shown in [3], depending on the declination the sensitivity of the 40+59-string sample with respect to the 40-string sample published in [1] improves by about a factor of 2.5. A factor of about 4 is achieved in the downgoing vertical region where use of the IceTop detector as a veto for muons leads to a more significant improvement [3]. It is to be noted that the search for astrophysical sources in IceCube extends to the entire sky but the sensitivity is different in the upgoing (Northern sky) and in the downgoing (Southern sky) regions. As a matter of fact, as explained in [1], the upgoing region is dominated by atmospheric neutrinos since muons are filtered by the Earth, while we select high energy muons in the downgoing region since we look for a clustering of astrophysical events characterized by a harder spectrum than atmospheric events.

All searches shown in this proceeding will be unblinded by the time of the conference, hence here we indicate preliminary sensitivities. P-values and corresponding fluxes will be given at the conference.

2 Stacking searches

Stacking multiple sources in neutrino astronomy can enhance discovery potential and further constrain astrophysical models for uniform populations of sources. The stacking method is described in detail in [1] where it is explained how the signal and background are integrated over a set of sources using the same weight for all sources or a weighting scheme from models for specific tests. As shown in [1], the fractional flux needed for discovery for stacked sources compared to single sources at 5σ CL is very close to the inverse of number of stacked sources. The stacking searches we perform were also performed in [1] on the 40-string sample with the exception of one catalog. We perform:

1. A stacking search for 17 Milagro TeV gamma ray sources, 9 of which have been reported as high significance-detections and another 8 which are lower in significance but also confirmed by Fermi[6, 7]. The sources include supernova remnants, pulsars, pulsar wind nebulae, and one unconfirmed hot-spot;

2. It was noticed with an *a posteriori* search [1], that some of the 6 supernova remnants (SNR) observed by Milagro at energies $> 1TeV$ and considered in [8] as interesting potential neutrino emitters are the most significant in the previous list above. When these 6 sources are analyzed as a single sub-group, an a posteriori p-value of 0.02 was found with best fit parameters n_s = number of signal events = 15.2 and γ = spectral index = 2.9. The true trial factor is incalculable from this search with 40 strings since this was done after unblinding. Hence we perform a search for these 6 sources using only the sample of 59-strings in order not to bias the final result;

3. a stacking search for 127 local starburst galaxies [9];

4. a stacking search for five nearby galaxy clusters (GCs), testing four different models for the CR spatial distribution [10]. The GCs we considered are Virgo, Centaurus, Perseus, Coma and Ophiuchus. The parameterization of the models, taken from [10] and described in detail in [1], consider scenarios where CRs are uniformly distributed within the cluster shock radius or the virial radius (Models A and B respectively), an Isobaric Model in which CRs follow the distribution of thermal gas, and a Central AGN Model in which CRs are accelerated in a central AGN. This last case is treated as a point source while other models include the extension of sources in the LH.

5. a stacking search of ultra-high energy cosmic rays (UHECRs) assuming the sources of these UHECRs are also neutrino sources. We include UHECRs observed by the Auger Observatory [11] and the HiReS [12] collaboration.

The UHECR search presented here looks for neutrinos originating from the same direction as observed UHECRs. However, for this search, we fit for the 'extension' of the sources in maximizing the LH. The 'extension' of the sources here represent the possible deflection of the UHECR from their sources which depends on the UHECRs energy and the distance and magnetic field strength they propagate through. The observation of a correlation between UHECR and neutrinos is only possible in proton dominated scenarios since heavy elements would be deflected too much by magnetic fields. This search fits for an average deflection of all events stacked. The average can still be insightful given the similar energies of the UHECRs. Furthermore, the width of a Gaussian centered at the UHECR directions is used as the fit variable, accounting for the possible event-by-event directional variation between the UHECRs and neutrinos. This search, like all other LH searches performed, incorporates the neutrino event point spread function of the IceCube detector as well. After fitting for the 'extension' of sources, we test a model describing the deflections of UHECRs in extragalactic magnetic fields [13] and constrain the degenerate parameter space of distance and B-field intensity assuming that UHECRs are protons. The Auger sample contains 69 events with reconstructed energy above 55 EeV [11] with angular resolution better than 0.9° for events that trigger more than 6 stations, and the HiRes sample contains 13 events [12] in the same energy range with angular resolution of 0.8° in stereo mode. The energy scale for these events is known at the level of 20%. In order to reduce the galactic magnetic field contribution, expected to be larger than the intergalactic one, UHECR events that cross the galactic plane are removed so the fitted extension represents the intergalactic magnetic deflection alone.

The sensitivities for these searches are shown in Tab. 1.

3 The Galactic plane

Neutrinos and photons are expected to be produced in the galactic plane via interaction of cosmic rays with the interstellar medium (ISM). Diffused cosmic rays are confined for million years in the galaxy and their spectrum is hence expected to approach $E^{-2.7}$ with a composition that becomes heavier above the knee at a few PeVs. The low density of the ISM allows secondary mesons to decay before reaching their interaction length, thus preserving the cosmic ray spectrum in their decay products and also fixing the ratio of neutrinos to photons. The Milagro collaboration have reported observation of TeV gamma-rays from the galactic plane [19], showing good agreement with the GALPROP model. The GALPROP code propagates cos-

Catalog	Data sample	Fit par.	Sensitivity	Disc. Pot.
Milagro 17	I+II	γ+n_s	0.28 $\times$ $E2$	1.05 $\times E2$
Milagro 6	II	γ+n_s	0.66 $\times$ FM	3.20 $\times FM$
Starbursts 127	I+II	γ+n_s	0.96 $\times$ $E2$	3.44 $\times E2$
GC - Model A	I+II	γ+n_s	1.39 $\times$ FM	4.85 $\times FM$
GC - Model B	I+II	γ+n_s	2.58 $\times$ FM	8.98 $\times FM$
GC - Isobaric	I+II	γ+n_s	1.26 $\times$ FM	4.84 $\times FM$
GC - AGN	I+II	γ+n_s	0.63 $\times$ FM	2.36 $\times FM$
UHECR	I+II	γ+σ+n_s	4.01 $\times$ $E2$	12.8 $\times E2^*$

Table 1: Median sensitivities of the stacking searches (90% CL) and the discovery potentials (p-value $< 2.87 \times 10^{-7}$) given as a sum of flux required from the sources in each catalog. Data sample I (II) represents data taken with the 40-string (59-string) configuration. Fit parameters are the spectral index γ, the extension of the sources σ, and the number of signal events n_s. $E2$ indicate units of E^2dN/dE [10^{-11} TeV cm^{-2} s^{-1}], while FM indicates the scaling to the predicted flux profile. *For UHECR, p-value $< 1.35 \times 10^{-3}$ (3σ significance of one-sided Gaussian) is used for discovery potential calculation.

mic rays in the galaxy with assumptions of the distribution of cosmic ray sources [15]. The Fermi telescope has prodcued a detailed map of the observed gamma-ray emission from the galactic plane region [17]. The GALPROP code and a fit for the cosmic ray flux are then used to separate the contribution from neutral pion decays, which the neutrino emission map should closely follow. We use this Fermi model of the relative flux of pion decays as the spacial template in the LH analysis for neutrinos from the galactic plane. Fig. 1 shows the relative neutrino signal strength expected in the 59-string IceCube configuration assuming a source emission pattern of the Fermi model. The strongest emission is expected near the galactic center and extends along the plane. However, because the center belongs to the Southern (downgoing) hemisphere, the signal strength is expected to be highest at the closest region on the plane to the galactic center that belongs to the Northern (upgoing) hemisphere, due to IceCube's background and event selection as described in the Introduction section. The LH analysis will combine data from both the 40 and 59-string configurations. One noteworthy issue is that while the Fermi model used here provides a relative flux expected from different regions of the sky, it does not provide the absolute scale of the predicted flux. Therefore, a detailed calculation of the neutrino flux must be made, or older flux predictions [16] must be used to translate event counts in IceCube into fluxes. The flux calculations of [16] predict 21 neutrino events in the combined 40-string and 59-string data.

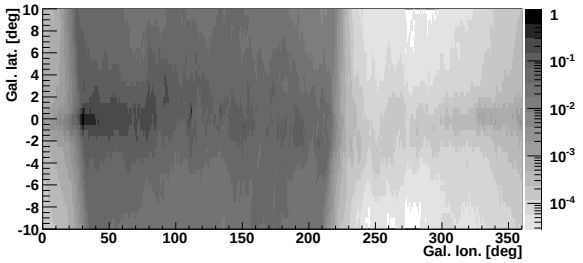

Figure 1: Relative signal strength from different parts of the sky expected from the galactic plane to be seen with the 59-string IceCube detector, plotted in galactic coordinates *(preliminary)*. The center belongs in the Southern (downgoing) hemisphere, so the signal strength is highest at the closest region on the plane to the galactic center that belongs to the Northern (upgoing) hemisphere as expected.

4 The Fermi Bubbles

Recently evidence has emerged of enormous features in the γ-ray sky observed by the Fermi-LAT instrument: bilateral "bubbles" of emission centered on the core of the Galaxy and extending to around 10 kpc from the Galactic plane. These structures are coincident with a nonthermal microwave "haze"' and an extended region of X-ray emission [18]. The bubbles γ-ray emission is characterized by a hard and relatively uniform spectrum, relatively uniform intensity, and an overall luminosity of $\sim 4 \times 10^{37}$ erg/s. The γ-ray luminosity between 1-100 GeV is measured to be around an order of magnitude larger than the microwave luminosity and more than an order of magnitude lower than the X-ray luminosity. In [20] the bubbles are explained as due to a population of relic cosmic ray protons and heavier ions in the energy range of $10 - 1000$ GeV trapped for timescales of about 10^{10} yrs undergoing pp collisions on the bubbles low density plasma that produce secondaries which in turn produce γ-rays and neutrinos. Accounting for ionization losses by sub-relativistic protons and adiabatic energy losses at all energies, bubble protons lose a total of about 10^{39} erg/s in steady state, precisely accounting for the CR power injected at the galactic center. This is compatible with observations in γ-rays around the galactic center by Fermi and at higher energies by HESS [20]. While in the galactic plane diffusive confinement of the CRs leads to a steepening of the steady-state spectrum to $\propto E^{-2.7}$, in the bubbles there is no energy-dependent confinement effect. So, given the almost energy-independent

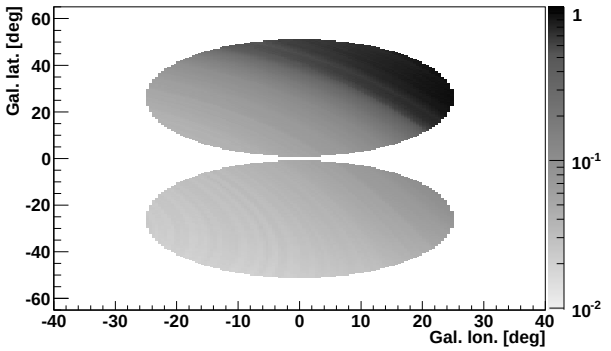

Figure 2: Relative signal strength expected from Fermi bubbles with the 59-string IceCube detector, plotted in galactic coordinates *(preliminary)*. Most of the signal is expected from the corner of the bubble that is in the Northern (upgoing) hemisphere when transformed to equatorial coordinates.

pp loss time, the observed spectrum of the CRs is as at the injection at their acceleration sites (evidently $\propto E^{-2.1}$) mirrored by the bubble $\gamma-$ rays. If the bubbles are a reservoir of CRs it is possible to think that the primary spectra reach energies above the knee and with a very hard neutrino spectrum. This makes these sources extremely interesting for neutrino telescopes.

The bubbles are parameterized as circular regions of 25° radii emitting a uniform flux of neutrinos per steradian. In Fig. 2, the relative signal strength expected from each region is simulated using the 59-string configuration of the IceCube detector. As expected, a part of one bubble that dips below the horizon in equatorial coordinates as seen by IceCube (upgoing hemisphere) has the largest expected signal. Thus the exact sensitivity of IceCube to the Fermi bubbles depends on the characterization of the shape of the bubbles. However, despite the extensive shape-fittings of the gamma emission performed in [18], due to the intrinsic haziness of the structure, the dependence on the fitting of other emission mechanisms contributing to the observed gamma-ray structure, and the unknown energy dependence of the shape at the high-energy region of our interest, we conclude that using a simple model of two circular neutrino-emission regions is adequate for an initial LH analysis. The LH analysis will combine data from both the 40 and 59-string configurations. Using this circular parameterization and assuming a continuous flux of $3.5 \times E^2 dN/dE$ [10^{-10} TeV cm^{-2} s^{-1}], motivated by an optimistic gamma-ray flux calculation [20], 164 events are expected in the combined 40 and 59-string configuration of IceCube.

References

[1] R. Abbasi *et al.*, 2011, Astrop. J. **732**:18.

[2] J. Braun *et al.*, 2008, Astropart. Phys. **29**: 299.

[3] IceCube Collaboration, 0909, these proceedings.

[4] IceCube Collaboration, 0784, these proceedings.

[5] IceCube Collaboration, 0289, these proceedings.

[6] A. A. Abdo *et al.*, 2009, Astrop. J. **700**: L127-L131.

[7] A. A. Abdo *et al.*, 2007, Astrophys. J. **664**L91.

[8] F. Halzen, A. Kappes & A. OMurchadha, 2008, Phys. Rev. **D78**: 063004.

[9] J. K. Becker, P. L. Biermann, J. Dreyer & T. M. Kneiske, 2009, arXiv:0901.1775.

[10] K. Murase, S. Inoue & S. Nagataki, 2008, Astrop. J. Letters **689**: L105.

[11] P. Abreu *et al.*, 2010, Astrop. Phys. **34**: 314.

[12] R. Abbasi *et al*, 2008, Astrop. Phys. **30**: 175.

[13] F. A. Aharonian, S. R. Kelner, A. Y. Prosekin, 2010, Phys. Rev. **D82**:043002.

[14] S. Hoover *et al.*, arXiv:1005.0035.

[15] Moskalenko *et al.*, `http://galprop.stanford.edu`, 2010.

[16] G. Ingelman & M. Thunman, 1996, Phys. Rev. D **54**: 4385

[17] Fermi-LAT Collaboration, `http://fermi.gsfc.nasa.gov/ssc/data/access/lat/BackgroundModels.html`, 2010.

[18] D. P. Finkbeiner, 2004, Astrop. J. **614**: 186; M. Su, T. R. Slatyer, & D. P. Finkbeiner, 2010, Astrop. J. **724**: 1044.

[19] A. A. Abdo *et al.*, 2008, Atrophys. J. **688:** 1078.

[20] R. M. Crocker & F. Aharoanian, 2011, Phys. Rev. Lett. **106**: 101102; F. Aharonian *et al.*, aXiv:1105:0131.

32ND INTERNATIONAL COSMIC RAY CONFERENCE, BEIJING 2011

Search for Galactic Cosmic-Ray Accelerators with the Combined IceCube 40-strings and AMANDA Detector

THE ICECUBE COLLABORATION
[1] *see special section of these proceedings*

Abstract: During the season 2008/2009, IceCube took data as a combined detector with AMANDA embedded into the 40-string array. With a smaller spacing between the sensors compared to IceCube, AMANDA improved the effective area below a few TeV and acted as a first generation low-energy extension of IceCube. The data obtained in this configuration is used to search for neutrino sources within the Galaxy. The TeV γ-ray spectra of some potential galactic cosmic-ray accelerators show cut-offs in the energy spectrum at energies of a few TeV. In the case of transparent TeV γ-ray sources, high-energy neutrinos will follow similar spectra and an improved effective area below a few TeV improves the sensitivity for these of sources.

Several tests including a scan of the galactic plane in the Northern Hemisphere and a dedicated analysis for the Cygnus region are presented. In the absence of a significant signal, upper limits are reported. The results provide the most restrictive upper limits for the Cygnus region obtained so far. Depending on the assumed energy cut-off, the upper limits obtained with this analysis are only a factor of two to three above the expected neutrino flux if all the TeV γ-rays observed in the region were of hadronic origin. This implies that during the coming years, IceCube will be able to either detect neutrinos from the Cygnus region, or to constrain the nature of the high-energy γ-ray emission in the region, and thus the fraction of interacting cosmic rays produced in one of the most active parts of the Galaxy.

Corresponding authors: Sirin Odrowski[1] (*Sirin.Odrowski@mpi-hd.mpg.de*), Elisa Resconi[2,3](*Elisa.Resconi@mpi-hd.mpg.de*), Yolanda Sestayo[1] (*Yolanda.Sestayo@mpi-hd.mpg.de*)

[1] Max-Planck-Institut fuer Kernphysik, 69117 Heidelberg, Germany

[2] T.U. Muenchen, 85748 Garching

[3] Friedrich-Alexander Universitaet Erlangen-Nuernberg, 91058 Erlangen

Keywords: neutrino astronomy, IceCube

1 High-Energy Neutrino Production in the Galaxy

One of the primary goals of the IceCube experiment [1] is the detection of astrophysical sources of high-energy neutrinos. A neutrino signal uniquely identifies the sites of hadron acceleration and interaction and thereby the sites of cosmic-ray production.

If protons are accelerated to sufficiently high energies in (galactic) sources, high-energy neutrinos can be produced through proton-proton interactions with the ambient gas. If such sources are transparent and the γ-ray emission from high-energy electrons is small compared to the total γ-ray emission, the high-energy neutrino spectra can be inferred from the γ-ray spectra [2].

Several objects within the Galaxy such as supernova remnants and pulsar wind nebulae, binary systems and the collective winds of massive stars might accelerate protons up to PeV energies [3]. Even though γ-rays up to several TeV have been observed from several of these objects, many of the observed γ-ray spectra have energy cut-offs below 10 TeV and/or their energy spectra are significantly steeper than an E^{-2} spectrum as expected from shock acceleration. A search for neutrino emission from within the Galaxy thus requires an approach that is optimized to retain a high efficiency for neutrinos with energies below 10 TeV. The predicted neutrino flux from galactic sources is very low and single point-like sources might elude a detection in the near future. In star forming regions, it is however possible that several (weak) sources produce an integrated signal strong enough for a discovery. In particular the Cygnus region as the most active part of the Galaxy in the Northern Hemisphere is of primary interest to IceCube in this context.

2 Methods and Targets

At energies between a few hundred GeV and a few TeV, the field of view of the 2008/2009 configuration of Ice-

Cube is restricted to the Northern Hemisphere where the atmospheric muon background is suppressed by several orders of magnitude by the shielding provided by the Earth. Within this field of view, a search for point-like, steady high-energy neutrino sources has been performed. We search for a significant excess of neutrinos over the uniform background of atmospheric neutrinos by a maximum likelihood ratio hypothesis test, described in [4]. The search is performed on a 0.25° grid covering the galactic plane within the field of view ($37.5^\circ < l < 212.5^\circ$, $-5^\circ < b < 5^\circ$). Since the angular grid size is smaller than the angular resolution of the detector, this search may be regarded as an unbinned analysis. The energy term in [4] is omitted as it is not relevant for soft spectra sources.

In addition, the same likelihood ratio hypothesis test is applied to six prominent γ-ray sources: the Crab Nebula, LSI +61 303, CasA, W51, SS433 and IC443. The sources were chosen due to their brightness in γ-rays and/or the presence of target material for proton-proton interactions in or near the sources.

To search for high-energy neutrino emission within the Cygnus region, a dedicated test based on a 2-point correlation function has been developed [5]. A search for a spatial clustering of events inside a 7°x11° region ($72^\circ < l < 83^\circ$, $-3^\circ < b < 4^\circ$) around the most active part of the Cygnus region is performed. The method is able to take advantage of extended emission regions and the emission of any sources within the region. If applied to the data sample used in this work, the discovery flux per point source is lower than in a standard search if more than two point sources are present within the region.

The analyzed data set is dominated by atmospheric neutrinos. Any potential astrophysical signal presents only a very small contribution in number of events. A data driven background estimation can thus be obtained by randomizing the arrival directions of the events, compatible with a homogeneous spatial distribution. All statistical tests reported here use this technique for the construction of their respective null hypothesis.

3 The Combined IceCube 40-string and AMANDA Detector

The full IceCube [1] neutrino telescope at the South Pole consists of a volume of approximately one cubic kilometer of clear Antarctic ice instrumented with light sensors. This instrumentation allows to detect muons from charged current interactions of neutrinos. 5160 digital optical modules are deployed in the ice along 86 strings that hold 60 optical modules each. The detector has been built in several stages and new strings have been added each Antarctic summer since 2004/2005.

AMANDA [8] is located at the same site as IceCube and consists of 677 optical modules deployed on 19 strings, most of them at depths between 1500 and 2000 m. Both the vertical and horizontal spacing of the optical modules in AMANDA are smaller than in IceCube. This provides a lower energy threshold and a higher collection efficiency for muons below a few TeV. As AMANDA is the precursor experiment to IceCube, many of the techniques employed in IceCube were developed and tested in AMANDA [9]. AMANDA took data as a stand-alone neutrino telescope until December 2006. Since 2007, AMANDA is fully surrounded by IceCube strings and was integrated into the IceCube data acquisition system as a low-energy extension of the IceCube detector until 2009 [10].

In the combined data taking mode, AMANDA initiates a read-out of IceCube whenever a multiplicity trigger condition in AMANDA is fulfilled. The data collected from both parts of the combined detector is then merged into a single event and reconstructions can be applied to either the full event information or to the IceCube or AMANDA information separately. The analysis presented here uses the information from both IceCube and AMANDA.

4 Neutrino Sample

The targets of this analysis are soft-spectrum sources or sources with high-energy cut-offs below the PeV range within the Galaxy. The event selection is thus aimed to improve the effective area for neutrino energies below this scale. This is achieved both through the use of AMANDA as an embedded array inside the 40 IceCube strings and through an event selection optimized for a larger acceptance of events below 10 TeV compared to the analysis presented in [11].

The current analysis uses data collected from April 5, 2008 to May 20, 2009. Both parts of the combined IceCube-AMANDA detector operated very stably during this time. For IceCube $\sim$ 375 days of data were collected. AMANDA was decommissioned before the end of the IceCube 40-string data taking period and $\sim$306 days of combined IceCube-AMANDA data were collected . The main causes for detector downtime were scheduled operations in the course of the integration of new strings into the detector.

The dominant class of recorded events are atmospheric muons incident from the atmosphere above the detector. The majority of this background is suppressed by a cut on the reconstructed direction such that only events from the Northern Hemisphere are accepted. Even after this cut, the atmospheric muons dominate over the atmospheric neutrinos by several orders of magnitude as a fraction of atmospheric muons are not well-reconstructed and as such end up as up-going muons. In particular coincidences between two muons from different air showers can mimic up-going events. An event selection is then applied to reduce this background by rejecting events with poor reconstruction quality and/or events with a high probability to be composed of two separate particles. An overview of reconstruction quality estimators and other event parameters that allow to distinguish signal from background is given in [11]. A subset of these parameters is used in this work.

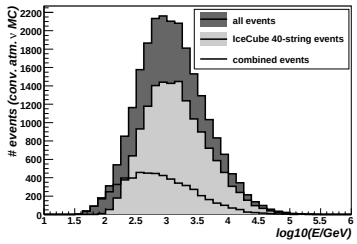

Figure 1: Energy distribution of atmospheric neutrino events in the combined IceCube 40-strings and AMANDA point source sample. Events with AMANDA trigger ("combined events") peak at lower energies than events with IceCube trigger. 90% of the events are contained in a central interval from 130 GeV to 7.5 TeV.

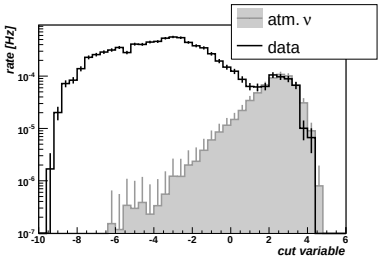

Figure 2: Distribution of the main cut variable for IceCube-triggered events before final cuts are applied. Shown are the data in black and atmospheric neutrino simulation based on the atmospheric neutrino flux model of [6] in gray. The final cut is placed at 1.0 as result of an optimization of the discovery potential [7].

The data collected in 2008/2009 contains events that triggered AMANDA, events that triggered IceCube and events that triggered both detectors. Most analyses performed on the data sample, such as [11], use only the events that triggered IceCube. The approach presented here extracts a neutrino sample from all three kinds of events. Combined IceCube-AMANDA events are selected by different event selection criteria than events that only have an IceCube trigger, as outlined below.

IceCube events without AMANDA trigger are selected by a series of one-dimensional cuts on event quality parameters followed by a multivariate classification based on the Neyman-Pearson rule (see for example [12]). The probability density functions for five quality parameters are generated from atmospheric muon-dominated data as background and from atmospheric neutrino simulation and combined in the cut. The main cut variable is the likelihood ratio between the atmospheric neutrino and the atmospheric muon hypothesis. The distribution of this main cut variable is shown in Figure 2 for data and for atmospheric neutrino simulation. For combined IceCube-AMANDA events, the Neyman-Pearson rule is not applied because a series of a series of one-dimensional cuts resulted in a similar performance for these events.

The energy distribution at the final event selection level is shown in Figure 1. The combined IceCube-AMANDA events peak at lower energies. The angular resolution of the sample depends on the energy of the events. An unbroken E^{-3} power law spectrum has been used to benchmark the performance of the analysis. For this very soft spectrum, a median angular resolution of 1.2° is achieved. From simulation of single and double coincident cosmic-ray air showers with CORSIKA [13], the atmospheric muon contamination of the cleaned data sample used in this analysis is estimated between 2% and 3%.

19797 neutrino candidates are selected from IceCube and AMANDA triggered events. This sample is predominantly background atmospheric neutrinos, which cannot be distinguished from the cosmic neutrino signal on an event-by-event basis [1]. These events are analyzed with the hypothesis tests described in the previous section to search for spatial clustering of events over the uniform atmospheric neutrino background.

5 Results

The results of the galactic plane scan are presented in Figure 3, from which it is seen that all observations are compatible with the background expectation. The largest clustering of events was observed at $(85.5^\circ, -2, 0^\circ)$ with a (pre-trial) probability to observe an equal or stronger excess at this position of 0.0935% due to background fluctuations only. Accounting for the trials introduced by the repetition of the test along the galactic plane, an equivalent or more significant observation is made in 88.02% of randomized data samples. Thus the observed excess in the scan is consistent with fluctuations of background. Also the results for the six γ-ray sources are compatible with the background expectation and preliminary 90% flux upper limits are summarized in Table 1 assuming a power-law with a spectral index of 3. The preliminary limits do not include the systematic uncertainty of the signal efficiency. The strongest preliminary flux limit can be set for Cas A at a flux of $5.9 \cdot 10^{-11}$ TeV^{-1} cm^{-2} s^{-1}. The upper limits are calculated using the approach of Feldman and Cousins [15].

With 55 events observed within the box defined around the most active part of the Cygnus region compared to a background expectation of 60 events, strong flux upper limits could be extracted for this region. Assuming an $E^{-2.6}$ spectrum as was fit to the MILAGRO γ-ray observations [16], a preliminary 90% flux upper limit of $3 \cdot 10^{-11}$ TeV^{-1}cm^{-2}s^{-1} (without systematic uncertainties) is obtained provided the astrophysical signal from the region has an exponential energy cutoff only at or above 1000 TeV.

1. An exception could be the use of a veto against atmospheric neutrinos as proposed in [14]

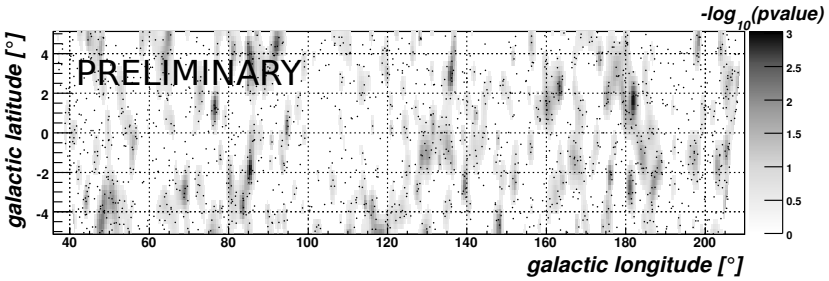

Figure 3: Result of the galactic plane scan using data collected by IceCube 40-strings as a combined detector with AMANDA. The significance of the observation at each grid point is expressed by the (pre-trial) pvalue which is shown together with the distribution of the events shown as black dots. The most significant excess of events is located at $(85.5°, -2, 0°)$ with a (pre-trial) pvalue of 0.000935 (-log10(pvalue)=3.03). The probability to observe a similar or stronger excess of events at any point of the galactic Plane is 88.02%. No neutrino sources have been detected.

	ra	dec	ns	upper limit
Crab	$83.63°$	$22.01°$	0	7.3
CasA	$350.85°$	$58.82°$	0	5.9
LSI +61 303	$40.13°$	$61.23°$	1.6	7.8
SS433	$287.94°$	$4.983°$	0	9.7
IC443	$94.18°$	$22.53°$	0	7.3
W51	$290.82°$	$14.15°$	0.6	8.3

Table 1: Position, best fit number of source events (ns) and **preliminary** 90% upper limits on the flux of muon neutrinos for each of the tested objects in units of 10^{-11} TeV^{-1} cm^{-2} s^{-1}. The upper limits are calculated without systematic uncertainties under the assumption of an E^{-3}-spectrum.

6 Outlook

The installation of the IceCube detector has been completed in 2010 and IceCube is now taking data in its final configuration of 86 strings. The collaboration continues to search for neutrino sources within and outside of the Galaxy. With the substantially larger detector, the sensitivity to galactic neutrino sources will improve significantly with respect to the analysis presented here.

In particular IceCube's observations of the Cygnus region will enter an interesting regime in the next few years. We have shown that the IceCube 40-string/AMANDA limits for the Cygnus region are only a factor of two to three above the expected flux if all of the γ-rays in the region were of hadronic origin. Applying the same test to the data obtained with larger configurations of IceCube, it will thus be possible to either detect neutrino emission in this region or to constrain the hadronic component in the γ-ray emission.

AMANDA has been decommissioned in 2009 and replaced by the DeepCore extension of IceCube. The positioning of a more densely instrumented volume in the deepest and clearest ice around the central IceCube string offers several advantages with respect to AMANDA. In particular, it offers the possibility to use veto techniques that allow the suppression of downgoing atmospheric muons and might open the Southern Hemisphere to neutrino astronomy below several tens of TeV from the South Pole.

References

[1] IceCube collaboration, Astroparticle Physics 20 (2004) 507.
[2] S. R. Kelner, F. A. Aharonian, Physical Review D, 2008, **78**(3): 034013-1 - 034013-16
[3] S. Gabici, F. A. Aharonian, Astrophysical Journal, 2007, **665**(2): L131 - L134
[4] J. Braun et. al., Astroparticle Physics, 2008, **29**(4): 299 - 305
[5] Y. Sestayo, PhD Thesis, Universitaet Heidelberg, 2010
[6] G. D. Barr et. al., Phys. Rev. D, 2004, **70**(2): 023006-1 - 023006-13
[7] G. Hill et. al., Proceedings of PHYSSTAT05, Oxford, UK, 2006, 108-111
[8] AMANDA collaboration, Nature, 2001, **410**: 441-443
[9] AMANDA collaboration, Nuclear Instruments and Methods in Physics Research A, 2006, **556**(1): 169 - 181
[10] A. Gross et. al. for the IceCube collaboration, Proceedings of the 30th International Cosmic Ray Conference, Merida, Mexico, 2007 : 12531256, http://arxiv.org/abs/0711.0353
[11] IceCube collaboration, Astrophysical Journal, 2011, **732**(1): 1 - 16
[12] A. R. Webb, Statistical Pattern Recognition, John Wiley & Sons, Ltd, 2002
[13] D. Heck et. al., Forschungszentrum Karlsruhe Report FZKA, 1998 **6019**)
[14] S. Schoenert et. al., Phys Rev. D, 2009, **79**(4): 043009-1 - 043009-5
[15] G. J Feldman, R. D. Cousins, Phys. Rev. D ,1998, **57**(7): 38733889
[16] A. A. Abdo et. al., Astrophysical Journal, 2007, **658**(1): L33 - L36

32ND INTERNATIONAL COSMIC RAY CONFERENCE, BEIJING 2011

Time-dependent search for neutrino multiflare sources with the IceCube 59-string data

THE ICECUBE COLLABORATION[1]
[1]*See special section in these proceedings*

Abstract: A time-dependent search for neutrino flares from pre-defined directions in the whole sky is presented. The analysis uses a time-clustering algorithm combined with an unbinned maximum likelihood method. This algorithm, by including a likelihood signal term describing the contribution of many small clusters of signal-like events, provides an effective way for looking for weak neutrino flares over different time-scales. The event selection is optimized to maximize the discovery potential for the IceCube 59-string (IC59) detector configuration. Sources are being selected based on data in the 0.1 to 100 GeV energy range as provided by the Fermi satellite. Subsequently, periods of interest based on electromagnetic data are scanned, over larger time-windows as compared to the duration of the corresponding electromagnetic flares.

Corresponding authors: Dariusz Góra[2,3] (*Dariusz.Gora@desy.de*), Elisa Bernardini[2] (*Elisa.Bernardini@desy.de*), Angel Cruz Silva[2] (*angelh@ifh.de*)
[2] *DESY, D-15738 Zeuthen, Germany*
[3]*Institute of Nuclear Physics PAN, Radzikowskiego 152, 31-342 Cracow, Poland*

Keywords: IceCube; Neutrino Flares; Time-dependent searches

1 Introduction

Finding neutrino point sources in the sky requires locating an excess of events from a particular direction over the background of atmospheric neutrinos and muons. Signal events might present additional features that distinguish them from background, for example a different energy spectrum or time structure. For sources which manifest large time variations in the emitted electromagnetic radiation, the signal-to-noise ratio can be increased by testing smaller time windows around the flare (time-dependent search). Following this idea there are in principle two approaches to neutrino time-dependent searches: Triggered and Untriggered. In the first case we are looking directly for photon-neutrino correlations using specific source lightcurves from Multi-WaveLength (MWL) observations [1]. In the second case, followed in this work, we perform a generalized search for neutrino flares from a pre-selected source list, motivated by (but not directly in time coincidence with) MWL observations. This approach allows to account for possible time lags between photon flares and the associated neutrino flares [2].

An untriggered unbinned flare search was first developed and applied to IceCube data, using a compact list of pre-defined source directions [3]. IceCube is km^3 scale neutrino detector at the South Pole sensitive to TeV-neutrinos [4]. A time-clustering algorithm [3, 5], and an unbinned maximum likelihood method [6] are the basis of this analysis. Such a method finds the most significant flare in a long period. The number of trials coming from all combinations of event times is increased, reducing the significance. However, for flares sufficiently shorter than the total observation period, the time clustering algorithm is more sensitive than a time-integrated analysis.

In this paper, we propose an extension of the method described in [3]. The proposed algorithm can extract not only the most significant flare, but also less significant clusters of events distributed over several weak flares. These weaker flares could have any separation in time and therefore may be very difficult to detect or even undetectable with other existing point-sources methods (like [6]).

2 Multiple flare search algorithm

A more detailed description of the proposed method and its application for multi-flare Monte Carlo simulation can be found in [7]. Here we only briefly describe the main steps of the proposed algorithm. In order to identify a series of weak flares, we first extract all *consecutive* doublets that can be formed out of all signal-like events ($S_i/B_i > 1$) over the data taking period $\Delta T_{\rm data}$[1], see Figure 1.

1. A signal-like event is defined as having $S_i/B_i > 1$, where S_i and B_i are the signal and background Probability Density Function (PDF), respectively, as defined for the time-integrated

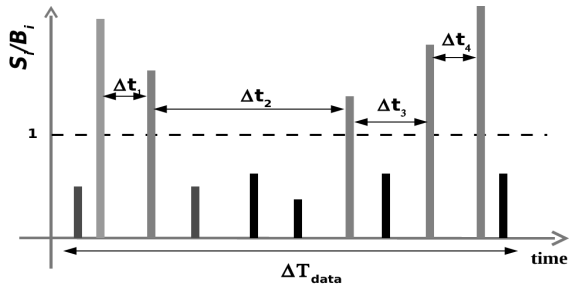

Figure 1: The basic idea of the time-clustering procedure.

This step serves to isolate all possible (and smallest) time windows (Δt_j) that compose the signal contribution in the tested data sample (the total number being M). We call these time windows "data segments". Note, that by using only doublets as data segments we do not need any assumptions about the distribution of signal events inside a data segment i.e. by definition the time probability $P^{\rm time}$ in the signal PDF is uniform in time and is given by $P^{\rm time} = \frac{1}{\Delta t_j}$.

Then for each data segment the best estimates of the number of signal events $\hat{n}_s$ and source spectral index $\hat{\gamma}_s$ are found by maximizing the one-source likelihood as defined in [6]. Then for each data segment the individual value of the test statistic $\mathrm{TS}_j|_{\Delta t_j}$ is calculated from the likelihood ratio of the background-only (null) hypothesis over the signal-plus-background hypothesis [6]. All data segments are then sorted according to $\mathrm{TS}_j|_{\Delta t_j}$. In the case that real signal events are present, some of these data segments will contain the signal events while the rest of them are due to background fluctuations. Our aim is to extract the optimal (best suited) number of data segments ($M_{\rm opt}$) which compose the total signal contribution in the overall period $\Delta T_{\rm data}$.

For this purpose, we used a modification of the single-source likelihood function ([6]) by replacing the one-source signal term S_i by the sum of signal sub-terms over m data-segments:

$$S_i \rightarrow \frac{\sum_{j=1}^{m} W^j \times S_i^j(\mid \vec{x}_i - \vec{x}_s \mid, E_i, \gamma, \Delta t_j)}{\sum_{j=1}^{m} W^j} \qquad (1)$$

where W^j is a weight which describes the strength (significance) of the doublet contained in each data segment. As was shown in [7] the test statistic is quite well correlated with the true number of injected signal events. Thus we take $W^j = \mathrm{TS}_j|_{\Delta t_j}$.

In order to estimate the optimal number of data segments $M_{\rm opt}$ for a given configuration of m segments (starting from $m = 1$) we maximize the modified $\log(\tilde{\mathcal{L}}(n_s, \gamma_s, m))$ with n_s and γ_s as free parameters. For a given number m the minimization returns the best estimates for the number of signal events $\hat{n}_s$ and for the spectral index of the source $\hat{\gamma}_s$, and the "global" test statistic is calculated from:

$$\widetilde{\mathrm{TS}}(m) \equiv -2\log\left[\frac{\tilde{\mathcal{L}}(\vec{x}_s, n_s = 0)}{\tilde{\mathcal{L}}(\vec{x}_s, \hat{n}_s, \hat{\gamma}_s, m)}\right]. \qquad (2)$$

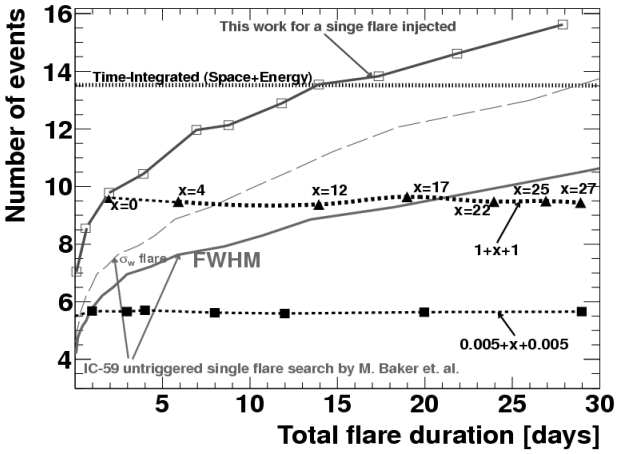

Figure 2: Number of events for a 5σ discovery as a function of the total flare duration obtained for one flare search and two flares search. See text for more details.

Then, the optimal number of data segments to be stacked ($M_{\rm opt}$) is chosen according to the maximum of $\widetilde{\mathrm{TS}}(m)$. The overall significance of the optimal configuration $M_{\rm opt}$ can be determined using MC simulations by applying the same procedure to a large number of scrambled data sets.

3 Data Sample

IceCube 59-string data from May 20, 2009 to May 31, 2010 is used. It spans 375 days with an overall effective detector uptime of 93% (i.e. 348 days). The whole sky (declination range from -85° to 85°) is scanned. Different selection criteria, due to different backgrounds, are applied for the northern and southern skies, see [8]. After selection the data set contains 107 569 events (43 339 events in the northern sky and 64 230 events in the southern sky) with a median angular resolution of 0.7° .

4 Expectations for IceCube 59-strings

Figure 2 shows the performance of the algorithm for a source with a E^{-2} energy spectrum located at declination $\delta = 22^\circ$. For a single flare search (solid line with open boxes) the number of events for a 5σ discovery decreases when we consider flares with shorter duration. As an example, for a flare with duration of 28, 10 and 0.1 days in average about 15, 12 and 7 events, respectively, are needed for discovery. Note, that for flares with relatively short durations (below about 15 days) the number of events is smaller compared to a time-integrated analysis, see dashed line in Figure 2 labeled: Time Integrated Analysis (Space+Energy). In Figure 2 the performance of the algorithm for two flare searches is also shown (horizontal dashed lines).

In this case two individual flares with duration $\Delta t^{(1)}_{flare}$ and $\Delta t^{(2)}_{flare}$, respectively, are separated in time by a time in-

method [6]. To calculate the ratio, $S_i/B_i > 1$, only the spatial and energy terms in the PDF's are included.

terval x. [2]. For two flares separated by x we can see that the number of events needed for discovery only slightly depends on the total flare duration $\Delta T(M_{opt})$ and equals the case of single flare with duration ($\Delta T(M_{opt}) = \Delta t^{(1)}_{flare} + \Delta t^{(2)}_{flare}$) i.e. $x = 0$. This is a consequence of the fact that the proposed algorithm looks for the total signal in the data sample but disregards how these signal events are distributed in time. In other words, signal events form in time one significant cluster of events (one flare) for a given source location, or theses events can be distributed among a few (sometimes less significant) flares separated in time. Figure 2 shows also that multiple flares have better discovery potential than that of one flare if the same method is used.

For comparison purposes, in Figure 2 the performance of an untriggered time-dependent analysis from [8] is shown. In this case calculations are performed using the standard unbinned likelihood method with the assumptions, that the shape of the flare follows the Gaussian distribution i.e. so called Gaussian burst [6] [3]. Comparing our results for a single flare with [8] we need about 50% more events for discovery in case all events are injected in one single flare. This is because our algorithm stacks also background fluctuations, and thus leads to a higher 5σ threshold than the threshold obtained by a single-source likelihood based method. However, if we consider two flares separated in time the differences in the number of events strongly decreases and with enough separation in time the multi-flare analysis requires fewer events for discovery than standard untriggered searches. As an example for two flares 1 day long each, if they are separated by more than 20 days, the multi-flare search performs better than [8]. A similar behavior is observed for individual flares with duration $\Delta t^{(1)}_{flare} = 0.005$ day, i.e. for time scales of the order of minutes.

In Figure 3 the fluence sensitivity for IceCube 59-string data is presented for six representative source directions. The fluence depends on the total data period $\Delta T_{\rm data}$ considered, being better for smaller data periods. The fluence increases when we consider flares with longer duration. The effect is well visible for $\Delta T_{\rm data} = 40$ days.

5 Source selection and results

The proposed algorithm was applied to selected sources which manifest large time variations in the electromagnetic flux. Using our multiple search algorithm we do not need a precise estimation of the starting time and ending time of each flare. As was shown in [7] the algorithm finds all signal events in the data period even if signal events are arranged as a few clusters separated in time. Thus we only need a first guess of the flare central time T_m and we set a larger time window: $T_m \pm 40$ days. This allows to search for neutrino flares near a γ, optical, x-ray or infra-red flare testing the correlation or anticorrelation in the neutrino-gamma emission.

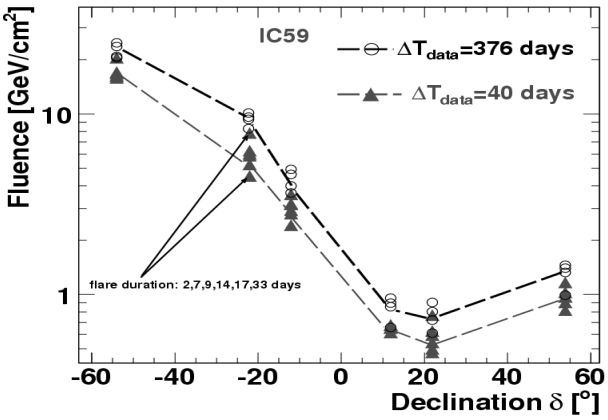

Figure 3: Fluence sensitivity from an E^{-2} spectrum neutrino signal plotted versus declination for different observation times using IceCube 59-string data.

In the context of hadronic models predicting high energy neutrino emission from objects such as Active Galactic Nuclei (AGN), there are several possible scenarios. For example in [2] Flat Spectrum Radio Quasars (FSRQ) are more promising, as neutrino sources, than BL-Lac objects, whereas in [9] the opposite is predicted. The proton blazar model [10] predicts that the Low synchrotron peaked BL-Lacs (LBL) are more likely to produce a significant neutrino emission than the High synchrotron peaked BL-Lacs (HBL). In [9] harder sources are selected as promising sources to be detected by IceCube once the prediction of the neutrino fluxes, within the assumed pp model, is combined with the IceCube instrumental response. On the other hand in [2] the considered $p\gamma$ model leads to the conclusion that FSRQs bright in the GeV range are promising neutrino sources without any assumption on the spectral index. In order to include these different predictions in this analysis data from the first Fermi LAT catalog [14] was used to select AGNs according to the following criteria:

- **BL-Lacs:** Average flux $[1 - 100$ GeV$] > 1 \times 10^{-9}$ ph cm^{-2}s^{-1} AND Spectral index < 2.3
- **FSRQs:** Average flux $[0.1 - 1$ GeV$] > 7 \times 10^{-8}$ ph cm^{-2}s^{-1}

In addition for both cases we include a variability index cut ($V > 23.21$) to select sources that are more likely to exhibit flaring periods [14]. For the selected sources, information about flaring states in different wavelengths, during the period of the 59-string configuration of IceCube was collected. The selected sources and periods are presented in Table 1.

2. In this case the total flare duration is defined as $\Delta T(M_{opt}) \equiv \Delta t^{(1)}_{flare} + x + \Delta t^{(2)}_{flare}$, so for example configuration $1 + x + 1$ corresponds to two one day flare each separated by time interval x ranging from 0 up to 27 days.

3. In this work simulated signal events are injected according to a uniform time distribution, while in [8] a Gaussian distribution with different standard deviation σ_w was considered. To make comparison, the corresponding width at half maximum $FWHM = 2\sqrt{2\ln 2}\sigma_w$ is calculated for a Gaussian flare, and then these results are compared with our calculations.

Table 1: Results for pre-defined variable astrophysical source candidates using the multi-flare algorithm.

Source	Type	ra [deg]	dec [deg]	#Atel / ref	T_m* (MJD)	p-value	$\Delta T(M_{\rm opt})$ [days]	Fluence Limit [GeV/cm^2]
PKS 0235+164	LBL	39.67	16.62	2207 / [11]	55085	0.27	0.0060	0.54
Mkn 421	HBL	166.12	38.21	2368 / [12]	55200	1.0	4.11	0.90
				2443 / [12]	55255	0.34	0.13	0.73
PKS 0426-380	LBL	67.16	-37.94	2366	55198	1.0	14.41	14.3
PKS 0537-441	LBL	84.72	-44.08	2124	55020	0.45	7.21	15.7
				2454	55247.5	1.0	25.68	17.44
				2591	55313	1.0	1.18	15.2
S5 0716+714	LBL	110.48	71.34	2353	55176.5	0.34	3.90	1.30
PKS 0447-439	HBL	72.38	-43.84	2350	55180	1.0	4.80	15.5
PKS 1424+240	HBL	216.75	23.8	2098	54977	1.0	0.44	0.59
PKS 0301-243	IBL	45.89	-24.11	2610	55319	0.36	0.775	7.37
3C 454.3	FSRQ	343.49	16.15	2534	55289	1.0	1.84	0.64
				2329 / [11]	55167	0.22	0.045	0.52
				2200 / [11]	55089	0.08	28.67	0.86
3C 279	FSRQ	194.05	-5.79	2154	55044	1.0	1.10	1.40
PKS 2023-07	FSRQ	306.42	-7.6	2175	55066	1.0	0.81	1.80
3C 273	FSRQ	187.28	2.05	2200 / [13]	55089	1.0	0.365	0.71
				2376	55203	1.0	1.28	0.81
4C +31.03	FSRQ	18.23	32.12	2054	54971	1.0	1.43	0.68
PKS 0805-07	FSRQ	122.05	-7.84	2136	55034	1.0	3.85	2.03
				2048	54958	1.0	10.34	1.91
PKS 0402-362	FSRQ	60.98	-36.06	2484	55228	1.0	13.17	12.88
B2 1520+31	FSRQ	230.55	31.73	2026	54941	1.0	4.85	0.65
OX 169 325.87	FSRQ	325.87	17.72	2393	55214	1.0	1.54	0.64
PKS 2052-47	FSRQ	314.09	-47.24	2160	55052	1.0	0.62	15.36
4C +38.41	FSRQ	248.77	38.14	2456	55250	1.0	3.17	0.81
				2136	55034	0.17	0.023	0.69
PKS 0906+01	FSRQ	137.27	1.44	2543	55294	0.16	0.154	0.71
PKS 0420-01	FSRQ	65.	-1.31	2402	55217	0.59	1.1	0.96
PKS 1830-21	FSRQ	278.41	-21.06	2242	55116.5	1.0	1.92	6.67
PKS 0244-470	FSRQ	41.5	-46.87	2440	55239	1.0	12.92	17.96

* T_m is the midpoint of the flare time interval reported in the alert (Atel) or in the corresponding reference when available.
$\Delta T(M_{opt})$ is the flare duration calculated for the optimal configuration of M_{opt} data segments.
The fluence upper limit is calculated by integrating $d\Phi/dE \times E$ over the 90% energy range and $\Delta T(M_{opt})$, assuming a neutrino energy spectrum of E^{-2}.

The proposed method was applied to the selected source candidates.No significant excess above the atmospheric background is found, therefore upper limits on the neutrino fluence were calculated. The results are presented in Table 1. The highest fluctuation observed corresponds to 3C 454.3 with a p-value of 8% (not including the trial factors due to looking at several sources). The limits for IC59 are on average about 50% better than for IceCube 40-strings data [15].

6 Summary

We presented a method to search for neutrino flares from point sources without an *a-priori* assumed time structure. The method considers only data segments which contain signal-like doublets, and uses a test-statistic term as their weights in a stacking-like calculation for the global maximum likelihood. For flares sufficiently shorter than the total observation period, the method is more sensitive than a time-integrated analysis and in some cases is also more sensitive than single flare searches already in use (like [8]). IceCube 59-string data was analyzed using the proposed method looking for neutrino multi-flares with no a-priori assumption on the time structure of the signal. A list of promising source candidates was selected based on different hadronic models. Since no deviation from the background-only hypothesis was found, upper limits on the neutrino fluence from these sources were derived.

References

[1] M. Baker et al., for the IceCube Collab., the 31st ICRC, Lodz, Poland, July 7-15, 2009 .
[2] A. Atoyan et al., New Astron. Rev., 2004, **48**: 381.
[3] J.L. Bazo Alba et al, arXiv:0908.4209.
[4] H. Kolanoski, IceCube summary talk, these proceedings.
[5] K. Satalecka et al; arXiv:0711.0353.
[6] J. Braun et al., Astropart. Phys. (2008) **29**: 299-305; J. Braun et al., Astropart. Phys., 2010, **33**:175-181.
[7] D. Góra et. al., Astropart. Phys. (2011) **35**: 201-210.
[8] IceCube Collab., paper 0784, these proceedings.
[9] A. Neronov et al., Phys. Rev. D, 2009, **80**: 083008.
[10] A. Mücke et al., Astropart. Phys., 2003, **18**: 593-613.
[11] R. Chatterjee et al., arXiv:1101.3815.
[12] N. Isobe et al., arXiv:1010.1003.
[13] A.A. Abdo et al., Astro. J. Lett., 2003, **714**: 615-627.
[14] A.A. Abdo et al., Astro. J. Supp., 2010, **188**: 405-436.
[15] The IceCube Collaboration; arXiv:1104.0075v1.

32ND INTERNATIONAL COSMIC RAY CONFERENCE, BEIJING 2011

Optical follow-up program of IceCube multiplets - testing for soft relativistic jets in Core-collapse Supernovae

THE ICECUBE COLLABORATION[1], CARL AKERLOF[2], FANG YUAN[3], WEIKANG ZHENG[2]
[1]*see special section in these proceedings,* [2]*University of Michigan, Ann Arbor,* [3]*Australian National University*

Abstract: Transient neutrino sources such as Gamma-Ray Bursts (GRBs) and Supernovae (SNe) are hypothesized to emit bursts of high-energy neutrinos on a time-scale of $\lesssim 100$ s. To increase the sensitivity to detect those neutrinos and identify their sources, an optical follow-up program for neutrinos detected with the IceCube observatory has been implemented. If a neutrino multiplet, i.e. two or more neutrinos from the same direction within 100 s, is found by IceCube a trigger is sent to the Robotic Optical Transient Search Experiment, ROTSE. The 4 ROTSE telescopes immediately observe the corresponding region in the sky in order to detect an optical counterpart to the neutrino events of IceCube. Data from the first year of operation of the optical follow-up program have been searched for a signal from supernovae. No statistically significant excess in the rate of neutrino multiplets has been observed and further no coincidence with an optical counterpart was found during the first year of data taking. This allows us to restrict current models predicting a high-energy neutrino flux from soft jets in core-collapse SNe. For the first time a stringent limit on the hadronic jet production in core-collapse SNe is derived.

Corresponding Author: Anna Franckowiak[3] (*franckowiak@physik.uni-bonn.de*)
[3]*Universität Bonn*

Keywords: neutrinos, supernovae, gamma-ray bursts

1 Introduction

High-energy astrophysical neutrinos are produced in proton interactions of charged cosmic rays with ambient photon or baryonic fields (for reviews see [1]). Acceleration of protons to very high energies takes place in astrophysical shocks. Neutrinos escape the acceleration region and propagate through space without interaction, while protons are deflected in magnetic fields and no longer point back to their source. Unlike gamma-rays, neutrinos are solely produced in hadronic processes and could therefore reveal the sources of the highest energy charged cosmic rays. Gamma-ray bursts could provide the environment and the required energy to explain the production of the highest energy cosmic-rays and hence are a plausible candidate. Recent observations imply a common physical origin of long GRBs and core-collapse supernovae (CCSNe): a massive stellar explosion (see [2] for a review). According to the collapsar model [3], long GRBs (duration $\gtrsim 2$ s) have their origin in the collapse of a massive, rapidly rotating star into a black hole surrounded by an accretion disk. Relativistic jets with Lorentz boost factors of 100-1000 form along the stellar axis. This GRB-SN connection gives rise to the idea that GRBs and SNe might have the jet signature in common and a certain fraction of core-collapse SNe might host soft relativistic jets. SN jets are suggested to be equally energetic and more baryon-rich, hence they are only mildly relativistic. Such soft relativistic jets would become stalled in the outer layers of the progenitor star, leading to essentially full absorption of the electromagnetic radiation emitted by the jet and at the same time an efficient production of high-energy neutrinos [4, 5]. This motivates a search for neutrino emission, as neutrinos would be able to escape from within the star.

The IceCube neutrino detector, located at the geographic South Pole, is built to detect high-energy astrophysical neutrinos [6]. So far GRB neutrino searches have been performed offline on AMANDA [7] and IceCube [8] data, triggered by gamma-ray satellite detections. Furthermore, a dedicated search for a neutrino signal in coincidence with the observed X-ray flash of SN 2008D has been conducted by IceCube [9] in order to test the soft jet scenario for CC-SNe. Neither the GRB nor the SN neutrino searches led to a detection yet, but set upper limits to the possible neutrino flux.

Early SN detections, as in the case of SN 2008D, are very rare since X-ray telescopes have a limited field of view. However, neutrino telescopes cover half of the sky at any time. If neutrinos produced in soft relativistic SN jets are detected in real time, they can be used to trigger follow-up observations [10]. This is realized with the optical follow-up program presented here. Complementary to the offline

searches, the optical follow-up program is an online search independent of satellite detections. It is sensitive to transient objects, which are either gamma-dark or missed by gamma-ray satellites. In addition to a gain in significance, the optical observations may allow to identify the transient neutrino source, be it a SN, GRB or any other transient phenomenon producing an optical signal. Hence it enables us to test the plausible hypothesis of a soft relativistic SN jet and sheds light on the connection between GRBs, SNe and relativistic jets.
In order to implement the optical follow-up program an online neutrino event selection was developed at the neutrino detector IceCube. The data are processed online by a computer farm at the South Pole. A multiplicity trigger selects neutrino burst candidates and the directional information is transferred to the four ROTSE telescopes, which start the follow-up immediately and continue observations for several days. The obtained optical data are analyzed in order to search for an optical supernova counterpart.

2 IceCube

The IceCube neutrino telescope has been under construction at the geographic South Pole since 2004 and was completed in the Antarctic summer of 2010/11. It is capable of detecting high energy neutrinos with energies above 100 GeV and is most sensitive to muon neutrinos within the energy range from TeV to PeV. High-energy muon neutrinos undergoing charged current interactions in the ice or the underlying rock produce muons in neutrino-nucleon interactions. The muon travels in a direction close to that of the neutrino and emits Cherenkov light. The deep ultra clear Antarctic ice is instrumented with light sensors thus forming a Cherenkov particle detector. After its completion it comprises a volume of $1\,\mathrm{km}^3$ with 5160 digital optical modules (DOMs) attached to 86 vertical strings at a depth of $1450\,\mathrm{m}$ to $2450\,\mathrm{m}$ [6]. Each DOM consists of a $25\,\mathrm{cm}$ diameter Hamamatsu photomultiplier tube (PMT) and supporting hardware inside a glass pressure sphere. Here we present the analysis of the data taken from the start of the follow-up program on 2008/12/16 to 2009/12/31. Initially 40 IceCube strings were taking data. In May 2009 an additional 19 strings were included. This corresponds to an uptime of 121 days with 40 and 186.4 days with 59 strings. In the following the deployment stages will be referred to as IC40 and IC59.

2.1 Online System

In order to rapidly trigger optical telescopes the first online analysis of high-energy neutrinos detected by IceCube was developed and implemented. Unlike in the offline analyses, which are performed on an entire dataset (usually ~ 1 year of data) with time consuming reconstructions on a large computer cluster, the data are processed online by a computer cluster at the South Pole. The processing includes event reconstruction and basic event selection. The first year of data presented here was taken with a latency of 6-8 h. With the start of operations with 79 strings the processing was upgraded reducing the latency to a few minutes. After the parallel processing the data arrive on a dedicated machine (analysis client), where a sophisticated event selection is applied based on the reconstructed event parameters. A multiplicity trigger selects neutrino burst candidates (see section 2.2). No further reconstruction algorithms need to be applied at the analysis client allowing a very fast filtering of the events ($\ll 1\,\mathrm{s}$). The directional information is transferred to Madison, Wisconsin, via the Iridium satellite network within about $10\,\mathrm{s}$. From there the message is forwarded to the four ROTSE telescopes via the internet through a TCP-socket connection for immediate follow-up observations. The stability and performance of the online system is constantly monitored in order to allow a fast discovery of problems. To achieve this, test alerts are produced at a much higher rate (~ 100 test alerts per day compared to 25 real alerts per year) by the same pipeline and are also send to the North. Their rate and delay time distributions are monitored using an automatically generated web page.

2.2 Neutrino Event Selection

The background in a search for muon-neutrinos of astrophysical origin can be divided into two classes. One consists of atmospheric muons, created in cosmic ray air showers, entering the detector from above. The other is given by atmospheric neutrinos which have their origin in meson decays in cosmic ray air showers. The expected neutrino signal according to the soft jet SN model can be calculated as a function of two model parameters: the boost Lorentz factor Γ and the jet energy E_{jet} [9]. Signal events are simulated following the predicted neutrino flux spectrum in order to develop and optimize selection criteria to distinguish signal and background events. Restricting the search to the Northern hemisphere and imposing requirements on the event reconstruction quality (e.g. the number of hits with small time residual or the likelihood of the reconstruction) allows a suppression of the mis-reconstructed muon background. To suppress the background of atmospheric neutrinos, which we cannot distinguish from the soft SN neutrino spectrum, we require the detection of at least two events within $100\,\mathrm{s}$ and an angular difference between their two reconstructed directions of $\Delta\Psi \leq 4^\circ$. The choice of the time window size is motivated by the jet penetration time. The observed gamma-ray emission from long GRBs has a typical length of $50\,\mathrm{s}$, which roughly corresponds to the time for a highly relativistic jet to penetrate the stellar envelope. The angular window $\Delta\Psi$ is determined by the angular resolution of IceCube and was optimized along with the other selection parameters. The final set of selection cuts has been optimized in order to reach a multiplet rate of ~ 25 per year corresponding to the maximal number of alerts accepted by ROTSE. The final data stream consists of 37% (70%) atmospheric neutrinos for IC40 (IC59). Combining the neutrino measurement with the optical measure-

ment allows the cuts to be relaxed yielding a larger background contamination and at the same time a higher signal passing rate. A doublet is not significant by itself, but may become significant when the optical information is added. Each multiplet is forwarded to the ROTSE telescopes. The doublet direction is calculated as a weighted mean from the single reconstructed directions comprising the multiplet. The single events are weighted with $1/\sigma^2$, where σ is the reconstruction error estimated by the paraboloid fit, which fits a paraboloid to the likelihood landscape around the minimum defined by the best fit. The resolution of the doublet direction is $\sim 0.8^\circ$.

3 Search for Optical Counterparts

The IceCube multiplet alerts are forwarded to the robotic optical transient search experiment (ROTSE), which consists of four identical telescopes located in Australia, Texas, Namibia and Turkey [11]. The telescopes stand out because of their large field of view (FoV) of $1.85^\circ \times 1.85^\circ$ and a rapid response with a typical telescope slew time of 4 sec to move the telescope from the standby position to the desired position. The telescopes have a parabolic primary mirror with a diameter of 45 cm. To be sensitive to weak sources no bandwidth filter is used. ROTSE is most sensitive in the R-band (~ 650 nm). The wide field of view is imaged onto a back-illuminated thinned CCD with 2048×2048 $13.5\,\mu$m pixels. For a 60 sec exposure at optimal conditions the limiting magnitude is around $m_R \approx 18.5$, which is well suited for a study of GRB afterglows during the first hour or more and SN light curves with peak magnitude ≤ 16. The corresponding FWHM (full width at half maximum) of the stellar images is less than 2.5 pixels (8.1 arcseconds). Observations are scheduled in a queue and are processed in the order of their assigned priority. IceCube triggers have second highest priority after GRB follow-ups triggered by the GRB Coordinate Network (GCN).

Once an IceCube alert is received by one of the telescopes, the corresponding region of the night sky will be observed within seconds. A predefined observation program is started: The prompt observation includes thirty exposures of 60 seconds length. Follow-up observations are performed for 14 nights. This was extended on 2009/10/27 to 24 nights, with daily observations for 12 nights and then observations during every second night up to day 24 after the trigger was received. Eight images with 60 seconds exposure time are taken per night. The prompt observation is motivated by the typical rapidly decaying light curve of a GRB afterglow, while the follow-up observation of 14 (or 24) nights permits the identification of a rising SN light curve. In the initial phase with IC40 and IC59, the online processing latency of several hours made the search for an optical GRB afterglow unfeasible. We therefore focus on the SN light curve detection in the ROTSE data.

Image correction and calibration are performed at the telescope sites. The images of each night are combined in order to obtain a deeper image. A reference image is subtracted from each combined image using the algorithm developed by [12]. As deep images are usually not available for the positions we would like to observe, we initially choose the deepest image of our observing sequence as the reference image. In 40% of the alerts we took another deep image roughly one year later. Both SN light curves and GRB afterglows would have faded after a few weeks, and would not be present in the newly taken reference image.

All extracted objects found in the subtracted images are candidates for variable sources. However, bad image quality, failed image convolution, bad pixels and other effects frequently cause artifacts in the subtraction process, requiring further selection of the candidates. A candidate identification algorithm including a boosted decision tree is applied to classify sources according to geometrical and variability criteria. The final candidates are summarized on a web page and are inspected visually by several trained persons, who have to classifly the candidate as a SN, a variable star or a subtraction artifact. SN candidate identification by the human eye works well as shown in the galaxy zoo SN project [13]. The visual scanning was performed by three individual persons to ensure no good candidate was missed and to avoid false positives.

4 Results

This paper presents the results from the analysis of data taking in the period of 2008/12/16 to 2009/12/31. Table 1 shows the number of detected and expected doublets and triplets for the IC40 and the IC59 datasets as well as the number of detected and expected optical SN counterparts. The IceCube expectation based on a background only hypothesis was obtained from scrambled datasets. To correctly incorporate detector asymmetries, seasonal variations and up-time gaps we used the entire IC40 and IC59 datasets and exchanged the event directions randomly while keeping the event times fixed. The number of doublets shows a small excess, which corresponds to a $2.1\,\sigma$ effect and is thus not statistically significant. The expected number of randomly coincident SN detections, $N_{\mathrm{SN}}^{bg} = 0.074$, is based on an assumed core-collapse SN rate of 1 per year within a sphere with radius 10 Mpc, i.e. $2.4 \cdot 10^{-4}\,\mathrm{y}^{-1}\,\mathrm{Mpc}^{-3}$, and a Gaussian absolute magnitude distribution with mean of -18 mag and standard deviation of 1 mag for CCSN [14]. In total 31 alerts were forwarded to the ROTSE telescopes. Five could not be observed be-

Table 1: measured and expected multiplets

	SN	Doublets		Triplets	
		IC40	IC59	IC40	IC59
measured	0	15	19	0	0
expected	0.074	8.55	15.66	0.0028	0.0040

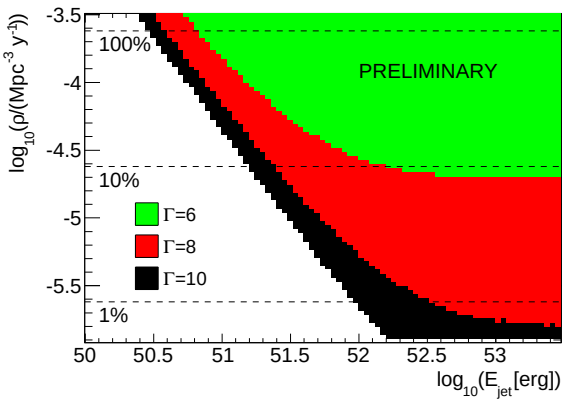

Figure 1: Limits on the choked jet SN model [5] for different boost Lorentz factors Γ as a function of the rate of SNe with jets ρ and the jet energy $E_{\rm jet}$ (colored regions are excluded at 90% CL). Horizontal dashed lines indicate a fraction of SNe with jets of 100%, 10% or 1%.

cause they were too close to the sun. For two alerts no good data could be collected. Seven alerts were discarded because the corresponding fields were too close to the galactic plane and hence too crowded. Thus 17 good optical datasets remained for the analysis. The data were processed as described above. No optical SN counterpart was found in the data.

We obtain the confidence level for different combinations of SN model parameters [5] by using a pre-defined test statistic based on a likelihood function. The limit is calculated for the jet boost Lorentz factors $\Gamma = 6, 8, 10$ as a function of the rate of SNe with jets ρ and the jet energy $E_{\rm jet}$. Systematic errors related to the simulated neutrino sensitivity and the SN sensitivity are included in the limit calculation. The 90% confidence regions for each Γ-value are displayed in the $E_{\rm jet}$-ρ-plane in figure 1 (colored regions are excluded at 90% CL). Including the optical information into the limit calculation improved the limit and allows tests of 5-25% smaller CCSN rates. The largest improvement is obtained for small jet energies and large CCSN rates. The most stringent limit can be set for high Γ-factors. Less than 4.2% of all SNe have a jet with $\Gamma = 10$ and a typical jet energy of $E_{\rm jet} = 3 \cdot 10^{51}$ erg. This is the first limit on CCSN jets using neutrino information.

5 Summary and Outlook

The optical follow-up program of IceCube neutrino multiplets realized by the four ROTSE telescopes proves the feasibility of the program. The technical challenge of analyzing neutrino data in real time at the remote location of the South Pole and triggering optical telescopes has been solved. First meaningful limits to the SN slow-jet hypothesis could be derived already after the first year of operation. Especially in cases of high boost Lorentz factors of $\Gamma = 10$ stringent limits on the soft jet SN model are obtained. Soderberg *et al.* [15] obtain an estimate on the fraction of SNe harboring a central engine from a radio survey of type Ibc SNe. They conclude that the rate is about 1%, consistent with the inferred rate of nearby GRBs. Our approach is completely independent and for the first time directly tests hadronic acceleration in CCSN, while the radio counterpart is sensitive to leptonic acceleration.

The volume of the IceCube detector has now increased to a cubic kilometer yielding a larger sensitivity to high-energy neutrinos. In addition the acquired uptime is growing continuously. The delay of processing neutrino data at the South Pole has been reduced significantly from several hours to a few minutes. This results in the possibility of a very fast follow-up and allows the detection of GRB afterglows, which fade rapidly below the telescope's detection threshold.

Because of the successful operation of the optical follow-up program with ROTSE, the program was extended in August 2010 to the Palomar Transient Factory (PTF) [16], which will provide deeper images and a fast processing pipeline including a spectroscopic follow-up of interesting SN candidates. Furthermore an X-ray follow-up by the Swift satellite of the most significant multiplets has been set up and started operations in February 2011 [17].

References

[1] Anchordoqui, L.A. and Montaruli, T., Ann. Rev. Nucl. Part. Sci., 2010, **60**: 129-162
[2] Woosley, S.E. and Bloom, J.S., Ann. Rev. Astron. Astrophys., 2006, **44**: 507-556
[3] MacFadyen, A. and Woosley, S.E., Astrophys.J., 1999, **524**: 262
[4] Razzaque, S. and Meszaros, P. and Waxman, E., Mod. Phys. Lett., 2005, **A20**: 2351-2368
[5] Ando, S. and Beacom, J.F., Phys. Rev. Lett., 2005, **95**: 061103
[6] Achterberg, A. *et al.* , Astropart. Phys., 2006, **26**: 155-173
[7] Achterberg, A. *et al.* , Astrophys.J., 2008, **674**: 357-370
[8] Abbasi, R. *et al.* , Phys.Rev.Lett., 2011, **106**: 141101
[9] Abbasi, R. *et al.* , Astron.Astrophys., 2011, **527**: A28
[10] Kowalski, M. and Mohr, A., Astropart.Phys., 2007, **27**: 533-538
[11] Akerlof, C. W. *et al.* , Publ. Astron. Soc. Pac., 2003, **115**: 132-140
[12] Yuan, F. and Akerlof, C.W., astro-ph/0801.0336, 2008
[13] Smith, A.M. *et al.* , astro-ph/1011.2199, 2010
[14] Richardson, D. and Branch, D. and Baron, E., Astron. J., 2006, **131**: 2233-2244
[15] Soderberg, A.M. *et al.* , Nature, 2010, **463**: 513-515
[16] Rau, A. *et al.* , Publ. Astron. Soc.Pac., 2009, **121**:1334-1351
[17] IceCube Collaboration, paper 535, these proceedings

SWIFT Follow-Up of IceCube neutrino multiplets

THE ICECUBE COLLABORATION[1], THE SWIFT COLLABORATION
[1]*See special section in these proceedings*

Abstract: The search for neutrinos of astrophysical origin is among the primary goals of the IceCube neutrino telescope. Point source candidates include galactic objects such as supernova remnants (SNRs) as well as extragalactic objects such as Active Galactic Nuclei (AGN), Supernovae (SNe) and Gamma-Ray Bursts (GRBs). To increase the sensitivity of the search for high-energy neutrinos from SNe and especially GRBs an X-ray follow-up with the Swift satellite has been developed. Triggered by interesting IceCube events the satellite will be repointed aiming for the detection of a transient X-ray counterpart, e.g. an X-ray GRB afterglow. In addition to typical GRBs the program is sensitive to SN shock breakouts, slightly off-axis GRBs and orphan GRB afterglows. The online event selection in IceCube as well as the X-ray observation strategy will be presented.

Corresponding Author: Andreas Homeier[2] (*ahomeier@icecube.wisc.edu*), Miles Smith[3,4] (*msmith@astro.psu.edu*)
[2]*University of Bonn*
[3]*Swift Mission Operations Team*
[4]*Penn State University*

Keywords: Neutrino, GRB, Swift, X-ray, Multimessanger

1 Introduction

1.1 Overview of the program

The X-ray Follow-Up with Swift is a multimessanger approach developed by the Swift and the IceCube collaboration to detect GRBs. It uses the IceCube neutrino telescope at the South Pole to look for signal like neutrino-multiplets (i.e. at least two neutrinos from the same direction within 100 seconds) to trigger for follow-up observations with the Swift satellite in the X-ray band. The implementation of the program makes use of the existing neutrino event selection of the Optical Follow-Up Program [1] (OFUP) at the South Pole. Neutrino multiplets are found online in quasi-real time with a typical latency of about 5 minutes. This low latency opens the possibility to search for fast decaying X-ray afterglows from GammaRaz Bursts (GRBs). Additional latency is expected on the Swift side, due to communication constraints with the spacecraft, the orbital position of Swift, and human-in-the-loop requirements for spacecraft commanding. Depending on the visibility of Swift to a ground relay station, the additional delay will be between 30 minutes to 4 hours. It is worth noting that the typical X-ray afterglow associated with long GRBs is visible to Swift for days and sometimes weeks.

1.2 Scientific Motivation

Astrophysical neutrino bursts are not necessarily always accompanied by an observable prompt electromagnetic flux but can be detected using neutrinos. Such objects could be GRBs whose narrow jets don't point directly towards earth [2] or choked GRBs [3] for which the jet may fail to penetrate the stellar envelope. Despite the lack of prompt γ-rays, the source is likely to be visible in X-rays from shock breakout after 10^3 s, and exhibit an optical counterpart similar to that seen in core collapse supernovae [4]. While no firm estimate exists, the number of these dark bursts might be ten times larger than γ-bright bursts. Therefore, the search for transient neutrino sources can to play an important part in the search for (γ-dark) GRBs, and may provide insights e.g. into the origin of the high energy cosmic rays. While an optical follow-up can be conducted by ground based telescopes (e.g. ROTSE [5]), Swift is uniquely capable of rapid follow up with X-ray observations.

NASA's Swift Explorer Mission is an ideal tool for studying the electromagnetic radiation from violent astrophysical events, such as GRBs. Three telescopes are supported by the Swift platform. A wide field of view instrument, the Burst Alert Telescope (BAT), monitors for the prompt γ-rays from a GRB. In response to a burst, Swift will slew into position to image the BAT error region with the X-Ray

Telescope (XRT) and UltraViolet and Optical Telescope (UVOT).

2 Alert chain

Swift is in high demand amongst the scientific community. Hence only limited observing time is available for the IceCube follow-up program. Using the setup of the OFUP, one obtains 25 multiplets triggers per year with IceCube. Most of these are due to atmospheric neutrinos and some atmospheric muons. The number of extensive follow-up observations can be reduced in two steps to one per year. The number of IceCube alerts can be decreased to approximately 7/year with very little loss in signal efficiency. This is achieved by making a likelihood method, as described in section 2.1. The second step involves a quick evaluation of the first available X-ray data (section 3.1), before triggering the extensive follow-up program.

2.1 IceCube Trigger Selection

For the optical follow-up program, the singlet data rate is reduced by the optical follow-up online level 3 filter [5] to $R_s \approx 2mHz$, almost reaching a pure (atmospheric) neutrino sample. Using this data sample, multiplets are selected if they arrive within $\Delta t = 100s$ and from the same direction within the reconstruction uncertainty of $\Delta\Psi = 3.5^\circ$. The trigger conditions reduce the detected number of coincident neutrinos from the isotropic background of atmospheric neutrinos to 25 false positives per year.

To maximize the discovery potential of the IceCube-Swift program a new test statistic was developed to test for the possibility that a neutrino doublet is of astrophysical origin and lies within Swift's field of view. As the derivation is beyond the scope of this paper, it is only described and motivated here. We begin with the following definitions:

$$\begin{aligned} \sigma_q^2 &= \sigma_1^2 + \sigma_2^2 \\ \sigma_w^2 &= \left(\frac{1}{\sigma_1^2} + \frac{1}{\sigma_2^2}\right)^{-1} \\ cos\psi &= \hat{r}_1 \cdot \hat{r}_2 \end{aligned} \quad (1)$$

where $\sigma_{1/2}$ are the reconstruction uncertainties of the participating neutrinos that arrive from the (reconstructed) directions $\hat{r}_{1/2}$ with an angular difference of ψ. Assuming a circular follow-up region, the test statistic

$$d = \left[\frac{\psi^2}{\sigma_q^2} + 2ln(2\pi\sigma_q^2)\right] - 2ln\left(1 - e^{-\frac{\theta_A^2}{2\sigma_w^2}}\right) + 2ln\left(\frac{\Delta t}{100s}\right) \quad (2)$$

tends to small values for signal-like doublets and larger values for background-like events. It takes various effects into account.

- The first two terms act together. While the first term favors events with a small angle ψ, indicating neutrinos from the same direction and possibly source, it also introduces a punishment for small reconstruction uncertainties. The qualitative explanation is that two neutrinos for which the error regions do not overlap are more likely background than signal. As a consequence the first term tends also to small values for large combined reconstruction uncertainties σ_q. The second term counteracts this effect, introducing a punishment for large uncertainties. Thus, the two first terms favor well reconstructed events from the same direction.

- The third term introduces the tiled Swift field of view with a radius of $\theta_A \approx 0.5^\circ$. It favors those events with small errors for which the reconstructed doublet direction matches well with the true direction, thus minimizing the possibility of observing a region of space during a follow-up which does not include the actual source within the FoV and supporting the first two terms in selecting well reconstructed events. Obviously, the Swift FoV need to be evaluated before a cut decision can be done.

- The time difference Δt between two neutrinos is considered in the fourth term. Normalized to the 100 s time window of the trigger, small values are reached for small time differences assuming they are an indicator for a neutrino bundle of an astrophysical source.

2.2 Swift Follow-Up

IceCube provides a median position resolution for selected events of less than one degree. However, the XRT field of view is only 0.4^o in diameter, which will cover only a fraction of roughly 20% of the IceCube space angle distribution. Due to the limited coverage by the XRT field of view, we are forced to tile the follow-up region with seven pointings of Swift, thus creating an artificially larger field of view. In this analysis we treat the regions where two fields overlap in an identical way to the other regions (i.e. we do not count them twice). The discovery potential for bright sources is not expected to improve for longer exposures and we choose to optimize the follow-up program for bright sources that are easily discovered in less than 1 ks. With this, a wider field is preferred over a deeper exposure.

Figure 1 shows the acceptance of an astrophysical source with an E^{-2} spectrum by the test statistic relative to the optical follow-up filter as a function of the estimated number of doublet triggers per year. Starting with loose cuts on the test statistic and 25 false positives, one can see the drop in the number of false positives as well as signal efficiency for tighter cuts reducing the background to zero doublets per year. The maximum acceptance equals 63% which is the fraction of IceCube's point spread function covered by the tiled follow-up region.

We decided to aim for seven observable alerts per year. This reduces the background by 72% while, in the case of an E^{-2} spectrum, there is only a loss of 10% (14%) for

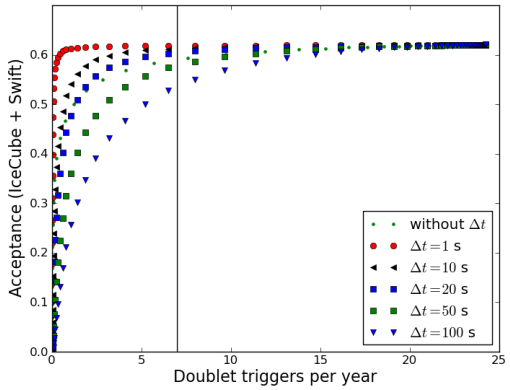

Figure 1: The acceptance of an astrophysical source with an E^{-2} spectrum of the test statistic relative to the optical follow-up filter as a function of the estimated number of doublet triggers per year. The effect of the Swift field of view is included, only accepting events within the FoV and reducing the acceptance to a maximum of 63%. It is displayed for four different cases assuming a signal with a time difference between the arriving signal neutrinos of Δt. The aim is to reduce the background to seven alerts per year.

events arriving with a time difference of 50 (100) seconds (figure 1) relative to the maximum acceptance. Almost all doublets with a short time difference will pass the cut.

3 Expected Results

Swift orbits the Earth every 96 minutes, with the IceCube trigger region becoming visible each time for approximately 2 ks. The spacecraft will be commanded to automatically observe the seven fields as soon as they rise above the Earth limb, providing approximately 285 s of observation time each per orbit. The observations will be repeated every orbit until a total of approximately 2 ks per tile is achieved, typically taking between 12 hours and a full day to complete.

In this way, any X-ray sources visible to Swift will be observed multiple times, generating a light curve. These products provide critical information for interpreting the nature of the source, possibly identifying a GRB via a typical GRB afterglow.

This might prove vital in the process of distinguishing between background sources accidentally found within the FoV and interesting transient objects. Two different significance tests are proposed. The level 1 test (section 3.1) provides a relatively quick test on the first day of data collected by Swift, to decide whether to initiate a multi-day follow-up program. The level 2 test (section 3.2), made on the full data set, provides a threshold for claiming a joint Swift-IceCube discovery of an X-ray afterglow in coincidence with an astrophysical neutrino source. The level 1 test is presented in its final form here, while the level 2 test is still under development.

3.1 Level-1 Significance Test

After several orbits, Swift may have detected one or more X-ray sources, with a position uncertainty that is typically on the order of a few arcsec, limited by the Swift XRT point spread function. The source position and an initial measurement of the flux will allow for a preliminary test of whether it stands out from the expected background of X-ray sources. The expected number of background X-ray sources depends strongly on the flux threshold. We will consider an X-ray source to have passed the level 1 significance test if it satisfies any of the following criteria for an (extra) galactic search.

A **Uncatalogued Sources:** The level 1 source is not in proximity to a catalogued X-ray object (i.e. not within 3 σ of the combined Swift and catalog position uncertainty), is brighter than a flux threshold $S_A = (5{\cdot}10^{-12})1{\cdot}10^{-10}$ erg/(cm^2 s), and occurs in a region of the sky where the ROSAT Bright Source Catalog would have observed it had it been in its current state when surveyed.

B **Variable Sources:** The source is brighter than a flux threshold $S_B = (5 \cdot 10^{-13})1 \cdot 10^{-11}$ erg/(cm^2 s) and exhibits significant variability across the first day of Swift data, with the p-value of a fit to a flat light curve being lower than some critical value P.

C **Active Catalogued Sources:** The level 1 source is within 3σ uncertainty of the position of a catalogued object but the new measurement is $M\times$ brighter than it appears in the catalog.

D **Poorly Catalogued Sources:** A source lies outside of the region covered by the ROSAT Bright Source Catalog (due to the low exposure time of ROSAT in that region) but is observed to be $M\times$ brighter than the threshold set by ROSAT for that region.

It is noted that there are significantly more serendipitous X-ray backgrounds in proximity to the galactic plane. As such, the analysis is carried out with different thresholds depending on galactic latitude (GL). Specifically, a higher threshold is used if $|GL| < 20°$.

Our intended goal is that the level 1 test will allow no more than one false positive per year. This is achieved by adjusting the above parameters (S_A, S_B, P, N, M) to keep the number of serendipitous X-ray sources to fewer than $N_S \leq 0.18$ deg^{-2}.If an X-ray source passes the level 1 test, then additional Swift data is accumulated over the following ≈ 1 week, to determine a light curve and spectrum for the source. The full data set is then utilized for the level 2 test.

The level 1 tests will first be applied once two observations have been made on each tile (i.e. after two Swift orbits). The analysis will continue on the accumulating data until the level 2 observations are triggered or a total of 2 ks have been observed for each tile, whichever is sooner. If a total of 2 ks has been accumulated for each tile without triggering the level 2 observations, then the fields will be declared uninteresting and no further observations or analysis will be carried out.

3.2 Level-2 Significance Test

Should an X-ray source be discovered that passes the level 1 test described above, a dedicated observing program will be initiated for that source. The tiled observations will be discontinued and Swift will take up a pointed observing mode, with the source at the center of a single XRT field of view (0.4° diameter). The level 2 test will determine the significance of all data accumulated over ≈ 1 week, in conjunction with the IceCube trigger data. Backgrounds will be significantly reduced from level 1 to level 2 by examining the larger data set, looking at additional features for transient behavior like the slope of the light curve, the shape of the X-ray spectrum and the source fading into obscurity.

It is anticipated that, for a given class of transient X-ray sources (GRB afterglow, AGN activity, etc), we will be limited by an irreducible background of similar events. A first estimate, based on the rate of BAT-triggered GRBs and the average light curve behavior, predicts that serendipitous GRB afterglows will be discovered only once per 3000 years with the Swift-IceCube program.

However, significant effort will be required to put a final limit on these chance events, requiring both an analysis of previously observed fields and a careful study of theoretical constraints to place limits on the number of untriggered GRBs like failed or γ-*dark* GRBs, off-axis or *orphaned* GRBs or ordinary GRBs that were not in the field of view of a telescope during the prompt outburst, but nonetheless produce a serendipitous X-ray afterglow.

Numerous studies have placed limits on the number of untriggered GRBs, typically of order 100 times the rate of regular GRBs [6, 7, 8]. This would place a limit on the Swift-IceCube level-2 false positive rate of once per 30 years.

4 Current Status and Outlook

The program was approved by the IceCube collaboration at the beginning of 2011 and is running since February, 11^{th}. Until the midst of May, one alert has been forwarded to Swift. The total latency between the neutrino events and the first observation by Swift was 90 minutes. All steps in the alert chain worked as planned and the event will be included in the final analysis of the program.

Considering the limitations in our Swift search to brighter GRBs, we use a conservative probability of 40% instead of the 90% detection efficiency of Swift for all X-ray afterglows. The OFUP has an detection efficiency of 40% for single neutrino events. Combining these two numbers with the fact that about 20% of the sky are not observable by Swift due to the sun, 13% of all GRB neutrino events could be identified as such [9]. Assuming the prediction of 10 GRB neutrinos in IceCube per year and hemisphere and requiring a doublet detection (introducing a reduction by a factor of 20 [9]) one obtains a detection rate of 0.064 GRBs per year of which 0.04 GRBs would lie within the FoV of Swift ($P_{FoV} = 63\%$). However, according to [6] there could be up to 5 times more γ-dark GRBs with an X-ray flux above our level 1 threshold of $5 \cdot 10^{-12}$ erg/(cm^2 s), increasing the number of expected detections possibly to about 0.2 GRBs per year.

A future extension triggering on high energy single neutrino events could overcome the reduction factor of 20 for doublet observations and add a signal which would be an order of magnitude higher. (these numbers might be updated and change slightly in the next week)

References

[1] A. Franckowiak for the IceCube collaboration, ICRC proceedings, 2011
[2] R. Yamazaki, K. Ioka, T. Nakamura, K. Toma , Adv. Sp. Res., 2006, **38**:1299
[3] P. Meszaros, Rept.Prog.Phys., 2006, **69**: 2259-2322
[4] S. Ando, J. F. Beacom, Phys. Rev. Lett., 2005,**95**: 171101-1 - 171101-4
[5] C. W. Akerlof et al., arXiv:astro-ph/0210238v1, 2002,
[6] T. Totani, A. Panaitescu, The Astrophysical Journal, 2002, **576**: 120-134
[7] J. Greiner et al., Astronomy and Astrophysics Supplement, 1999, **138**: 441-442
[8] Achterberg et al., The Astrophysical Journal, 2007, **664**: 397-410
[9] M. Kowalski, A. Mohr, Astropart. Phys., 2007, **27**: 533-538

32ND INTERNATIONAL COSMIC RAY CONFERENCE, BEIJING 2011

Limits on Neutrino Emission from Gamma-Ray Bursts with the 59 String IceCube Detector

THE ICECUBE COLLABORATION[1]
[1]*see special section in these proceedings*

Abstract: IceCube is the first neutrino telescope that has sensitivity to the TeV neutrino flux from GRBs below theoretical predictions and hence is able to put constraints on the model parameters and the cosmic-ray flux from GRBs above 10^{18} eV. The analysis of data from the IceCube 59-string configuration presented here is a dedicated search for neutrinos produced via $p\gamma$-interactions in the prompt phase of the GRB fireball. Yielding no significant excess above the background, the result from this analysis is then combined with the IceCube 40-string configuration result and a stringent limit on the model is set. The combined limit is 0.22 times the predicted neutrino flux. Finally, the implications for the fireball model are discussed.

Corresponding Author: Peter Redl (redlpete@umd.edu), University of Maryland

Keywords: IceCube, GRB, fireball model, neutrino

1 Introduction

Gamma-ray Bursts (GRBs) are prime candidates for the production of the highest energy cosmic rays because of the enormous energy that is released in such an event [1] ($\mathcal{O}(10^{51} - 10^{54}\mathrm{erg} \times \Omega/4\pi)$ in gamma rays, where Ω is the opening angle of a possible beamed emission). If the prime engine accelerates protons and electrons with similar efficiencies this would be sufficient energy to account for the observed ultra high energy cosmic rays. The observed gamma-rays would originate from high energy electron synchrotron emission and inverse Compton scattering, while high energy neutrons would escape the fireball's magnetic field and later decay to protons, which would be responsible for the high energy cosmic ray flux seen on Earth. The observation of high energy gamma-rays confirms the presence of high energy electrons in the fireball; however, because high energy protons are deflected in inter-galactic and the Galactic magnetic fields no direct observation of protons from GRBs is possible. Nevertheless, if high energy protons are present in the fireball along with high energy electrons it is reasonable to assume that pions will be produced through $p\gamma$ interactions near the source, which would give rise to neutrinos. Guetta et al. [2] gives a detailed account of the expected neutrino flux from such interactions and is the model that is used for the theoretical neutrino prediction in this paper. Previous searches with IceCube and other experiments have given null results, with the most recent search done in IceCube achieving a 90% upper limit that is slightly below the predicted model flux [3]. In this contribution, a further improved limit is presented, which is then combined with the previous one.

2 IceCube

IceCube is a km^3-scale neutrino detector at the South Pole sensitive to TeV-scale neutrinos and above. Construction of the detector finished in December, 2010. IceCube detects Cherenkov light emitted by secondary charged particles produced in neutrino nucleon interactions and uses that information to reconstruct neutrinos. The finished detector is made up of 5160 optical modules (DOMs), with 60 optical modules placed on each of the 86 strings. The results presented here were obtained with the 59-string configuration of IceCube, which took data from 05/20/09 to 05/31/10. IceCube is able to detect all known neutrino flavors; however, in this analysis the focus was on ν_μ. Furthermore, IceCube is sensitive to the entire sky; however, because of the large cosmic-ray muon background in the southern sky, this analysis only considers events that were reconstructed as coming from the northern sky and consequently, only GRBs in that part of the sky were analysed. In this region, the best sensitivity for ν_μ can be achieved in part because of the good angular resolution for muons (0.7° for $E_\nu \gtrsim 10$ TeV) and the low background. The background consists of mis-reconstructed muons (a reducible background) and atmospheric neutrinos (an irreducible background). Both backgrounds have a softer spectrum than the predicted neutrinos from GRBs so event

energy information can be used to improve the signal to background ratio.

3 Event Reconstruction

Events in IceCube are reconstructed by fitting the spatial and temporal Cherenkov light hit pattern observed by the DOMs in a muon event using a maximum likelihood method [4][5]. In the energy range that IceCube is sensitive to, neutrinos have sufficiently high energy for the charged current interaction between the neutrino and the nucleon to be forward and hence the muon and neutrino move in a nearly collinear manner, which enables the determination of the neutrino direction from the reconstructed muon. The shape of the likelihood space near the maximum gives an estimate of the reconstruction error of the fit [6]. In addition to knowing the direction of the neutrino, knowing the energy helps to separate signal from background. The stochastic nature of the muon energy loss in the ice, and the fact that many tracks originate outside of the detector makes it impossible to measure the energy of a muon at the neutrino-interaction point directly. Nevertheless, it is possible to measure the energy loss rate of a muon as it traverses the detector, which is correlated to the energy of the muon inside the detector for energies $\gtrsim$ 1 TeV [7]. The energy resolution achieved in this way is 0.3 to 0.4 in $\log_{10}(E)$.

4 The GRB sample

During the IC59 data taking period, 105 GRBs were observed in the northern sky and reported via the GRB Coordinates Network (GCN) [8]. Of those GRBs 9 had to be removed, because IceCube was not taking physics data. GRB090422 and GRB090423 happened during 59-string test runs before the official start of the IceCube-59 runs and were included in the final GRB list as well, which brings the final catalog to 98 GRBs. The GRB localization is taken from the satellite that has the smallest reported error. The start (T_{start}) and stop (T_{stop}) times are taken by finding the earliest and latest time reported for gamma emission. The fluence, and gamma-ray spectral parameters are taken preferentially from Fermi (GBM), Konus-Wind, Suzaku WAM, and *Swift* in this order. The gamma-ray spectra reported by the satellites were used to calculate the neutrino spectra and flux as outlined in Appendix A of [2]. The neutrino energy spectrum was calculated as a power law with two breaks, with the first break corresponding to the break in the photon spectrum and with the second break corresponding to synchrotron losses of muons and pions (Fig 1). GCN does not always report values for all of the parameters used in the neutrino spectrum calculation. In that case average values are used for the parameters not measured by the satellites. GRBs are classified into two groups: long soft bursts, which are all bursts with a duration longer than 2 seconds and short-hard bursts, which are all bursts with a duration of less than 2 seconds. Average parameters from [3] were used.

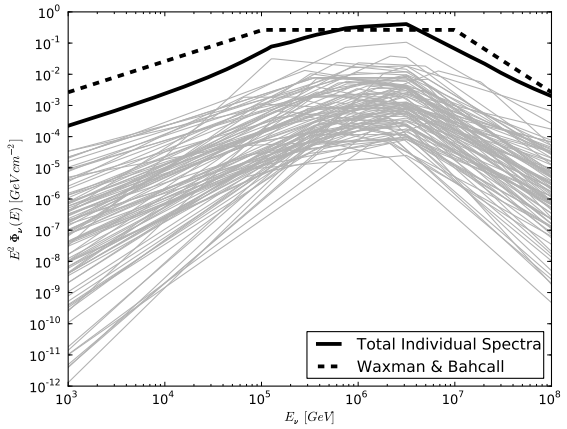

Figure 1: Neutrino spectra of the GRBs used in this analysis. The thin lines represent the individual bursts while the solid thick line represents the sum of all bursts. Finally, the dashed line shows the Waxman 2003 [9] prediction normalized to the number of GRBs observed.

5 Analysis

The analysis presented here was designed to be sensitive to neutrino production from $p\gamma$ interactions in the prompt phase of the fireball. To separate signal from background a Boosted Decision Tree [10] was trained. The analysis was then optimized for discovery with respect to the Boosted Decision Tree score. The optimized value resulted in a final data sample of 85% atmospheric neutrinos and 15% miss-reconstructed cosmic ray muons in the off time data sample (any events not within $\pm$2 hours of a GRB). An unbinned maximum likelihood search [11] was performed and each event passing the boosted decision tree cut was assigned a probability of being a signal event from a GRB or a background event. The final likelihood is the product of three PDFs based on the location of an event with respect to a GRB, the timing information of the event with respect to the prompt gamma-ray emission, and the energy. The directional signal PDF is a two-dimensional Gaussian:

$$\mathrm{PDF}_i^S(\vec{x}) = \frac{1}{2\pi(\sigma_i^2 + \sigma_{GRB}^2)} e^{\frac{|\vec{x}_i - \vec{x}_{GRB}|^2}{2(\sigma_i^2 + \sigma_{GRB}^2)}} \qquad (1)$$

where σ_i is the directional uncertainty for the i^{th} event and σ_{GRB} is the uncertainty of the GRB location as reported by GCN. $|\vec{x}_i - \vec{x}_{GRB}|$ is the angular difference between the reconstructed muon direction and the GRB location reported by GCN. The background spacial PDF was constructed from off-time data, taking into account the direction-dependent acceptance of the detector.

The time PDF is flat over the duration (T_{100}) of the burst and falls off smoothly as a Gaussian on either side. The

width, σ, of the Gaussian is equal to the T_{100} of the burst with a minimum of 2 s and a maximum of 25 s .

The third component of the likelihood is an energy PDF. In previous analyses, a single energy PDF for the whole northern sky was used [3, 11]. However, because the Earth is opaque to neutrinos above ~ 100 TeV, the northern sky was split into three zenith regions in order to account for this effect. The signal energy PDFs were computed from the reconstructed muon energy-loss (dE/dx) from signal simulation and averaged over all GRBs in a region. The energy background PDF was computed from the dE/dx distributions of all off-time data in each region.

The final likelihood is maximized by varying the assumed number of signal events n_s and a test statistic λ is computed from the likelihood ratio $L(n_s = \hat{n}_s)/L(n_s = 0)$, where $\hat{n}_s$ is the number of signal events for the maximized likelihood. A distribution, λ, for the background-only case is constructed from off-time data by scrambling it in time a sufficient number of times. By comparing the λ value for the on-time data with the background-only distribution a p-value for the measurement is derived, which is a measure for the compatibility of the measurement with the background-only hypothesis.

6 Result

No events were found in the on-time data to be on-source (within 10° of a GRB) and on time with a GRB and the likelihood maximization yielded $\lambda = 0$. In total 24 background events (not necessarily on source) were expected to be in the total time window and 21 were observed (none on-source). From the Guetta et al. model [2] 5.8 signal events were predicted and a final upper limit of 0.46 times the predicted flux can be set. This limit includes a 6% systematic uncertainty. The systematic uncertainty is estimated by varying parameters in the signal simulation and recomputing the limit, with the dominant factor being the efficiency of the DOMs (the uncertainty of the DOM-efficiency is $\sim 10\ \%$).

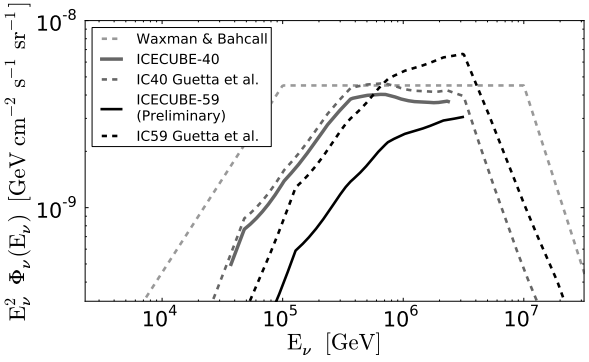

Figure 2: This plot shows the result of this analysis along with the result of the previous analyses. The flux lines from the predictions from Guetta et al. [2] and Waxman 2003 [9] are shown as well.

The corresponding model dependent result presented in a previous analysis [3] sets a limit of 0.82 of the model flux. This limit was obtained using data from the IceCube detector in the 40-string configuration. It is possible to combine this limit with the limit presented in this paper [3], because both analyses obtain a null result. The limits are combined by using signal simulation from each analysis and combining them into one signal simulation data set. From the combined signal data set a new limit is calculated by finding the fraction of total signal flux that would have yielded a *test statistic* that was greater than zero in either analysis in 90% of the cases. This new fractional signal flux is the combined limit and is 0.22 times the flux calculated according to Guetta et al. [2]. Systematic uncertainties were handled by combining the worst limit from each analysis which makes the combined limit conservative with respect to systematic uncertainties. Figure 3 shows the combined limit from these two analyses.

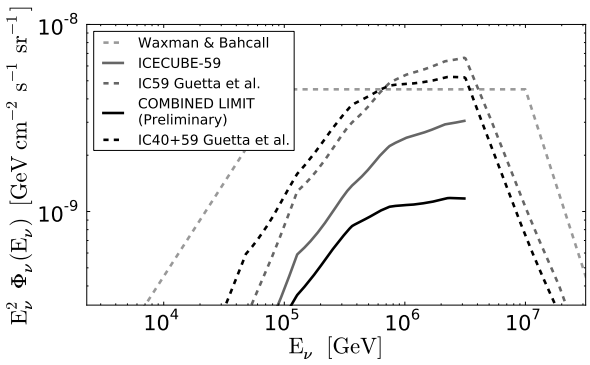

Figure 3: The combined limit of the IC40+59 analysis is shown in addition to the limits and flux predictions displayed in Fig.2.

7 Discussion

Previous results have excluded the neutrino production models outlined in [2] and [9] at a level where it may still have been explained by statistical fluctuations. This analysis is able to exclude the models with high confidence and if the result is combined with the previous result the model in question is strongly disfavored. The caveat is that there are parameters in the model for which average values, or theoretically calculated values are used, because they are not measured (or rarely measured) by the satellites. The bulk Lorentz Factor Γ is one of these values. The lower limit on this value is established by pair production arguments [2], but the upper limit is less clear. Recent papers [12, 13, 14] suggest that Γ can take values of up to 1000 (316 was used in this analysis as well as in [11, 3]). Γ is an important parameter, because in this analysis the GRBs that have the highest neutrino expectation also have the highest energy gamma-rays observed by Fermi's LAT [15]. Because of pair production arguments [2], this indicates higher Γ factors, which implies that the theoretical

brightest GRBs in the neutrino sky would be suppressed in practice. Another unmeasured parameter that could contribute to the non-detection of a neutrino flux from GRBs is the variability of the observed γ-ray light curve, t_{var}. This parameter is assumed to be the characteristic time scale between the collision of different shock fronts in the GRB fireball. Conceptually, if this time is shorter, shock fronts will collide more frequently, causing a greater number of accelerated particles and therefore more neutrinos. Recent limits on t_{var} indicate that if t_{var} is varied by a factor of 10 (either higher or lower) UHECR could still be explained as originating from GRBs [16]. Therefore, t_{var} was varied by a factor of 10 and the limit was recomputed in incremental steps from $0.1 - 10$ times the standard t_{var} value. In Fig. 4 the limit of this analysis is plotted as a function of Γ and t_{var}. It is also useful to ask, how well IceCube will do in

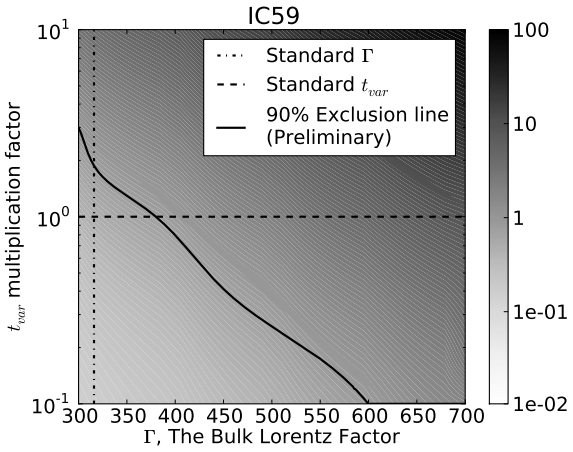

Figure 4: Limit set by the IC59 analysis as a function of the t_{var} multiplication factor and Γ assuming the Guetta et al. model [2]. The gray scale indicates the fraction of the model flux that can be excluded at each point of the phase space at 90% CL. The thick black line indicates where $1\times$ the model can be excluded at $90\ \%$ CL, while the dashed lines indicated the standard values used in this analysis. The excluded region is the region found to the left and below the exclusion line.

the 86-string configuration with respect to constraining this parameter space. To get a handle on this the GRB catalog from the 59-string configuration was used to estimate the 86-string sensitivity from Monte Carlo simulations. The result for 3-years of 86-string operation is plotted in Fig. 5. As seen from the plot, 3-years of IceCube-86 can exclude a large portion of the allowed parameter space with the portion that is not excluded being disfavored by theory. The parameters that are treated here are not the only variable parameters in the model that are important to the neutrino flux. However, the above parameters alone could account for the null result seen in IceCube so far. Future observations with the completed IceCube detector will be able to exclude or confirm GRBs as the major sources of UHECR production in a few years.

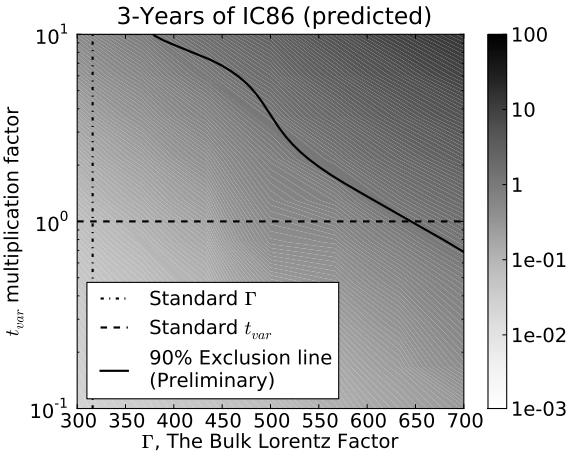

Figure 5: Projected sensitivity of IC86 after 3 years of operation with respect to Γ and t_{var}.

References

[1] E. Waxman. *Phys. Rev. Lett.*, 75:386–389, July 1995.

[2] D. Guetta, D. Hooper, J. Alvarez-Muñiz, F. Halzen, and E. Reuveni. *Astroparticle Physics*, 20:429–455, January 2004.

[3] R. Abbasi et al. *Phys. Rev. Lett.*, 106:141101, 2011.

[4] J. Ahrens, (AMANDA Collaboration), et al. *Nucl. Instrum. and Meth. A*, 524:169–194, May 2004.

[5] N. van Eijndhoven, O. Fadiran, and G. Japaridze. *Astropart. Phys.*, 28:456–462, 2007.

[6] T. Neunhöffer. *Astroparticle Physics*, 25:220–225, April 2006.

[7] Sean Grullon, David Boersma, Gary Hill, Kotoyo Hoshina, and K. Mase. In *Proc. of 30th ICRC, Merida, Mexico*, 2007.

[8] GRB Coordinates Network. `http://gcn.gsfc.nasa.gov`.

[9] E. Waxman. *Nucl. Phys. B Proc. Suppl.*, 118:353–362, April 2003.

[10] Andreas Hoecker, Peter Speckmayer, Joerg Stelzer, Jan Therhaag, Eckhard von Toerne, and Helge Voss. *PoS*, ACAT:040, 2007.

[11] R. Abbasi, (IceCube Collaboration), et al. *ApJ*, 710:346–359, February 2010.

[12] Johan Bregeon et al. *Astrophys. J.*, 729:114, 2011.

[13] En-Wei Liang et al. *Astrophys. J.*, 725:2209–2224, 2010.

[14] Alicia M. Soderberg and Enrico Ramirez-Ruiz. *AIP Conf. Proc.*, 662:172–175, 2003.

[15] NASA. Fermi: Gamma ray space telescope. 2008. `http://fermi.gsfc.nasa.gov/`.

[16] M. Ahlers, M. C. Gonzalez-Garcia, and F. Halzen. *submitted to ApJ*, 2011. arXiv:1105.2326.

Detecting Neutrinos from Choked Gamma Ray Bursts with IceCube's DeepCore

THE ICECUBE COLLABORATION[1]
[1]*See special section in these proceedings*

Abstract: The detection of astrophysical point sources of neutrinos is a prime goal of the IceCube neutrino telescope. Probable high-energy neutrino sources of interest include transient events such as core-collapse supernovae and gamma ray bursts (GRBs). It has been proposed that jets are present not only in supernovae that lead to long GRBs but also more frequently in so called choked GRBs that lack a high-energy electromagnetic signature. Choked GRBs may be detectable by IceCube's DeepCore subdetector. The transient nature of these events coupled with the angular direction and current filtering algorithms should allow strong background rejection. We will present simulations of choked GRB signal at trigger level and with preliminary data selection cuts applied.

Corresponding authors: Jacob Daughhetee [2] (*daughjd@gatech.edu*), IgnacioTaboada[2] (*ignacio.taboada@gatech.edu*)
[2] *School of Physics. Georgia Institute of Technology, Atlanta, USA*

Keywords: IceCube, DeepCore, GRB, neutrino

1 Introduction

Long duration gamma-ray bursts (GRBs) have shown a strong association with core collapse supernovae [1]. The leading model of GRBs attributes the production of gamma rays to Fermi-accelerated electrons in internal shocks of relativistic jets driven by the core collapse of the progenitor [2]. These GRBs require heavy progenitors ($M \geq 25$ $M_{\odot}$) and highly relativistic jets (Lorentz boost factor $\Gamma \geq 100$) that break through the surrounding stellar envelope. Although long duration GRBs appear correlated with supernovae, very few ($\leq 10^{-3}$) observed supernovae themselves are associated with GRBs [3].

It is conceivable that a large fraction of core collapse SNe produce mildly relativistic jets. Unlike GRBs, these jets never breach the stellar envelope and are essentially 'choked' within the progenitor. The inability of the jet to break through the envelope could arise from either the envelope itself being more massive than that of a GRB event or simply due to a lack of sufficient energy. These choked GRBs could be part of a continuum class of astronomical objects with long duration GRBs (having highly relativistic jets) representing the far end of the spectrum. Recently, evidence for mildly relativistic jets has been observed in supernovae 2007gr [4] and 2009bb [5], as well as in the observed asymmetry in the explosions of core collapse supernovae [6, 7]. This lends credence to the notion that central engines with less relativistic jets might occur more frequently than observable, fully developed GRBs.

Both hidden and visible jets can accelerate protons in shocks, resulting in the production of neutrinos. Despite lacking an elecromagnetic signature like typical GRBs, these choked GRB events would still have an associated burst of neutrinos that could provide information about hidden jets. One model for this type of event has been proposed by Razzaque, Mészáros and Waxman [8], and it has been extended upon by Ando and Beacom to include kaon production [9]. This model will hereafter be referred to as RMW/AB. The neutrino spectrum predicted by RMW/AB is fairly soft but high in fluence, and should be within reach of the IceCube detector ($\geq$ 100 GeV sensitivity) and the DeepCore subdetector ($\geq$ 10 GeV sensitivity). Due to the soft nature of the RMW/AB spectrum, DeepCore will be better suited to detecting choked GRBs.

IceCube is a neutrino detector located at the South Pole optimized for neutrino energies on the TeV scale. Finished in December of 2010, it detects Cherenkov light emitted by secondary charged particles produced in a neutrino nucleon interaction. The completed detector is made up of 5160 optical modules, with 60 optical modules placed on each of the 86 strings. These optical modules contain PMTs with onboard digitizers and are more succintly referred to as DOMs (Digital Optical Modules). The DeepCore subarray includes 8 densely instrumented infill strings optimized for low energies plus 12 adjacent standard IceCube strings.

Complete PMT waveforms are recorded by the DOMs that meet the Hard Local Coincidence (HLC) condition. HLC requires hits in a DOM and its nearest or next to nearest neighbor in a time window of $\pm$ 1 μ sec. IceCube also

records compact information for Soft Local Coincidence, or SLC, hits that do not meet HLC. DeepCore's trigger requires 3 HLC hits in a time window of 2.5 μ sec.

Despite its smaller detector volume, DeepCore's enhanced sensitivity to lower energies greatly increases the observable flux. In addition, the location of DeepCore inside the IceCube detector should allow for significant background rejection through utilization of IceCube itself as a veto. For these reasons this analysis focuses on simulating the response of the DeepCore detector under its standard triggering and filtering, and we calculate the expected event count from a sample choked GRB for the fully completed DeepCore under the RMW/AB model.

2 Neutrino Production in Jets

The RMW/AB model assumes a mildly relativistic baryon-rich jet with a bulk Lorentz factor Γ_b = 3 and an opening angle $\theta_j \sim \Gamma_b^{-1}$ = 0.3. The kinetic energy of the jet is set to E_j = 3×10^{51} erg, a typical energy for GRBs. The variability timescale of the engine mirrors that of observed GRBs as well and is set as $t_v \sim 0.1$ s. Shocks within the jet accelerate protons with a spectrum $\sim E_p^{-2}$ up to a maximum proton energy of 2×10^6 GeV determined by the acceleration timescale and radiative cooling. Neutrinos are the product of the kaons and pions produced in p-p interactions of the accelerated protons with the stellar envelope. Energies and densities involved are similar to those in neutrino production in the Earth's atmosphere. In the case of neutrinos from pion decay, the neutrino flavor flux ratio $\phi_{\nu_e} : \phi_{\nu_\mu} : \phi_{\nu_\tau}$ is 0:1:0. Secondary neutrinos from muon decays can be ignored here because the muons from pion decay are immediately subjected to radiative cooling. As for neutrinos from kaon decay, the small flux of ν_e from K_L^0 decay is neglected by RMW/AB. Thus, a flavor flux ratio of 0:1:0 is also assumed for neutrinos from kaon decay. After accounting for vacuum oscillations, the expected flavor flux ratio at Earth becomes ∼1:2:2 for both contributions. Neutrinos are emitted over a time window of O(∼10 s), set by the star's size ($\Delta t \sim R_\star/c$).

The shape of the neutrino spectrum is dependent upon that of the mesons from the p-p interactions. Initially, these mesons have the same E^{-2} spectrum as the protons, but mesons undergo hadronic and radiative cooling before decay. The result is a meson spectrum with two break energies at which the spectrum becomes steeper. The neutrino spectrum will match the meson spectrum, and it can be modeled as a doubly broken power law. For a given supernova at 10 Mpc with Γ_b = 3, opening angle $\theta_j \sim \Gamma_b^{-1}$ = 0.3, and $E_j = 3 \times 10^{51}$ erg, the spectrum is of the form:

$$\frac{d\Phi_\nu}{dE} = F_\nu \begin{cases} E^{-2} & E > E_\nu^{(1)} \\ E_\nu^{(1)} E^{-3} & E_\nu^{(1)} < E < E_\nu^{(2)} \\ E_\nu^{(1)} E_\nu^{(2)} E^{-4} & E_\nu^{(2)} < E < E_{max} \end{cases} \quad (1)$$

F_ν is the all flavor flux normalization where $d\Phi_\nu/dE$ is 5×10^{-2} GeV^{-1}cm^{-2}(5×10^{-5} GeV^{-1}cm^{-2}) at $E_\nu^{(1)}$ for pions(kaons). The break energies $E_\nu^{(1)}$ and $E_\nu^{(2)}$ denote the onset of hadronic and radiative cooling respectively where $E_\nu^{(1)}$=30 GeV (200 GeV) and $E_\nu^{(2)}$=100 GeV (20 TeV) for pions(kaons). The neutrino flux from both pion and kaon contributions is shown as a function of energy in Fig. 1.

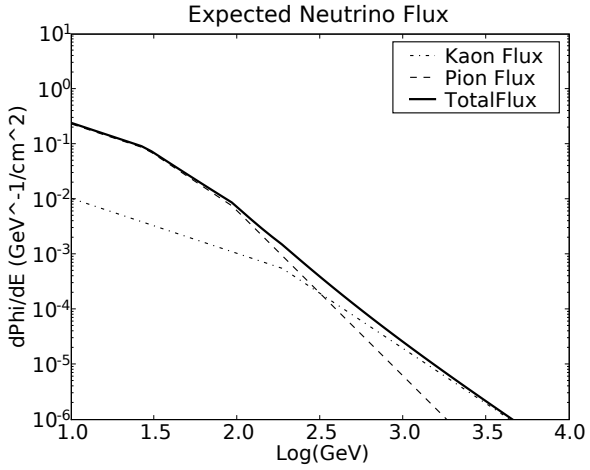

Figure 1: All flavor neutrino flux from pion, kaon and combined contributions.

3 Effective Area of DeepCore and Expected Events

We calculate the expected number of observed IceCube+DeepCore neutrino events N_{obs} given a flux $d\Phi_\nu/dE$ and detector effective area A_{eff} by

$$N_{obs} = \int dE A_{eff}(E) \frac{d\Phi_\nu}{dE} \quad (2)$$

In order to properly estimate the number of expected events from an astrophysical source, the neutrino effective area must be calculated through detailed simulation of a benchmark incident flux and the detector hardware. We briefly describe the calculation of the effective area.

The effective area of the detector has been calculated by simulating neutrinos in the nearby volume surrounding the detector, propagating them, and forcing them to interact (preventing the simulation of events that do not interact within the volume). These events are re-weighted to reflect the probability that the interaction would actually occur. All flavors of neutrinos used in this proceeding were simulated with NUGEN (a modified version of ANIS [10] that works with IceCube software). Simulation with NUGEN includes several effects including the ice/rock boundary below the detector, Earth neutrino absorption, neutral current regeneration, etc. The flavor flux ratio is taken from the ratio predicted by the RMW/AB jet model for neutrinos originating from both pions and kaons. Vacuum oscillations are

included [11], and the ratio of neutrino to anti-neutrino is assumed equal for all flavors. The propagation of muons within the detector has been simulated with MMC [12]. Detection of events is determined by simulating the detector response to light produced by the daughter lepton (or cascade) of the interacting neutrino. Events are considered detected if they activate the standard DeepCore trigger. The calculated neutrino effective area under the standard DeepCore trigger is shown for all flavors in Fig. 2.

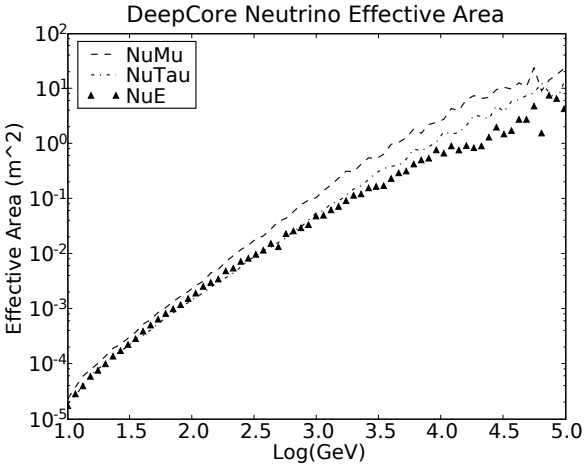

Figure 2: Effective area of the DeepCore detector given standard DeepCore SMT3 triggering for all flavor (ν_e-triangle symbols, ν_μ-dashed line, ν_τ-dashdot line). The effective area has been averaged over the entire sky.

As Fig. 2 shows, higher energy ν_μ events are significantly more visible than either ν_e or ν_τ. This can be attributed to muons produced outside of the physical DeepCore volume that then propagate near or through the ice occupied by DeepCore DOMs. At lower energies however, these muon tracks become shorter and more closely resemble cascade events.

It should be noted that there are some aspects of the simulation which are not accurate. Although NUGEN performs adequately at higher energies typical of IceCube analyses ($\geq$ 100 GeV), the cross-sections, and consequently interaction probabilites it predicts, lose accuracy at lower energies (between 10-100 GeV). This is particularly true for ν_τ as the simulation used does not properly take into account the kinematics of the τ lepton, and it is likely that the actual rate of ν_τ will be appreciably lower.

Combining the calculated effective areas with the flux predicted by the RMW/AB model via Eq. 1 yields an estimation on N_{obs} for the DeepCore detector. The number of expected events by flavor and the predicted background rate are listed in Table 1.

The result for a reference supernova at 10 Mpc is an all-flavor expectation of $\sim$10.5 events in the IceCube+DeepCore detector under standard DeepCore triggering. This event expectation is subject to large variation due to uncertainties in the jet parameters of the RMW/AB model. After application of the DeepCore filter, which discards events that show causal relation to hits in the non-DeepCore IceCube strings (veto region), the all-flavor event expectation is about 9 events. This decrease in events is mostly due to the rejection of ν_μ and ν_τ interactions outside of DeepCore's fiducial volume. Events with the best possibility of reconstruction will be those neutrinos that interact within the DeepCore fiducial volume. Therefore, it is of interest to estimate the number of events that actually interact inside DeepCore. Examination of the simulated interaction vertices reveals the number of trigger level events originating in DeepCore to be 5.7 (1.1 due to ν_e, 2.4 due to ν_μ, and 2.2 due to ν_τ). The predicted event spectra for all flavors at trigger level is shown as a function of energy in Fig. 3.

Flavor	Trigger	Filter	Preliminary Data Cuts
ν_e	1.6	1.5	1.5
ν_μ	4.6	3.9	3.3
ν_τ	4.3	3.6	3.1
Corsika	250 Hz	7 Hz	1.2 Hz

Table 1: Event expectation in DeepCore by flavor for RMW/AB model choked GRB at 10Mpc. Background is simulated with CORSIKA, and rates are estimated by taking the product of the DeepCore trigger rate and the simulated rejection factor at each cut level. Event estimation for ν_τ may be overly optimistic due to issues in NUGEN simulation at lower energies.

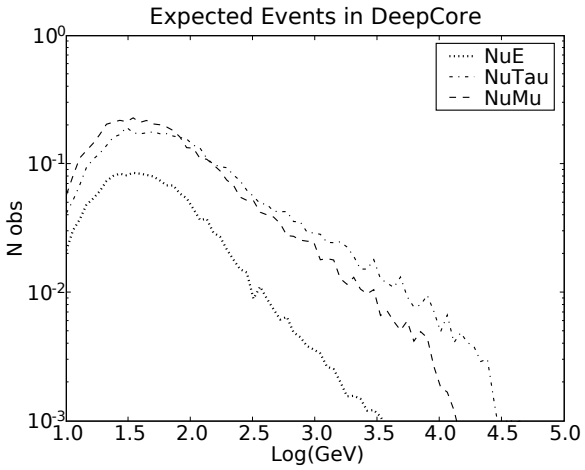

Figure 3: Expected trigger level signal in DeepCore as a function of energy for all flavors.

The plot shows a peak in event expectation at about 40 GeV for all flavors. This places most of the expected events below the typical IceCube threshold and well into the energy range of DeepCore.

4 Atmospheric Muon and Neutrino Background

A major goal of the DeepCore detector is to open up the southern sky to analysis to obtain a full 4π sr view. In order

to do this, extensive steps towards reducing the large atmospheric muon background must be taken. The expected rate of atmospheric neutrinos in DeepCore is about 10^5 events per year over 2π while the atmospheric muon rate in DeepCore is a factor of $\sim 10^6$ larger. We are currently developing techniques to be used in conjunction with the IceCube veto that will allow for a rejection of atmospheric muons by a factor $\geq 10^6$ while maintaining high signal efficiency. For more information on DeepCore and its background rejection capabilities, see reference [13].

We have already begun investigating other background rejection methods. Some possible simple cuts include a modified version of the current filter, an algorithm using a reconstruction to search for correlated single detector hits (such hits are often cleaned in analysis), and a cut on the ratio of DOM hits inside and outside of the DeepCore detector. Taken in combination, these three additional data cuts can reduce background after standard filtering by an additional factor of six while maintaining a signal efficiency of $\sim$94%. The effect of these cuts on the number of expected events is shown in Table 1. Any future analyses will require a reduction in background to about the atmospheric neutrino level ($\sim$ 3 mHz).

5 Discussion

By simulating a choked GRB in accordance with the RMW/AB model, we have predicted the expected neutrino event count in the IceCube+DeepCore detector. For a reference supernova at 10 Mpc with a bulk Lorentz boost factor Γ_b = 3, opening angle $\theta_j \sim \Gamma_b^{-1}$ = 0.3, jet energy $E_j = 3 \times 10^{51}$ erg, and time variability $t_v \sim 0.1$ s, we expect $\sim$10.5 trigger level neutrino events in DeepCore. This level of event expectation would make a search for neutrinos in coincidence with known supernova on a distance scale $\sim$ 10 Mpc possible.

One possibile sensitivity enhancement is the expansion of DeepCore to a 2-layer IceCube veto (roughly doubling the detector volume used). This option would be particularly useful in a search for correlated neutrinos from known sources. The higher rate of background acceptance brought on by expanding the detection volume should be mitigated by the increase in signal rate for an overall increase in detection capability.

We also expect the event rate predictions to be modified when a more accurate simulation of the detector response is implemented. Most of this improvement will come from the use of superior neutrino cross-section simulation provided by GENIE [14]. A version of GENIE compatible with IceCube software has recently been developed to simulate lower energy neutrinos with much greater accuracy than that of the NUGEN based simulation used presently. This will greatly improve the simulation of ν_τ events in particular, which, due to oscillations, constitute $\sim$ 40% of the incident flux.

One promising method for searching for neutrino bursts from choked GRBs is a rolling time window search [15]. In this type of search, a time window for bursts is set by the characteristic neutrino emission time ($\Delta t \sim R_\star/c$). This fixed time window slides across the dataset looking for a statistical excess of events. For choked GRBs, the time window would be about 10-100 s. Only background events falling inside a time window seeing an excess would be kept, thus greatly reducing the amount of background accepted. An advantage of the rolling search is that it is not dependent on any optical observations, allowing it to look for photon-dark neutrino sources as expected for choked GRBs.

In addition to searching for choked GRBs, it may also be possible for DeepCore to detect neutrinos from high luminosity GRBs. A model using parameters inferred from observations by *Fermi* developed by P. Mészáros and M.J. Rees predicts a neutrino spectrum of luminosity comparable to the photon component [16]. The model predicts a muon neutrino energy spectrum centered around $\sim$ 12 GeV. We are curently investigating the event rate expected in DeepCore.

Observations of neutrinos in the DeepCore detector on the order of 10-100 GeV in coincidence with supernova would be strong evidence for the existence of choked jets from the central engine. Such an observation would help to uncover the relationship between long duration gamma ray bursts and core collapse supernovae, a relationship that is not currently fully understood.

References

[1] S. E. Woosley and J. S. Bloom, Ann. Rev. Astron. Astrophys., 2006, **44**: 507-556

[2] B. Zhang, P. Mészáros, Int. J. Mod. Phys. A, 2004, **19**: 2385.

[3] E. Berger et al., Astrophys. J., 2003, **599**: 408.

[4] Z. Paragi et al., Nature, 2010, **463**: 516.

[5] A.M. Soderberg et al., Nature, 2010, **463**: 513.

[6] J.R. Maund et al., Astrophys.J (to be published); arXiv:0909.2841.

[7] M. Tanaka et al., Astrophys.J, 2009, **700**: 1680

[8] S. Razzaque, P. Mészáros and E. Waxman, Phys. Rev. D, 2003, **68** (083001).

[9] S. Ando and J.F. Beacom, Phys. Rev. Lett., 2005, **95** (061103).

[10] A. Gazizov and M. Kowalski, Comput. Phys. Commun., 2005, **172**: 203.

[11] S. Razzaque, A. Yu. Smirnov, JHEP, 2010, **3**: 31.

[12] D. Chirkin and W. Rhode (unpublished). arXiv:hep-ph/0407075.

[13] C. Wiebusch et al., in *proceedings of the 31st Int. Cosmic Ray Conf., Lodz, Poland, 2009*; arXiv:0907.2263.

[14] C. Andreopoulos et al., Nucl.Instrum.Meth.A, 2010, **614**: 87-104.

[15] Achterberg A. et al., Astrophys. J., 2007, **664**: 397.

[16] P. Mészáros and M.J. Rees, ApJ, 2011, **733**: L40.

32ND INTERNATIONAL COSMIC RAY CONFERENCE, BEIJING 2011

Neutrino triggered high-energy gamma-ray follow-up with IceCube

THE ICECUBE COLLABORATION[1]
[1]*See special section in these proceedings*

Abstract: We present the status of a program for the generation of online alerts issued by IceCube for gamma-ray follow-up observations by Air Shower Cherenkov telescopes (e.g. MAGIC). To overcome the low probability of simultaneous observations of flares of objects with gamma-ray and neutrino telescopes a neutrino triggered follow-up scheme is developed. This mode of operation aims at increasing the availability of simultaneous multi-messenger data which can increase the discovery potential and constrain the phenomenological interpretation of the high energy emission of selected source classes (e.g. blazars). This requires a fast and stable online analysis of potential neutrino signals. We present the work on a significance based alert scheme for a list of phenomenologically selected sources. To monitor the detector and the alert system reliability, monitoring systems have been implemented on different levels. We show data from the first weeks of running this system.
Corresponding authors: Robert Franke[2] (*robert.franke@desy.de*), Elisa Bernardini[2] (*elisa.bernardini@desy.de*)
[2]*DESY Zeuthen, 15738 Zeuthen, Germany*

Keywords: IceCube, neutrino, NToO, blazars

1 Introduction

The major aim of neutrino astrophysics is to contribute to the understanding of the origin of high energy cosmic rays. A point-like neutrino signal of cosmic origin would be an unambiguous signature of hadronic processes, unlike γ-rays which can also be created in leptonic processes. The detection of cosmic neutrinos is however very challenging because of their small interaction cross-section and because of a large background of atmospheric neutrinos. Parallel measurements using neutrino and electromagnetic observations (the so-called "multi-messenger" approach) can increase the chance to discover the first neutrino signals by reducing the trial factor penalty arising from observation of multiple sky regions and over different time periods. In a longer term perspective, the multi-messenger approach also aims at providing a scheme for a phenomenological interpretation of the first possible detections.

The search of occasional flares with a high-energy neutrino telescope is motivated by the high variability which characterizes the electromagnetic emission of many neutrino candidate sources. Recent results obtained by the IceCube Collaboration [1] indicate that high-energy neutrino telescopes have reached a sensitivity to neutrino fluxes comparable to the observed high energy gamma-ray fluxes of Blazars in the brightest states (e.g. the flares of Markarian 501 in 1997 [2] and Markarian 421 in 2000/2001 [3]). With the assumption that the possibly associated neutrino emission would be characterized by a flux enhancement comparable to what is observed in gamma-rays in such states, neutrino flares could be extracted from the sample of neutrino-like events with a reasonable significance.

These astrophysical neutrinos can be searched for in several ways. Here we present a methods for a neutrino point source search that looks for events coming from a restricted angular region, which could be identified with a known astrophysical object. Finding neutrino point sources in the sky means to locate an excess of events from a particular direction over the background of cosmic-ray induced atmospheric neutrinos and muons. These events might present additional features that distinguish them from background, for example a different energy spectrum or time structure. For sources which manifest large time variations in the emitted electromagnetic radiation, the signal-to-noise ratio can be increased by searching for periods of enhanced neutrino emission (a time-dependent search). Of special interest is the relation of these periods of enhanced neutrino emission with periods of strong high-energy γ-ray emission. However, as Imaging Air Cherenkov Telescopes (IACTs) have a small field-of-view and are not continuously operated such correlation studies are not always possible to do after the fact. Therefore it is desirable to ensure the availability of simultaneous neutrino and high-energy γ-ray data for periods of interests. This is achieved by an online neutrino flare search that alerts a partner IACT ex-

periment when a possible neutrino flare from a monitored source is detected.

Such a Neutrino Triggered Target of Opportunity program (NToO) using a list of pre-defined sources was developed already in 2006 using the AMANDA array to initiate quasi-simultaneous gamma-ray follow-up observations by MAGIC [4]. We present here a refined and enhanced implementation using the IceCube neutrino detector.

IceCube is a one cubic kilometer neutrino detector operating in the glacial ice at the geographical South Pole. It consists of 86 strings equipped with 5160 digital optical modules (DOMs). Each DOM contains a photomultiplier tube to detect Cherenkov light of charged ultra-relativistic particles.

2 Neutrino event selection

The basis for the neutrino event selection is an on-line filter that searches for high-quality muon tracks. The full-sky rate of this filter is about $35\,\mathrm{Hz}$ for IceCube in its 2010/2011 configuration with 79 deployed strings. This rate is strongly dominated by atmospheric muons. As the computing resources at the South Pole are limited one can not run more elaborate reconstructions at this rate, so a further event selection has to be done. This so called Online Level2 filter selects events that were reconstructed as upgoing ($\theta > 80°$, $\theta = 0°$ equals vertically down-going tracks) with a simple likelihood reconstruction that only takes into account the arrival time of the first photon at each Digital Optical Module. By requiring a good reconstruction quality the background of misreconstructed atmospheric muons is reduced. The parameters used to assess the track quality are the likelihood of the track reconstruction, the number of unscattered photons with a small time residual w.r.t. the Cherenkov cone and the distribution of these photons along the track. The reduced event rate of approximately $3.6\,\mathrm{Hz}$ can then be reconstructed with more time intensive reconstructions, like a likelihood fit seeded with different tracks (iterative fit) and a likelihood-fit that takes into account the total number of photo-electrons registered in each module (multi-photoelectron fit). Based on this reconstruction the final event sample is selected by employing a zenith angle cut of $\theta > 90°$ for the multi-photoelectron fit and further event quality cuts based on this reconstruction. These cuts are optimized to achieve a good sensitivity for flares of different time durations. The event selection results in a median angular resolution of $0.48\,°$ for an E^{-2} signal neutrino spectrum, the median resolution for events with $E > 10^6\,\mathrm{GeV}$ is $< 0.4\,°$. For each event an angular uncertainty estimate is calculated.

The resulting event rate compared to the rate of atmospheric neutrinos as predicted by Monte Carlo as a function of zenith angle can be seen in Figure 1.

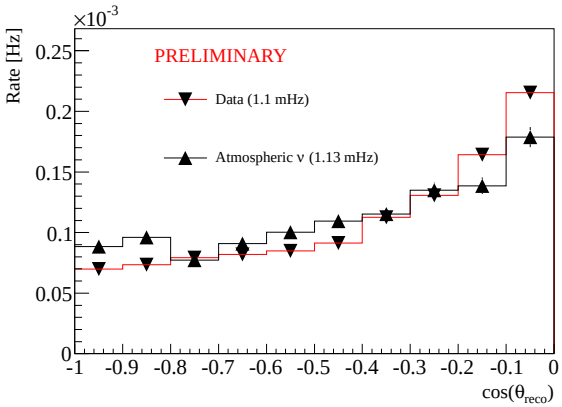

Figure 1: Comparison of the rate of selected events to the predicted rate of atmospheric neutrinos based on Monte-Carlo for IceCube in its 2010/2011 configuration with 79 deployed strings. The atmospheric neutrino prediction is based on the Bartol conventional flux model and the Naumov prompt flux model.

3 The time-clustering algorithm

The timescale of a neutrino flare is not fixed a-priori and thus a simple rolling time window approach is not adequate to detect flares. The time clustering approach that was developed for an unbiased neutrino flare search [6] looks for any time frame with a significant deviation of the number of detected neutrinos from the expected background. The simplest implementation uses a binned approach where neutrino candidates within a fixed bin around a source are regarded as possible signal events. To exploit the information that can be extracted from the estimated reconstruction error and other event properties like the energy an unbinned maximum-likelihood method is under development.

If a neutrino candidate is detected at time t_i around a source candidate the expected background $N_{\mathrm{bck}}^{i,j}$ is calculated for all other neutrino candidates j with $t_j < t_i$ from that source candidate. To calculate $N_{\mathrm{bck}}^{i,j}$ the detector efficiency as a function of the azimuth angle and the uptime has to be taken into account. The probability to observe the multiplet (i,j) by chance is then calculated according to:

$$\sum_{k=N_{\mathrm{obs}}^{i,j}-1}^{\infty} \frac{(N_{\mathrm{bck}}^{i,j})^k}{k!} e^{-N_{\mathrm{bck}}^{i,j}} \qquad (1)$$

where N_{obs} is the number of detected on-source neutrinos between t_j and t_i. It has to be reduced by 1 to take into account the bias introduced by the fact that one only does this calculation when a signal candidate is detected. As typical flares in high energy gamma-rays have a maximal duration of several days we constrain our search for time clusters of neutrinos to 21 days.

If the cluster with the highest significance exceeds a certain threshold (e.g. corresponding to $3\,\sigma$) the detector stability

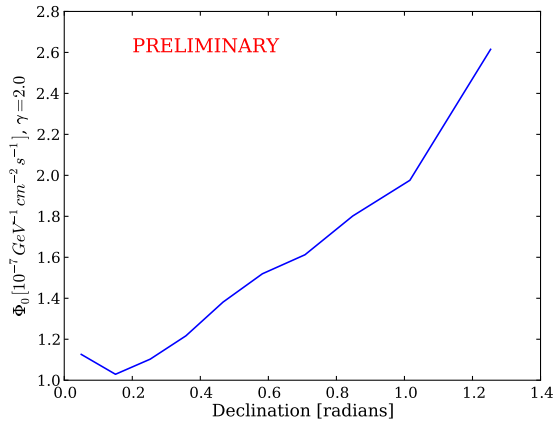

Figure 2: Neutrino flux needed from a given source declination to trigger a flare with a significance of $3\,\sigma$ with a probability of 50%. The neutrino spectrum is assumed to be an unbroken power law with a spectral index of -2.

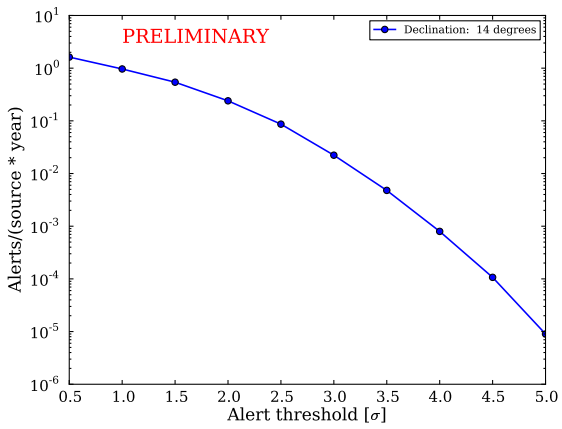

Figure 3: Expected number of accidental background alerts per year for a source at a declination of 14° as a function of the alert threshold expressed in units of standard deviations corresponding to a one-sided p-value.

will be checked and an alert will be sent to a Cherenkov telescope to initiate a follow-up observation. Figure 2 shows the flux needed as a function of declination for a neutrino spectrum with a spectral index of -2 to trigger a flare with a significance of $3\,\sigma$ with a probability of $50\,\%$.

To not overwhelm the partner experiment with follow-up requests one has to know the number of accidental background alerts caused by atmospheric neutrinos. This is shown in Figure 3 as a function of the alert threshold.

4 Stability monitoring

Data quality is very important for any online alert program to minimize the rate of false alerts due to detector or data aquisition (DAQ) instabilities. IceCube has a very extensive monitoring of the DAQ system and South Pole on-line processing. However, most of the information is only available with a certain delay after data-taking and thus not useful for a follow-up program which requires fast alerts. To ensure that alerts are triggered by neutrino multiplets that were detected during stable running conditions a simple but powerful stability monitoring scheme has been developed. It is based on a continuous measurement of the relevant trigger and filter rates in time bins of 10 minutes. These rates are inserted into an SQL database at the South Pole and are generally accessible a few minutes after the respective time bin ended. The rates and ratios of rates relevant for the selection of good quality neutrino-induced muon tracks are compared to an exponential running average of these rates to detect significant deviations. The running average is necessary as slow seasonal changes in the atmosphere and faster weather changes influence the rate of atmospheric muons which dominate the Level-2 rate. This system was tested off-line on data from IceCube in its 59-string configuration and proved to correlate very well with the extensive off-line detector monitoring. The fraction of data that has to be discarded because it was flagged as bad by this method was about $1.6\,\%$.

To generate a sufficient number of alerts to monitor the alert generation and forwarding itself we add 2000 so-called monitoring sources to the sourcelist (see Section 5). They are randomly distributed over the northern sky. To guarantee blindness for these sky locations the alerts for the monitoring sources are generated from blinded data events. The blindness is achieved by using the previous event time in the transformation from detector to sky coordinates for the current event instead of its own time. Due to the low event rate on the order of 10^{-3} Hz this results in a sufficient random shift of the event right ascension.

5 Sources

For a test run of this program we used selection criteria based on FERMI measurements [5]. For the galactic sources we choose sources that were observed in TeV and had a FERMI variability index > 15. Blazars were chosen according to the following criteria:

- Redshift < 0.6
- Fermi variability index > 15
- Spectral index as observed with FERMI < 2.4 (BL Lacs only)
- FERMI flux $1 - 100$ GeV $> 1 \cdot 10^{-9}$ph cm^{-2} s^{-1} (BL Lacs only)
- FERMI flux $0.1 - 1$ GeV $> 0.7 \cdot 10^{-7}$ph cm^{-2} s^{-1} (FSRQs only)

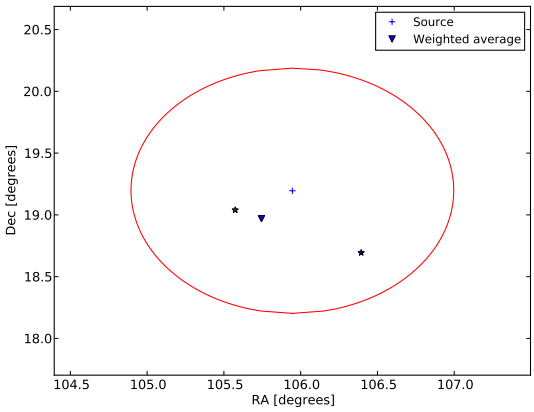

Figure 4: Angular distribution of events (star symbols) for one of the alerts that were generated during a test run of this follow-up program from March, 21st 2011 till May, 13th 2011 (see Section 7). The events contributing to this alert were blinded using the procedure described in this paper. The weighted average of the contributing events is calculated using an event-by-event angular resolution estimator. The circle indicates the size of the on-source bin.

These criteria are motivated by a compilation of different hadronic models that provide the guidelines to identify the most promising neutrino candidate sources. 22 sources (one galactic source, three FSRQs and 18 BL Lac objects) were selected according to these criteria in the northern hemisphere ($\delta > 0$).

6 Technical design of the alert system

After the alerts for this follow-up program are generated at the South Pole they are sent to the University of Wisconsin via the Iridium satellite communication system. This low bandwidth connection allows to send short messages from the South Pole without any significant delay. Once the message arrives in the North it is checked to see whether it represents a real alert or a test alert from a monitoring source. If it is a real alert, the alert is forwarded to the partner experiment. Depending on the technical setup this can happen e.g. via email or a dedicated socket connection.

All alerts (real and test) are filled into a database and a monitoring web page is updated. Each alert can be reviewed and basic information like the coordinates of the contributing events can be inspected. This allows a fast human inspection of alerts, even before the full IceCube event data arrives in the North. For each generated alert the time and space distribution of the contributing events can be inspected (see Figure 4). Furthermore global properties of the alerts, like their rate, significance and time length distribution are plotted and monitored.

The total time delay between the time the (latest) neutrino event is detected by IceCube and the moment it is forwarded to the partner experiment is on the order of several minutes ($\sim$ 10 min). This time is dominated by the delay until the detector rate is available in the database and the event processing time in the South Pole system.

7 Testrun results and Outlook

The system described here was tested online with the IceCube 79-string configuration from March, 21st 2011 till May, 13th 2011. During the test run neutrino triggers were generated online but not forwarded to any IACT. 199 alerts were generated during this test run for all sources combined, including the monitoring sources, while 219 where expected for a 52 day period. Besides statistical fluctuations, part of the discrepancy is also due to the limited event history available during the first days of running the program.

We plan to run this neutrino triggered high-energy gamma follow-up program using IceCube in its final 86-string configuration. Several enhancements are possible and planned. A maximum-likelihood based significance calculation taking into account an event-by-event angular reconstruction uncertainty estimation and an energy estimation of the event will further improve the sensitivity to neutrino flares.

References

[1] J.L. Bazo Alba *et al.* for the IceCube Collaboration, Proc. 31st ICRC, 2009, arXiv:0908.4209
[2] F. Aharonian *et al.* , A&A, 1999, **349**: 11-28
[3] F. Aharonian *et al.* , A&A, 2002, **393**: 89-99
[4] M. Ackermann *et al.* , Proc. 29th ICRC, 2005, arXiv:astro-ph/0509330.
[5] The Fermi LAT Collaboration, Astrophys.J.Suppl., 2009, **183**: 46-66
[6] K. Satalecka *et al.* for the IceCube collaboration, Proc. 30th ICRC, 2007

The Shadow of the Moon in Cosmic Rays measured with IceCube

THE ICECUBE COLLABORATION[1], H. STIEBEL[2]
[1]*See special section in these proceedings*
[2]*Stockholm University, Department of Physics, SE 106 91 Stockholm, Sweden*

Abstract: The observation of a deficit of cosmic rays from the direction of the Moon is an important experimental verification of the absolute pointing accuracy of the IceCube detector and the angular resolution of the reconstruction methods. This Moon shadow in the downward-going muon flux has been observed with a statistical significance of more than 10 sigma in an initial analysis based on a binned counting approach. An unbinned maximum likelihood method was developed to reconstruct the shape and the position of this shadow more precisely, to compare the performance of different reconstruction algorithms and to verify the correctness of the angular error estimate.

Corresponding Authors: D.J. Boersma[3] (*boersma@icecube.wisc.edu*), L.E. Gladstone[4] (*gladstone@icecube.wisc.edu*), J. Blumenthal[3] (*blumenthal@physik.rwth-aachen.de*), H. Stiebel[2] (*hust7801@student.su.se*)
[3]RWTH Aachen University, III. Phys. Institut B, Otto-Blumenthal-Strae, 52074 Aachen, Germany
[4]UW Madison, 222 West Washington Avenue, Madison 53703 WI, USA

Keywords: IceCube, cosmic rays, Moon shadow, pointing capability, neutrino astronomy

1 Introduction

IceCube [1] is a cubic kilometer scale Cherenkov detector at the geographical South Pole, designed to search for muons from high energy neutrino interactions. The arrival directions of these muons, which are reconstructed with $\mathcal{O}(1^\circ)$ accuracy, are used to search for point sources of astrophysical neutrinos [2], one of the primary goals of IceCube.

The main component of IceCube is an array of 5160 Digital Optical Modules (DOMs) deployed in the glacial ice at depths between 1450 m and 2450 m. During construction, with the first string of 60 DOMs deployed in January 2005 and the 86th and final string deployed in December 2010, the detector already took high quality data. The data analyzed and reported here were taken in the 40 and 59 string configurations, which were in operation between April 2008 and June 2010, with a configuration switch in May 2009.

For downward-going directions, the vast majority of the detected muons do not originate from neutrino interactions, but from high energy cosmic ray interactions in the atmosphere. While these cosmic ray muons are the dominant background in the search for astrophysical neutrinos, they can be used to study the performance of our detector. In particular, we can verify the pointing capability of IceCube by studying the shadow of the Moon in cosmic ray muons. Cosmic rays at TeV energies propagate through the solar system nearly uniformly in all directions. The Moon blocks some cosmic rays from reaching the Earth. This creates the shadow of the Moon, a relative deficit of cosmic ray muons from the direction of the Moon.

The idea of a Moon shadow was first proposed in 1957 [3], and has become an established observation for a number of astroparticle physics experiments [4, 5, 6, 7]. Experiments have used the Moon shadow to calibrate detector angular resolution and pointing accuracy [8]. The shift of the Moon shadow due to the Earth magnetic field has also been observed [9].

For an observer at the geographic South Pole, the Moon rises and sets once per orbital period of 27.32 days. The number of cosmic ray induced muons reaching IceCube decreases with increasing declination (i.e. for increasingly horizontal directions), since the Earth and the Antarctic ice sheet filter low energy muons. Therefore, the shadow of the Moon is best observed as far above the horizon as possible, i.e. at low declinations. However, the minimum declination of the Moon in an orbital period varies slowly over time with a period of 18.6 years and is currently increasing. In April 2008, 2009 and 2010 the minimum declination of the Moon was -26.89°, -25.85° and -24.47°, respectively. Fig. 1 shows the energy spectrum of cosmic ray primaries that result in one or more muons triggering IceCube. For the declination greater than -30°, the energy threshold is about 2 TeV.

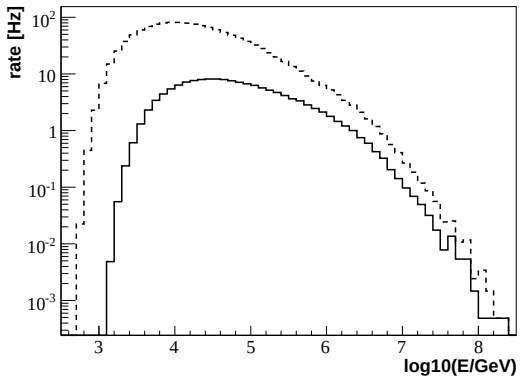

Figure 1: The energy spectrum of cosmic ray (CR) primaries with muons triggering IceCube, as simulated using CORSIKA [10]. Dashed: all events; solid: primaries with $\delta_{\rm CR} > -30^\circ$.

The Moon shadow in cosmic rays was first observed with IceCube using data taken during the first 8 orbital periods in the 40-string configuration, using a binned analysis [11]. In the analysis using the full data sets from the 40-string and 59-string configurations, a log-likelihood based analysis [12] has now been developed to study the point spread function of IceCube for muons.

The observed Moon shadow can be characterized with the following observables:

- The apparent shift of the Moon shadow from its nominal position (as computed from the time at which each muon event was recorded). A shift of order 0.1° is expected due to the Earth's magnetic field. Other contributions to a shift could come from e.g. a possible bias in track reconstruction or an error in the clock used to record the event times.
- The apparent width and ellipticity of the shadow. The apparent radius of the Moon is $\sim 0.25^\circ$, significantly smaller than the estimated angular resolution for muon tracks in IceCube. Hence the width of the shadow provides an experimentalal verification of the angular resolution estimate, which could for instance be different in zenith and azimuth directions.
- The number of shadowed events should be compatible with the measured flux of cosmic-ray induced muons (at the declination of the Moon) and the solid angle subtended by the Moon. Any significantly deviating result would be an indication of a systematic error.

2 Event selection

The trigger rate from cosmic ray muons was about 1.2-1.3 kHz in the 40-string configuration and close to 2 kHz in the 59 string configuration. However, most of those muons detected by IceCube travel nearly vertically, and thus they cannot have come from directions near the Moon.

The online event selection is defined as follows:

- the Moon must be at least 15° above the horizon
- at least 12 DOMs must register each event
- at least 3 strings must contain hit DOMs
- the reconstructed direction must be within 10° of the Moon in declination
- the reconstructed direction must be within $40^\circ/\cos(\delta_\mu)$ of the Moon in right ascension; the $\cos(\delta_\mu)$ factor corrects for spherical projection effects

where δ_μ denotes the declination of the reconstructed track.

The online Moon shadow filter was active (i.e., the Moon was more than 15° above the horizon) for 7-9 days during each 27.3 day orbital period. In that time, between 10M and 20M events were selected, depending on the number of active installed strings, atmospheric conditions and detector stability. This is about one percent of all events triggering IceCube during those days.

The event sample that passed online selection is subject to the same higher level track fitting algorithms as used in the searches for point sources of astrophysical neutrinos. The track likelihood function used in the fit is based on a simplified model of the scattering and absorption of light in ice [13]. In the offline processing, the track fit is repeated using several different seeds. For the majority of the events, this leads to a solution which is close to the online fit with a slightly improved angular resolution, when studied in simulated data. For a fraction of all events, the track fit is ambiguous and the iterative fit may yield a completely different direction.

In the Moon shadow analysis, we characterize each event by the zenith angle difference $\Delta\theta = \theta_{\leftmoon} - \theta_\mu$ (which is equivalent to the the declination difference, thanks to the unique geographic location of the detector) and the azimuth angle difference $\Delta\phi = (\phi_{\leftmoon} - \phi_\mu) \cdot \sin\theta_\mu$ between the direction of the offline reconstructed track and the nominal position of the Moon at the time of the event.

In the analysis, on-source and off-source subsamples are defined using the offline reconstruction. They are again defined by an angular window, namely $|\Delta\theta| \leq 8^\circ$ and $|\Delta\phi + \phi_{\rm off}| \leq 8^\circ$. Here $\phi_{\rm off} = 0^\circ$ for the on-source sample, and $\phi_{\rm off} = \pm 18^\circ$ for the left and right half of the off-source sample, respectively. The on-source samples for the full year data sets of the 40-strings and 59 strings configurations contain 19M and 22M events, respectively.

The per-event directional error estimate is derived from the variation of the track likelihood function near the solution obtained with the track fit [14]. It can be characterized either by the 3 parameters describing the 1σ error ellipse, or by a single average angular error estimate. In this work, we use the latter characterization.

The reliability of the directional error estimate was studied in simulated data, and simple quality selection criteria were developed to ensure that the pull (ratio of real and estimated angular error) is on average equal to unity. Moreover, for numerical stability, only events with an error estimate in the range from 0.075° to 1.5° were accepted. About half of the events in the on-source and off-source samples satisfy all these criteria.

3 Likelihood analysis

An unbinned likelihood analysis was applied to both data sets, using an approach similar to the likelihood approach taken for the IceCube point source searches [2]. The likelihood for the Moon having shadowed n_s events centered around $\vec{x}_s$ out of the on-source data sample is expressed as:

$$L(\vec{x}_s, n_s) = \sum_i^N \log\Big(\frac{n_s}{N} S_i + (1 - \frac{n_s}{N}) B_i\Big), \quad (1)$$

where $\vec{x}_s = (\Delta\theta, \Delta\phi)$ is the position relative to the nominal Moon position, n_s is the number of signal events, N is the total number of events, S_i is the signal probability density, and B_i is the background probability density. Note that Eq. 1 includes no explicit energy-dependent term; this a major difference between the IceCube Moon analysis and the IceCube point source searches. For the Moon shadow, we expect the number of signal events to be negative, as the Moon produces a deficit.

The signal probability density function S_i was assumed to be Gaussian, with a width given for each event by the estimated error on the reconstructed position [14]. The background probability density function B_i was estimated by using the normalized (Moon-centered) declination distribution obtained from the two off-source regions, and by assuming a uniform distribution in (Moon-centered) right ascension.

The likelihood (1) was maximized at every point $\vec{x}_s$ in an angular grid around the nominal Moon position, allowing the number of "signal" events n_s to vary.

4 Results

The distribution of the reconstructed number of signal events n_s is shown in Figures 2 and 3 as a function of the offset coordinates of the center of the shadow from the nominal Moon position. The shadow of the Moon is observed as a significant deficit centered at the nominal Moon position.

These results are directly compared with the same distributions from the off-source samples, as shown in Fig. 4. The distributions of the off-source samples are consistent with null shadowing effect from the Moon. The RMS values of the n_s distributions obtained for the left and right halves the off-source are considered as two independent estimates of the standard deviation of the background fluctuations.

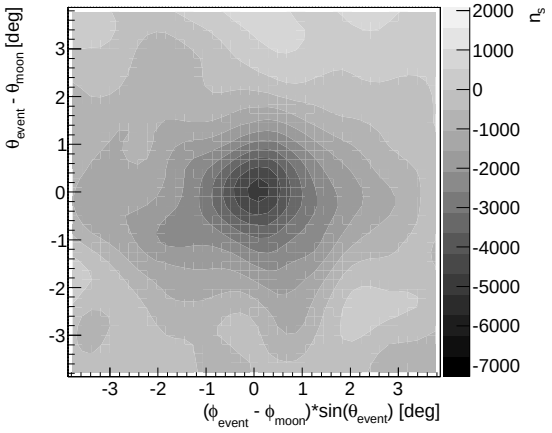

Figure 2: The Moon Shadow from the 40-string configuration *(preliminary)*. See text for details.

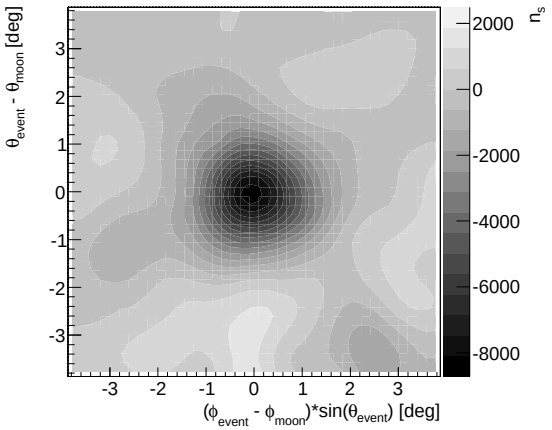

Figure 3: The Moon Shadow from the 59-string configuration *(preliminary)*. See text for details.

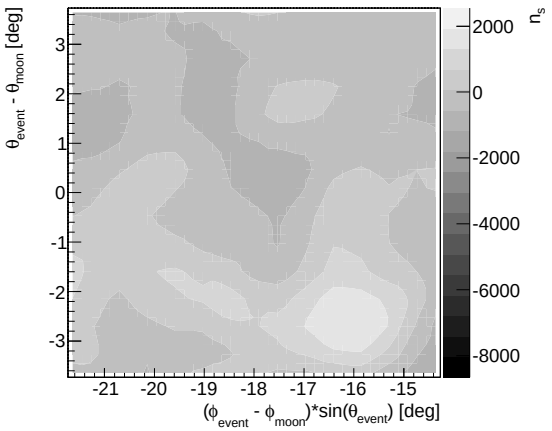

Figure 4: Fluctuation in n_s around the background model in one half of the off-source sample for the 59-string data set *(preliminary)*. See text for details.

	40 strings	59 strings
orbital periods	15	14
expected deficit	5734 ± 76	8192 ± 91
observed deficit	$5326 \pm 544 \pm 498$	$8660 \pm 565 \pm 681$
significance	10-11σ	13-15σ
θ offset	0.0°	0.0°
ϕ offset	0.0°	0.0°

Table 1: Results obtained in the Moon shadow analyses of the 40-string and 59-string data sets. Note that the two uncertainties given for the observed deficit are the estimates for the statistical uncertainty obtained from the left and right half of the off-source data samples; the numbers do *not* specify a systematic error.

The distributions of these values have means compatible with zero, as expected for the off-source regions. The RMS values of these distributions are now used as two independent estimates of the standard deviation of the background fluctuations (see Table 1).

The number of shadowed events found through likelihood maximization are also compared with the *expected* number of shadowed events. The expected number is calculated from the average apparent radius of the Moon and the off-source flux of downward-going muons from the declination of the Moon.

The depth of the observed shadow is compatible with the expected number of shadowed events. The significances of the shadows shown in Figures 2 and 3 are calculated to be 10-11σ and 13-15σ, respectively. The results for both detector configurations are summarized in Table 1.

The larger number of strings is the main reason for the larger significance of the result with the 59-strings configuration. With more optical sensors, more events are recorded, which are reconstructed with better angular resolution. On the other hand, the minimum declination reached by the Moon between April 2008 and May 2009 was more than a degree less than between May 2009 and June 2010. Moreover, the 40-string data sample contains livetime from one more orbital period.

To further confirm our results, the data from the 40-string configuration have also been analyzed using a different track fit algorithm and a corresponding angular error estimate. Simulation studies of this different reconstruction algorithm indicated an average pull of 1.55. Without correcting for this pull, the Moon shadow analysis resulted in a central n_s value of -3574 ± 434, differing by more than 5 standard deviations from the expectation: -6373 ± 80. Redoing the analysis with the angular error estimates rescaled by a factor of 1.55 resulted in a fitted n_s value compatible with expectation.

The log-likelihood-based analysis relies on the error estimate of the reconstructed track direction, ranging in this data sample from 0.075° to 1.5°. If we were not correctly estimating the angular errors, then we would find a shadow depth which is significantly smaller than expectation. The agreement between expected and observed shadow depth is a verification of the directional error estimate of the default track reconstruction algorithm as used in the analyses of the data taken with IceCube in these configurations.

5 Conclusions and Outlook

The shadow of the Moon in cosmic rays has been observed with a significance of more than 10σ in IceCube data collected between April 2008 and June 2010. The shadow depth is compatible with the expected number of shadowed events and has no significant systematic offset. These results confirm the pointing capability of IceCube.

We have started performing an observation of the shadow of the Sun. The shadow depth of the Sun should be comparable to that of the Moon, but a larger offset is expected due to the solar magnetic field. This offset should be correlated to the energy of the observed muons. Furthermore, if there is a component of high energy antiprotons in cosmic rays, then this should result in a faint second shadow with the opposite offset.

References

[1] H. Kolanoski, IceCube summary talk, these proceedings.

[2] J. Braun *et al.*, Astroparticle Physics **29** (2008) 299-305, [arXiv:0801.1604 [astro-ph]].

[3] G.W. Clark, Physical Review **108** (1957) p. 450-457.

[4] A. Karle for the HEGRA collaboration, Ann Arbor Proceedings (1990), High Energy Gamma-Ray Astronomy, p. 127-131.

[5] N. Giglietto, Nuclear Physics B Proceedings Supplements, Volume **61** (1997), Issue 3, p. 180-184.

[6] M.O. Wasco for the Milagro collaboration, 1999, arXiv:astro-ph/9906.388v1.

[7] The Soudan 2 collaboration, 1999, arXiv:hep-ex/9905.044v1.

[8] The Tibet AS Gamma Collaboration, M. Amenomori *et al.*, arXiv:astro-ph/0810.3757v1.

[9] L3 Collaboration, P. Achard *et al.*, Astropart. Phys. **23** (2005) p. 411-434, arXiv:astro-ph/0503472v1.

[10] D. Heck, J. Knapp, J.N. Capdevielle, G. Schatz, T. Thouw, FZKA **6019** (1998).

[11] D.J. Boersma, L. Gladstone, A. Karle, for the IceCube Collaboration, Proceedings of the 31^{st} ICRC, LODZ, POLAND (2009), arXiv:1002.4900.

[12] J. Blumenthal, Diplomarbeit in Physik (2011), Rheinisch-Westfälischen Technischen Hochschule Aachen, available upon request.

[13] G. Japaridze, M. Ribordy, arXiv:astro-ph/0506136v1.

[14] T. Neunhöffer and L. Köpke, Nuclear Instruments and Methods **A558** (2006) p. 561-568.

[15] H. Stiebel, Master Thesis (2011), Stockholm University, available upon request.